Fermilab

SDC SOLENOID DESIGN NOTE #154

TITLE: Buckling and Stress Analysis of the SDC (Isogrid) Vacuum Shell

AUTHOR: Lyle W. Swenson, Jr., PS Associates, Inc.

DATE: Aug 30, 1991

Buckling and Stress Analysis of the SDC (Isogrid) Vacuum Shell (Task 1)

Prepared For

Fermilab (PO B14690)

August 30, 1991

Prepared by

Lyle W. Swenson, Jr.

PS▲A

PS Associates, Inc.
5755 Oberlin Drive, Suite 300
San Diego, CA 92121-4717

1.0 Introduction

This report supersedes our report dated May 9, 1991 and presents analysis results for the SDC vacuum shell covering general instability and static stresses resulting from external pressure, bulk head reaction loads, and structural weight. Chimney loading conditions are not covered in this report. The following presentation is contained in nine sections and two appendices.

Section 2.0 is a description of the finite element model used to perform the static stress analyses. Material properties, model geometry, applied loading, and boundary conditions are presented in detail.

Section 3.0 presents buckling analyses for the outer (Isogrid) shell. Three sources were used and all produced consistent results validating the Isogrid design geometry.

Section 4.0 discusses the structural deformation resulting from the structural weight alone and from the structural weight combined with all applied loads. Deformation plots are also given.

Sections 5.0 through 8.0 presents static stress results for the four primary components of the vacuum shell: 1) outer (Isogrid) shell, 2) "second" bulk head, 3) inner shell, and 4) "first" (chimney-end) bulk head, respectively. For each component, internal loads, stresses, and effective von Mises stresses are presented.

Section 9.0 presents a summary of the results and collects the principal minimum and maximum values for all analyses.

Appendix A gives a brief derivation of the Isogrid stress-strain equations used in this report and shows the relations between Isogrid skin and rib stresses and the internal stress resultants.

Finally, Appendix B contains a discussion on the CGA-341 requirement for a minimum shell thickness of 1/8 inch and an interpretation of this requirement for the current Isogrid design.

2.0 Finite Element Modelling of the SDC Vacuum Shell

2.1 Material Properties

All vacuum shell structure is considered made from aluminum 2219-T851.

Properties for this material are taken from MIL-HDBK-5C [1] and are given in Table 2-1 below.

Table 2-1. Properties for Al 2219-T851 (Room Temperature)

Young' Modulus	10.5×10^6 psi
Poisson's Ratio	0.33
Weight Density	0.102 lb/in^3
Tensile Ultimate Strength	62,000 psi
Tensile Yield Stress	47,000 psi
Allowable Stress	15,500 psi

The allowable stress value given above is determined from the ASME Pressure Vessel Code rule (cf. [2], Appendix P):

allowable stress = MIN (0.25 * ultimate strength, 0.67 * yield stress)

2.2 Model Geometry

Basic geometry for the vacuum shell was specified by Fermilab as presented in Table 2-2 below.

Table 2-2. Basic Vacuum Shell Geometry

Outer Shell Diameter	160 in
Outer Shell Length	360 in
Inner Shell Diameter	134 in
Inner Shell Length	360 in
Inner Shell Thickness	0.25 in
Bulk Head Outer Radius	80 in
Bulk Head Inner Radius	67 in
Bulk Head Thickness	0.5 in

The current Isogrid design geometry is given below. See Appendix A for a discussion of the dimensionless parameters and computation of section details.

Table 2-3. Isogrid Geometry

Node Spacing	a	6.9930 in
Web Width	b	0.1500 in
Flange Depth	c	0.2900 in
Web Depth	d	1.8000 in
Triangle Height	h	6.0561 in
Flange Width	w	1.0000 in
Skin Thickness	t	0.1100 in

Table 2-4. Isogrid Dimensionless Parameters

$\alpha = bd/ht$	0.4053
β	49.917
$\delta = d/t$	16.364
$\tau = c/t$	2.6264
$\mu = wc/ht$	0.4353

Table 2-5. Isogrid Section Parameters

Effective Area	A	0.2025 in^2/in
Flange Fiber Distance	Cf	1.4617 in
Skin Fiber Distance	Cs	0.7383 in
Shell Modulus	E*	7.13×10^5 psi
Bending Rigidity	D	1.77×10^6 in-lb
Moment of Inertia	I	0.1502 in^4/in
Extension Stiffness	K	2.39×10^6 lb/in
Effective Thickness	t_{eff}	0.2025 in
Shell Thickness	t*	2.9832 in
Weight Thickness	t_{bar}	0.3874 in

The SDC vacuum shell is modelled using a symmetric three-dimensional finite element representation, see Figure 2.1. The origin of the global coordinate system is located at the center of the "first" (chimney-end) bulk head, with the x-axis horizontal, the y-axis vertical, and the z-axis increasing away from the "second" bulk head.

The finite element model consists of 592 shell elements and 666 nodes. The outer and inner shell each consist of 240 elements, while the bulk heads each consist of 56 elements. Figure 2.2 shows the outer shell element numbers 1-240 (note that the "chimney-end" bulk head is to the left). Figure 2.3 shows the "second" bulk head element numbers 241-296, Figure 2.4 shows the inner shell element numbers 297-536, and Figure 2.5 shows the "first" (chimney-end) bulk head element numbers 537-952.

2.3 Applied Loading

In addition to an external pressure loading of 15 psi, applied loading on the bulk heads was supplied by Fermilab as given below. The node numbers refer to the model presented in this report.

Table 2-6. Radial Loads on "First" Bulk Head

Node	Radial
649	941.51310
650	1855.1823
651	1775.8899
652	1657.2195
653	1517.2386
654	1377.2575
655	1258.5877
656	1179.2948
657	575.72552

Table 2-7. Radial and Axial Loads on "Second" Bulk Head

Node	Radial	Axial
289	143.31421	-857.20356
290	264.80999	-1583.9046
291	202.67690	-1212.2686
292	109.68776	-656.07344
293	0.0	0.0
294	-109.68772	656.07441
295	-202.67653	1212.2668
296	-264.81012	1583.9057
297	-143.31418	857.20345

2.4 Boundary Conditions

Boundary conditions specified on the bulk heads were supplied by Fermilab. The "first" (chimney-end) bulk head is unconstrained at the support attachments only in the radial direction. The "second" bulk head is constrained at the support attachments only in the circumferential direction.

3.0 Outer Shell Buckling Analysis

Computation of the critical buckling pressure for the outer (Isogrid) shell was determined using three sources: ASME Boiler and Pressure Vessel Code [2], CGA-341 [3], and NASA SP-8007 [4]. Analyses following the procedures set forth in each of these documents is presented in the following three sections.

3.1 Buckling Analysis via ASME Code

From the ASME Boiler and Pressure Vessel Code [2], computations proceed as follows. From Section UG-28 (c) the following steps were performed:

(0) $Do/t' = 160/1.217 = 131.47 > 10.0$

(1) $L/Do = 360/160 = 2.25$

(2,3) From Figure 5-UG0-28.0 find: $A = .000386$

(4,5) From Figure 5-UNF-28.20 find: $B = 1900$

(6) Compute allowable pressure: $Pa = 4B/3(Do/t') = 19.27$ psi

(7) $Pa > 15$ psi.

The result in (7) validates the requirement that allowable pressure (Pa) equal or exceed the maximum loading pressure of 15 psi. As stated in UG-28 (e), "The external design pressure or maximum allowable external working pressure shall not be less than the maximum expected difference in operating pressure that may exist between the outside and the inside of the vessel at any time".

The following assumptions were made in performing the above calculations. First, in step (0) the effective shell thickness used is that determined from Isogrid theory based on the Isogrid shell area moment of inertia, cf. Appendix A. That is,

$$I = t^3 b^2/12(1+\alpha+\mu) = (t')^3/12$$

or,

$$t' = t\,[b^2/(1+\alpha+\mu)]^{1/3}.$$

Using the skin thickness value of $t = 0.11$ (cf. Table 2-3) and the Isogrid dimensionless parameters in Table 2-4, the effective skin thickness is computed to be $t' = 1.217$.

Second, in step (4,5), data presented in Figure 5-UNF-28.20 for aluminum 5456 is assumed representative of 2219-T851. Properties for 2219-T851 do not appear in [2].

3.2 Buckling Analysis via CGA Standard

CGA-341 [3] requires that vacuum vessels be designed for a minimum collapse pressure of 30 psi (that is, a safety factor of 2 is specified). The critical collapse pressure is to be determined by the following equation:

$$Pc = 2.6\ E^* (t^*/Do)^{2.5}/[\ (L/Do) - 0.45(t^*/Do)^{0.5}].$$

Using material properties and geometry given in tables in Section 2.0, the critical pressure is found to be:

$$Pc = 2.6(713{,}000)(2.9832/160)^{2.5}/[\ (360/160) - 0.45(2.9832/160)^{0.5}]$$

$$Pc = 40.21 \text{ psi}$$

The critical buckling equation suggested in CGA-341 is effectively the same equation recommended by NASA (as presented in the next section). However, NASA suggests multiplying this equation by a correlation coefficient (the ratio of experimental measurement to theoretical expectation) with a value of 0.75. Following this suggestion, the "corrected" critical buckling pressure is given by:

$$Pc = 30.16 \text{ psi.}$$

3.3 Buckling Analysis via NASA SP-8007

NASA [4] recommends that the critical buckling pressure for cylindrical shells under external pressure be computed using the following equation:

$$Pc = [0.855/(1-n^2)^{3/4}]\ E^*\ \phi\ (t^*/R)^{2.5}/(L/R).$$

For aluminum Isogrid, Poisson's ratio is $n = 1/3$, therefore,

$$Pc = 0.934\ E^*\ \phi\ (t^*/R)^{2.5}/(L/R).$$

This equation is essentially the same as that recommended in CGA-341 with the outer diameter Do replaced by the radius R and the small second term in the denominator omitted. In this equation ϕ is the correlation coefficient with a suggested value is 0.75.

Substituting numerical values given in Section 2.0, the critical buckling pressure is found to be:

$$Pc = 0.934(713{,}000)(0.75)(2.9832/80)^{2.5}/(360/80)$$

$$Pc = 29.8 \text{ psi.}$$

Clearly, CGA-341 and NASA SP-8007 give essentially the same result for the critical buckling pressure for the Isogrid shell.

4.0 Structural Deformation

Structural deformation results are presented here for weight loading alone and for weight loading plus applied loads.

Figure 4.1 shows the deformation of the SDC vacuum shell for weight loading only. As expected, because of its greater effective weight the outer (Isogrid) shell suffers greater center sag than the inner shell. The center vertical displacement of the outer shell was computed to be 0.00247 inches, while the vertical displacement of the inner shell was 0.00182 inches. As can be seen in Figure 4.1, the "first" (chimney-end) bulk head is bent into a "C"-shaped cross section at the top of the shell, and into a reversed "C"-shaped cross section at the bottom of the shell.

Figure 4.2 shows the deformation of the SDC vacuum shell for combined weight loading and applied loads (pressure loading and bulk head reaction loads). For this case the "second" bulk head suffers the most bending deformation. As the outer shell deforms inward (due to pressure loading) it expands longitudinally and pushes the "second" bulk head away from the "first" bulk head (0.0403 inches). Conversely, as the inner shell deforms outward (again due to pressure loading) it contracts longitudinally and pulls the "second" bulk head toward the "first" bulk head (0.0367 inches).

Figures 4.3 and 4.4 show the original and deformed shapes for the outer and inner shells, respectively. The maximum radial deformation of the outer shell is 0.0456 inches inward, while the maximum radial deformation of the inner shell is 0.0284 inches outward. The bending deformation of the "second" bulk head can clearly be seen in both of these figures.

5.0 Stress Results for the Outer (Isogrid) Shell

Results for the internal load resultants and stresses for the outer (Isogrid) shell are presented in this Section. For plots in this section, the circumferential direction is referenced as the x-direction and the longitudinal direction is referenced as the y-direction. (This is because results are plotted in the element coordinate system.)

Figures 5.1 and 5.2 show internal moment resultants and internal force resultants versus element number, respectively. As seen from Figure 5.1, the longitudinal moment resultant dominates both the circumferential and twisting moment resultants and is restricted to the ends of the shell. Figure 5.2 shows the internal force resultants with the circumferential resultant relatively uniform over the length of the shell except near the ends. The circumferential force resultant is essentially uniform and is given by:

$$Nx = -pR = -(15)(80) = -1{,}200 \text{ lb/in},$$

with a peak value of -1,210 lb/in.

The Isogrid skin stresses are shown in Figure 5.3. Clearly the circumferential stress is dominated by the circumferential force resultant. The circumferential stress is essentially uniform and is given by:

$$Sx = -pR/t_{eff} = -(15)(80)/0.2025 = -5{,}926 \text{ psi},$$

with a peak value of -5,963 psi.

The von Mises effective stress (based on distortional energy theory) can be used as a criterion for comparison with the allowable stress (15.5 ksi). This stress is plotted in Figure 5.4 and shows a peak value of 5,765 psi. Clearly this result is dominated by the circumferential stress.

Outer fiber stresses in the Isogrid ribs are shown in Figure 5.5. The circumferential rib is denoted "BS1" and the diagonal ribs by "BS2" and "BS3". The circumferential rib stress follows a pattern nearly identical with the skin stress, with essentially the same stress (a peak value of -5,818 psi). This result is expected over the shell away from the ends where the bending moments are near zero.

As an interesting comparison with the results presented above, Figures 5.6 through 5.10 show exact results for a circular cylinder clamped at its ends and subjected to external pressure and longitudinal loading consistent with the structure being considered. (I will call this a simple model since it neglects weight loading and bulk head reaction loads.) Comparison of finite element method (FEM) results with the simple model are given in Table 5-1 below.

Table 5-1. Min/Max FEM Results versus Simple Model Results

	FEM	Simple
Disp.	0.0456	0.0435
Mx	-174	-343
	86	72
My	-502	-1041
	238	216
Mxy	-17	0
	26	0
Nx	-1220	-1249
	-370	-59
Ny	-186	-179
	-86	-179
Nxy	-38	0
	31	0
Sx	-5963	-6116
	-1955	-1537
Sy	-1338	-6000
	468	179
Sxy	-22	0
	135	0
S1	-5818	-5873
	-1560	-31
S2	-1680	-1994
	196	6163
S3	-1750	-1994
	46	6163

As can be seen, results from the simple model are in good agreement with the finite element results except at the bulk head interface. This, of course, is expected since the simple model neglects the bulk head reaction loads.

6.0 Stress Results for the "Second" Bulk Head

Results for the internal load resultants and stresses for the "second" bulk head are presented in this Section. For plots in this section, the circumferential direction is referenced as the x-direction and the inward radial direction is referenced as the y-direction. (This is because results are plotted in the element coordinate system.)

Figures 6.1 and 6.2 show internal moment resultants and internal force resultants versus element number, respectively. As seen from Figure 6.1, the radial moment resultant dominates both the circumferential and twisting moment resultants and reaches a maximum value of -431 in-lb/in in the element interface with the bottom of the outer shell.

Bulk head stresses are given in Figure 6.3 (vacuum side) and Figure 6.4 (pressure side). Note that the pattern of radial stress follows the radial moment, indicating dominance of the radial moment in contributing to the radial stress. Peak radial stresses occur at the interface of the bulk head with the bottom of the outer shell. The peak tensile stress (10,040 psi) occurs on the outside surface of the bulk head and the peak compressive stress (-10,630 psi) occurs on the inside surface of the bulk head.

The von Mises effective stress (based on distortional energy theory) can be used as a criterion for comparison with the allowable stress (15.5 ksi). This stress is plotted in Figure 6.5 and shows a peak value of 9,397 psi on the bulk head inside surface. Note, this is the largest stress found in the structure.

7.0 Stress Results for the Inner Shell

Results for the internal load resultants and stresses for the inner shell are presented in this Section. For plots in this section, the circumferential direction is referenced as the x-direction and the longitudinal direction is referenced as the y-direction. (This is because results are plotted in the element coordinate system.)

Figures 7.1 and 7.2 show internal moment resultants and internal force resultants versus element number, respectively. As seen from Figure 7.1, the longitudinal moment resultant dominates both the circumferential and twisting moment resultants and is restricted to the ends of the shell. Figure 7.2 shows the internal force resultants with the circumferential resultant relatively uniform over the length of the shell except near the ends. The circumferential force resultant is essentially uniform and is given by:

$$Nx = pR = (15)(67) = 1{,}005 \text{ lb/in},$$

with a peak value of 1,040 lb/in.

Inner shell stresses are given in Figure 7.3 (vacuum side) and Figure 7.4 (pressure side). Clearly, the circumferential stress is dominated by the circumferential force resultant except near the bulk heads. The circumferential stress is essentially uniform and is given by:

$$Sx = pR/t = (15)(67)/0.25 = 4{,}020 \text{ psi},$$

with a peak value of 4,262 psi.

The von Mises effective stress (based on distortional energy theory) can be used as a criterion for comparison with the allowable stress (15.5 ksi). This stress is plotted in Figure 7.5 and shows a peak value of 4,342 psi. This result is seen to be dominated by the circumferential stress.

8.0 Stress Results for the "First" (Chimney-end) Bulk Head

Results for the internal load resultants and stresses for the "first" bulk head are presented in this Section. For plots in this section, the circumferential direction is referenced as the x-direction and the outward radial direction is referenced as the y-direction. (This is because results are plotted in the element coordinate system.)

Figures 8.1 and 8.2 show internal moment resultants and internal force resultants versus element number, respectively. As seen from Figure 8.1, the radial moment resultant dominates both the circumferential and twisting moment resultants and reaches a maximum value of -165 in-lb/in in the element interface with the bottom of the outer shell.

Bulk head stresses are given in Figure 8.3 (vacuum side) and Figure 8.4 (pressure side). Note that the pattern of radial stress follows the radial moment, indicating dominance of the radial moment in contributing to the radial stress. Peak radial stresses occur at the interface of the bulk head with the bottom of the outer shell. The peak tensile stress (3,716 psi) occurs on the outside surface of the bulk head and the peak compressive stress (-4,216 psi) occurs on the inside surface of the bulk head.

The von Mises effective stress (based on distortional energy theory) can be used as a criterion for comparison with the allowable stress (15.5 ksi). This stress is plotted in Figure 8.5 and shows a peak value of 3,717 psi on the inside surface of the bulk head.

9.0 Discuss of Results

For pressure, weight, and bulk head loads, the SDC vacuum shell satisfies all requirements for deformation, critical buckling pressure, and static stress. Critical buckling pressure results are given in Table 9-1.

Table 9-1. Critical Buckling Pressure for Isogrid Shell

ASME Code	19.27 psi
CGA-341	30.16 psi
NASA SP-8007	29.80 psi

Note that the ASME Code requires that the computed result not be less than the maximum expected shell pressure (15 psi), while CGA-341 requires a safety factor of 2 when using their equation for computing buckling pressure. The CGA-341 result includes a correlation coefficient reduction factor (0.75) as suggested in NASA SP-8007.

Peak internal loads and stress values for the four vacuum shell components are given below in Tables 9-2 through 9-5.

Table 9-2. Summary of Outer (Isogrid) Shell Peak Results

Displacement	0.0456 in (inward)
Axial Moment	190 in-lb/in
Hoop Force	-1,210 lb/in
Hoop Stress	-5,963 psi
von Mises Stress	5,765 psi

Table 9-3. Summary of Inner Shell Peak Results

Displacement	0.0284 in (outward)
Axial Moment	3.82 in-lb/in
Hoop Force	1,040 lb/in
Hoop Stress	4,262 psi
von Mises Stress	4,342 psi

Table 9-4. Summary of Chimney-end Bulk Head Peak Results

Radial Moment	-165 in-lb/in
Radial Force	-129 lb/in
Radial Stress	-4,216 psi (+3,716 psi)
von Mises Stress	3,717 psi

Table 9-5. Summary of "Second" Bulk Head Peak Results

Radial Moment	-431 in-lb/in
Radial Force	-152 lb/in
Radial Stress	-10,630 psi (+10,040 psi)
von Mises Stress	9,397 psi

The peak radial stress values of -10,630/+10,040 psi located in the "second" bulk head, at its interface with the bottom of the outer shell, are the largest found in the structure. While these values are well below the maximum allowable stress of 15,500 psi, it would be prudent to examine this area of the bulk head in more detail.

In order to evaluate the contribution of pressure and bulk head loads to the stresses in the outer shell and "second" bulk head, two analyses were

performed considering pressure loading and bulk head loading separately. Figures 9.1 through 9.10 give results for the outer shell and "second" bulk head due only to pressure loading, while Figures 9.11 through 9.20 give results for the outer shell and "second" bulk head due only to bulk head reaction loads.

Table 9-6 summarizes the outer shell results for all loads, pressure loads, and bulk head loads. Similarly, Table 9-7 summarizes results for the "second" bulk head for all loads, pressure loads, and bulk head loads.

Table 9-6. Outer Shell Loading Comparison

		All Loads	Pressure	Bulk Head
Axial Moment	(in-lb/in)	190	189	-34
Axial Force	(lb/in)	-172	-132	44
Hoop Force	(lb/in)	-1,210	-1,210	12
Axial Stress	(psi)	-1,338	-989	-382
Hoop Stress	(psi)	-5,963	-5,963	55
von Mises Stress	(psi)	5,765	5,692	372

Table 9-7. "Second" Bulk Head Loading Comparison

		All Loads	Pressure	Bulk Head
Radial Moment	(in-lb/in)	-431	-375	-56
Radial Force	(lb/in)	-152	-150	9
Radial Stress	(psi)	-10,630	-9,299	-1,352
von Mises Stress	(psi)	9,397	8,219	1,198

These results clearly indicate that the pressure loading is the significant contributor to the outer shell and bulk head internal loads and stresses. The bulk head reaction loads contribute only 1.3 percent to the outer shell von Mises stress and less than 13 percent to the bulk head von Mises stress.

References

[1] MIL-HDBK-5C, Military Standardization Handbook, Metallic Materials and Elements for Aerospace Vehicle Structures. September 15, 1976.

[2] ASME Boiler and Pressure Vessel Code, Section VIII Rules for Construction of Pressure Vessels, Division I. 1989 Edition, July 1, 1989.

[3] CGA-341, "Standard for Insulated Cargo Tank Specification for Cryogenic Liquids", Compressed Gas Association. Third Edition, 1987.

[4] NASA SP-8007, "Buckling of Thin-walled Circular Cylinders", National Aeronautics and Space Administration, September 1965, Revised August 1968.

[5] Isogrid Design Handbook. NASA Contractor Report NASA CR-124075, February 1973.

Appendix A

An Overview of Isogrid Stress and Strain Equations

This appendix provides a synopsis of Isogrid theory in order to provide the reader with enough information to appreciate the Isogrid parameters and stress-strain relations used in this report. The final authority, however, resides with the Isogrid Design Handbook [5].

Figure A.1 shows the sign conventions used for the shell resultant forces and moments. Note that Nxy and Mxy used here are the negative of the same quantities used in [5]; this is because our finite element program uses the conventions shown in the figure.

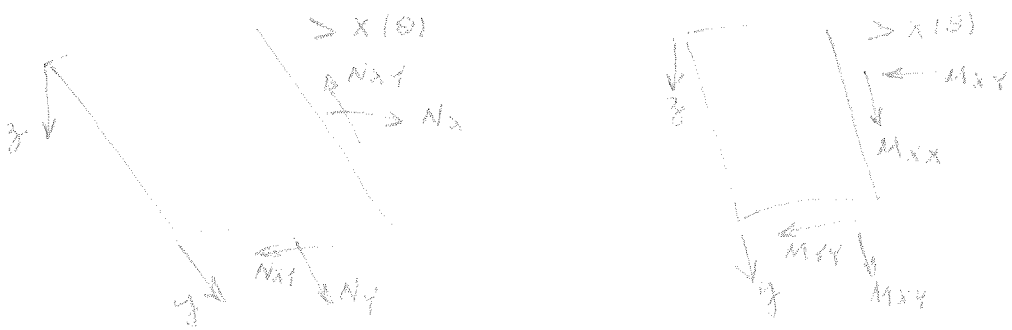

A.1 FORCE & MOMENT POSITIVE SIGN CONVENTION

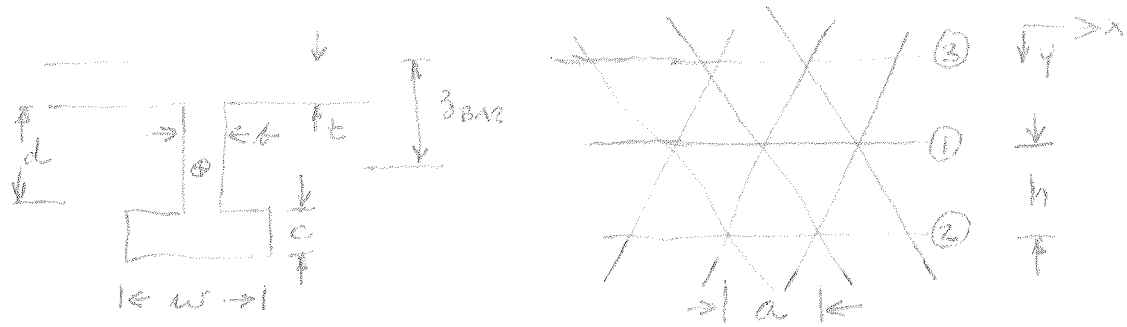

A.2 ISOGRID GEOMETRY

Figure A.2 shows the plan view of an Isogrid construction and a typical rib cross section. From this figure, the following geometrical dimensions are defined:

Table A-1. Isogrid Geometrical Parameters

a = Node Spacing
b = Web Thickness
c = Flange Thickness
d = Web Depth
h = Triangle Height
w = Flange Width
t = Skin Thickness

Table A-2. Isogrid Dimensionless Parameters

$\alpha = bd/ht$
$\beta = (1+\alpha+\mu)\,[(3(1+\delta)^2 + 3\mu(\delta+\tau)^2 + 1 + \alpha\delta^2 + \mu\tau^2] - 3[(1+\delta) - \mu(\delta+\tau)]^2$
$\delta = d/t$
$\tau = w/t$
$\mu = wc/ht$

Table A-3. Isogrid Section Parameters

A = Effective Area
Cf = Flange Fiber Distance
Cs = Skin Fiber Distance
E^* = Shell Modulus
D = Bending Rigidity
I = Moment of Inertia
K = Extension Stiffness
t_{eff} = Effective Thickness
t^* = Shell Thickness
t_{bar} = Weight Thickness
z_{bar} = Centroid Location

The section parameters given above are computed as follows:

$$
\begin{aligned}
A &= t\,(1 + \alpha + \mu) \\
Cf &= t + d + c - z_{bar} \\
Cs &= -z_{bar} \\
E^* &= E\,(1 + \alpha + \mu)^2/\beta \\
I &= t^3\,\beta^2/12(1 + \alpha + \mu) \\
D &= 9/8\,E\,I \\
K &= 9/8\,E\,A \\
t_{eff} &= A \\
t^* &= t\,\beta/(1 + \alpha + \mu) \\
t_{bar} &= t\,(1 + 3\alpha + 3\mu) \\
z_{bar} &= t + d/2 - t\,[1 + \delta - \mu\,(\delta+\tau)]/2(1 + \alpha + \mu)
\end{aligned}
\tag{1}
$$

From shell theory, the force and moment stress resultants are given by the following equations (note that for aluminum Isogrid, Poisson's ratio equals 1/3):

$$
\begin{Bmatrix} N_x \\ N_y \\ N_{xy} \end{Bmatrix} = K \begin{bmatrix} 1 & 1/3 & 0 \\ 1/3 & 1 & 0 \\ 0 & 0 & -1/3 \end{bmatrix} \begin{Bmatrix} \varepsilon_x^\circ \\ \varepsilon_y^\circ \\ \gamma_{xy}^\circ \end{Bmatrix}
\tag{2}
$$

and

$$
\begin{Bmatrix} M_x \\ M_y \\ M_{xy} \end{Bmatrix} = -D \begin{bmatrix} 1 & 1/3 & 0 \\ 1/3 & 1 & 0 \\ 0 & 0 & 1/3 \end{bmatrix} \begin{Bmatrix} \chi_x \\ \chi_y \\ 2\chi_{xy} \end{Bmatrix}
\tag{3}
$$

respectively. In these equations, ε° and X are the centroidal axis strains and curvatures, respectively.

The shell strains at a distance z from the reference surface are given by:

$$
\begin{Bmatrix} \varepsilon_x \\ \varepsilon_y \\ \gamma_{xy} \end{Bmatrix} = \begin{Bmatrix} \varepsilon_x^\circ \\ \varepsilon_y^\circ \\ \gamma_{xy}^\circ \end{Bmatrix} - z \begin{Bmatrix} \chi_x \\ \chi_y \\ 2\chi_{xy} \end{Bmatrix}
\tag{4}
$$

If equations (1) and (2) are inverted,

$$\begin{Bmatrix} \varepsilon_x^0 \\ \varepsilon_y^0 \\ \gamma_{xy}^0 \end{Bmatrix} = \frac{9}{8K} \begin{bmatrix} 1 & -1/3 & 0 \\ -1/3 & 1 & 0 \\ 0 & 0 & -8/3 \end{bmatrix} \begin{Bmatrix} N_x \\ N_y \\ N_{xy} \end{Bmatrix} \tag{5}$$

and

$$\begin{Bmatrix} \chi_x \\ \chi_y \\ 2\chi_{xy} \end{Bmatrix} = \frac{-9}{8D} \begin{bmatrix} 1 & -1/3 & 0 \\ -1/3 & 1 & 0 \\ 0 & 0 & 8/3 \end{bmatrix} \begin{Bmatrix} M_x \\ M_y \\ M_{xy} \end{Bmatrix} \tag{6}$$

and substituted into equation (3), the shell strains can be written as:

$$\begin{Bmatrix} \varepsilon_x \\ \varepsilon_y \\ \gamma_{xy} \end{Bmatrix} = \frac{9}{8K} \begin{bmatrix} 1 & -1/3 & 0 \\ -1/3 & 1 & 0 \\ 0 & 0 & -8/3 \end{bmatrix} \begin{Bmatrix} N_x \\ N_y \\ N_{xy} \end{Bmatrix} + \frac{9z}{8D} \begin{bmatrix} 1 & -1/3 & 0 \\ -1/3 & 1 & 0 \\ 0 & 0 & 8/3 \end{bmatrix} \begin{Bmatrix} M_x \\ M_y \\ M_{xy} \end{Bmatrix} \tag{7}$$

or,

$$\begin{Bmatrix} \varepsilon_x \\ \varepsilon_y \\ \gamma_{xy} \end{Bmatrix} = \frac{1}{EA} \begin{bmatrix} 1 & -1/3 & 0 \\ -1/3 & 1 & 0 \\ 0 & 0 & -8/3 \end{bmatrix} \begin{Bmatrix} N_x \\ N_y \\ N_{xy} \end{Bmatrix} + \frac{z}{EI} \begin{bmatrix} 1 & -1/3 & 0 \\ -1/3 & 1 & 0 \\ 0 & 0 & 8/3 \end{bmatrix} \begin{Bmatrix} M_x \\ M_y \\ M_{xy} \end{Bmatrix} \tag{8}$$

Use of the definitions of A and I were made in equation (8).

Isogrid Skin Stresses

Isogrid skin stresses are computed using the constitutive relations for plane stress:

$$\begin{Bmatrix} \sigma_x \\ \sigma_y \\ \sigma_{xy} \end{Bmatrix} = \frac{9E}{8} \begin{bmatrix} 1 & 1/3 & 0 \\ 1/3 & 1 & 0 \\ 0 & 0 & 1/3 \end{bmatrix} \begin{Bmatrix} \varepsilon_x \\ \varepsilon_y \\ \gamma_{xy} \end{Bmatrix} \tag{9}$$

If the shell strains in equation (8) are substituted into equation (9), and the extreme shell fiber z = Cs is identified, then the skin stresses are given by:

$$\begin{Bmatrix} \sigma_x \\ \sigma_y \\ \sigma_{xy} \end{Bmatrix} = \frac{1}{A} \begin{Bmatrix} N_x \\ N_y \\ -N_{xy} \end{Bmatrix} + \frac{C_s}{I} \begin{Bmatrix} M_x \\ M_y \\ M_{xy} \end{Bmatrix} \tag{10}$$

Isogrid Rib Stresses

Isogrid rib stresses can be computed for strains as follows [5]:

$$\begin{Bmatrix} \sigma_1 \\ \sigma_2 \\ \sigma_3 \end{Bmatrix} = \frac{E}{4} \begin{bmatrix} 4 & 0 & 0 \\ 1 & 3 & \sqrt{3} \\ 1 & 3 & -\sqrt{3} \end{bmatrix} \begin{Bmatrix} \varepsilon_x \\ \varepsilon_y \\ \gamma_{xy} \end{Bmatrix} \tag{11}$$

If the shell strains in equation (8) are substituted into equation (11), and the extreme rib fiber z = -Cf is identified, then the rib stresses are given by:

$$\begin{Bmatrix} \sigma_1 \\ \sigma_2 \\ \sigma_3 \end{Bmatrix} = \frac{1}{A} \begin{bmatrix} 1 & -1/3 & 0 \\ 0 & 2/3 & -2/\sqrt{3} \\ 0 & 2/3 & 2/\sqrt{3} \end{bmatrix} \begin{Bmatrix} N_x \\ N_y \\ N_{xy} \end{Bmatrix} - \frac{C_f}{I} \begin{bmatrix} 1 & -1/3 & 0 \\ 0 & 2/3 & 2/\sqrt{3} \\ 0 & 2/3 & -2/\sqrt{3} \end{bmatrix} \begin{Bmatrix} M_x \\ M_y \\ M_{xy} \end{Bmatrix} \tag{12}$$

Subscripts on the rib stresses are indicated in Figure A.2.

Appendix B

Discussion of the CGA-341 1/8 inch Shell Thickness Requirement

This appendix is added at the request of Ron Fast to discuss the requirement of CGA-341 that the minimum metal thickness of an aluminum outer vacuum shell not be less than 0.125 inches. This note is in order since the skin thickness of the current Isogrid design is 0.110 inches.

I will address the issue only from a structural aspect; it may be that the CGA requirement is governed by handling or road-worthiness considerations and, therefore, not a structural requirement at all.

Although the Isogrid skin is only 0.110 inches thick, because of the rib stiffening members, the construction is actually "thicker". Specifically, two effective thicknesses can be considered. First, a "membrane stress thickness" (t_{eff}) can be considered. This thickness is the effective Isogrid shell thickness used to compute membrane stresses in the absence of bending effects, and is given by:

$$t_{eff} = t\ (1 + \alpha + \mu)$$

where t is the Isogrid skin thickness and α and μ are Isogrid dimensionless parameters (cf. Appendix A). For the current design, the effective thickness is:

$$t_{eff} = 0.202 \text{ inches.}$$

Second, a "bending stress thickness" (t') can be considered. This thickness is determined from Isogrid theory based on the Isogrid shell area moment of inertia (cf. Appendix A), and is given by:

$$I = t^3\ \beta^2/12(1+\alpha+\mu) = (t')^3/12$$

or,

$$t' = t\ [\beta^2/(1+\alpha+\mu)]^{1/3}$$

where β is an Isogrid dimensionless parameter. For the current design, the bending thickness is:

$$t' = 1.217 \text{ inches.}$$

These considerations demonstrate that membrane and bending structurally effective thicknesses for the current Isogid design exceed the CGA minimum shell thickness requirement.

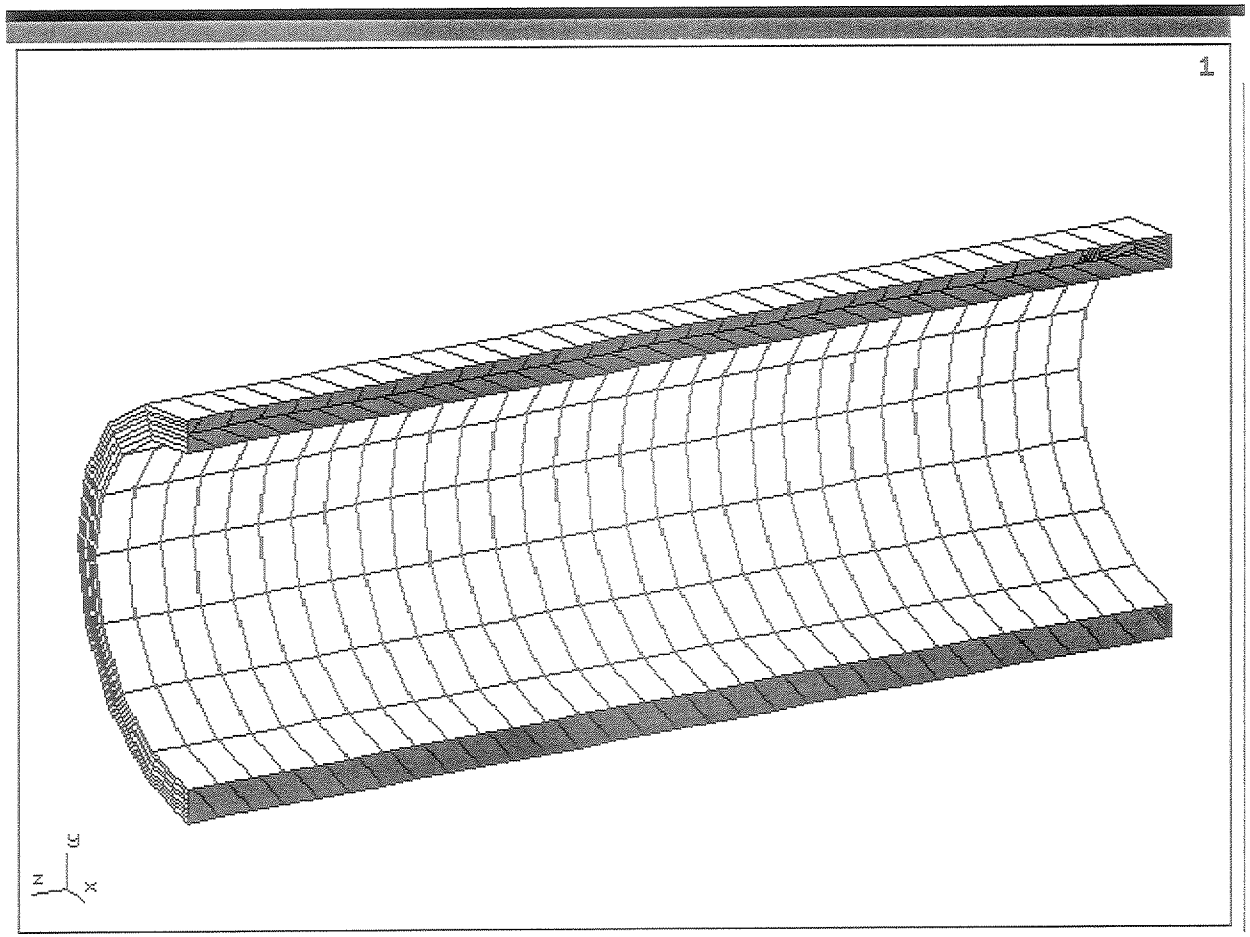

Figure 2.1 Finite Element Model of the SDC Vacuum Shell

1	9	17	25	33	41	49	57	65	73	81	89	97	105	113	121	129	137	145	153	161	169	177	185	193	201	209	217	225	233
2	10	18	26	34	42	50	58	66	74	82	90	98	106	114	122	130	138	146	154	162	170	178	186	194	202	210	218	226	234
3	11	19	27	35	43	51	59	67	75	83	91	99	107	115	123	131	139	147	155	163	171	179	187	195	203	211	219	227	235
4	12	20	28	36	44	52	60	68	76	84	92	100	108	116	124	132	140	148	156	164	172	180	188	196	204	212	220	228	236
5	13	21	29	37	45	53	61	69	77	85	93	101	109	117	125	133	141	149	157	165	173	181	189	197	205	213	221	229	237
6	14	22	30	38	46	54	62	70	78	86	94	102	110	118	126	134	142	150	158	166	174	182	190	198	206	214	222	230	238
7	15	23	31	39	47	55	63	71	79	87	95	103	111	119	127	135	143	151	159	167	175	183	191	199	207	215	223	231	239
8	16	24	32	40	48	56	64	72	80	88	96	104	112	120	128	136	144	152	160	168	176	184	192	200	208	216	224	232	240

Y X
Z

Figure 2.2 Outer (Isogrid) Shell Element Numbers

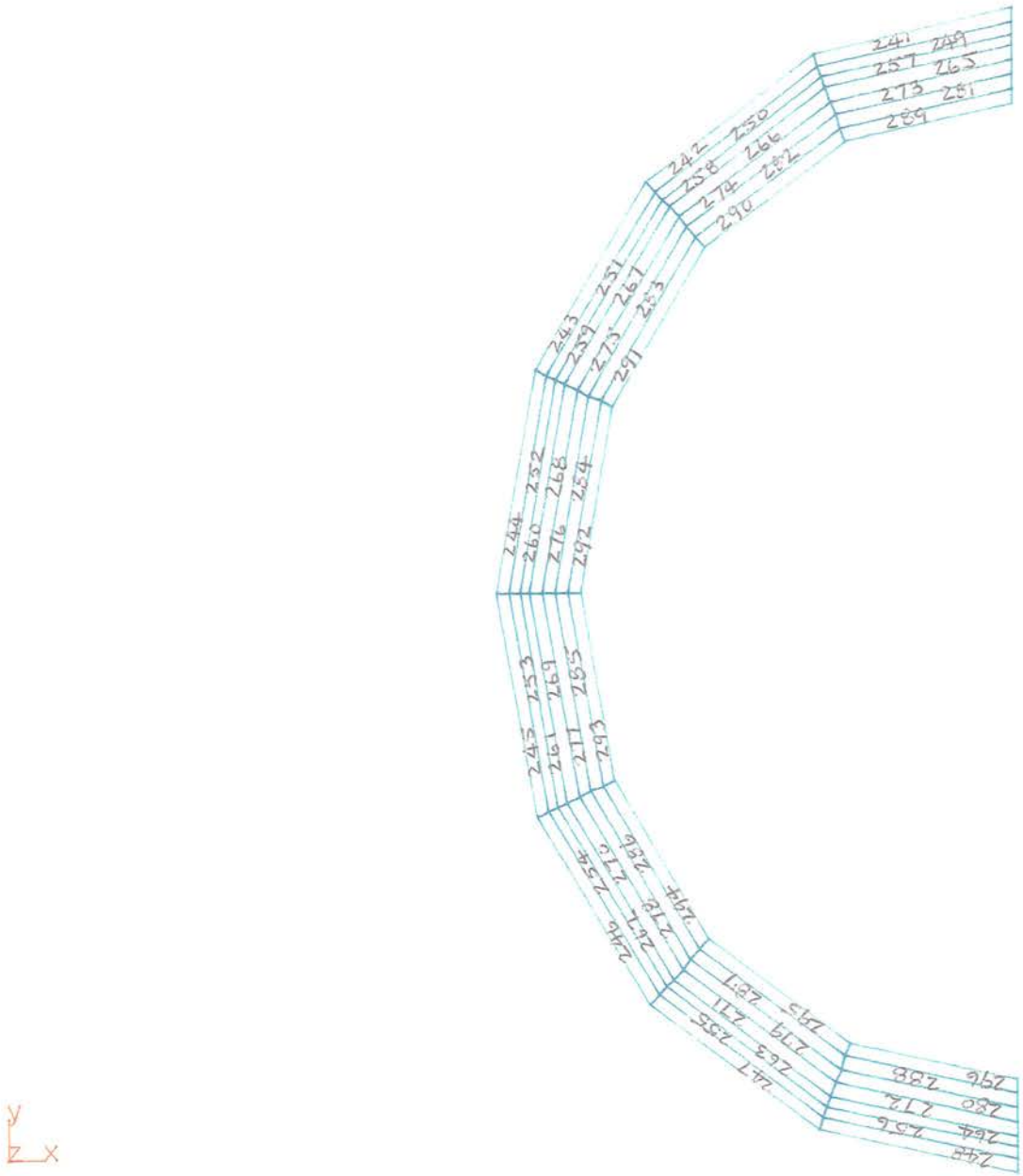

Figure 2.3 "Second" Bulk Head Element Numbers

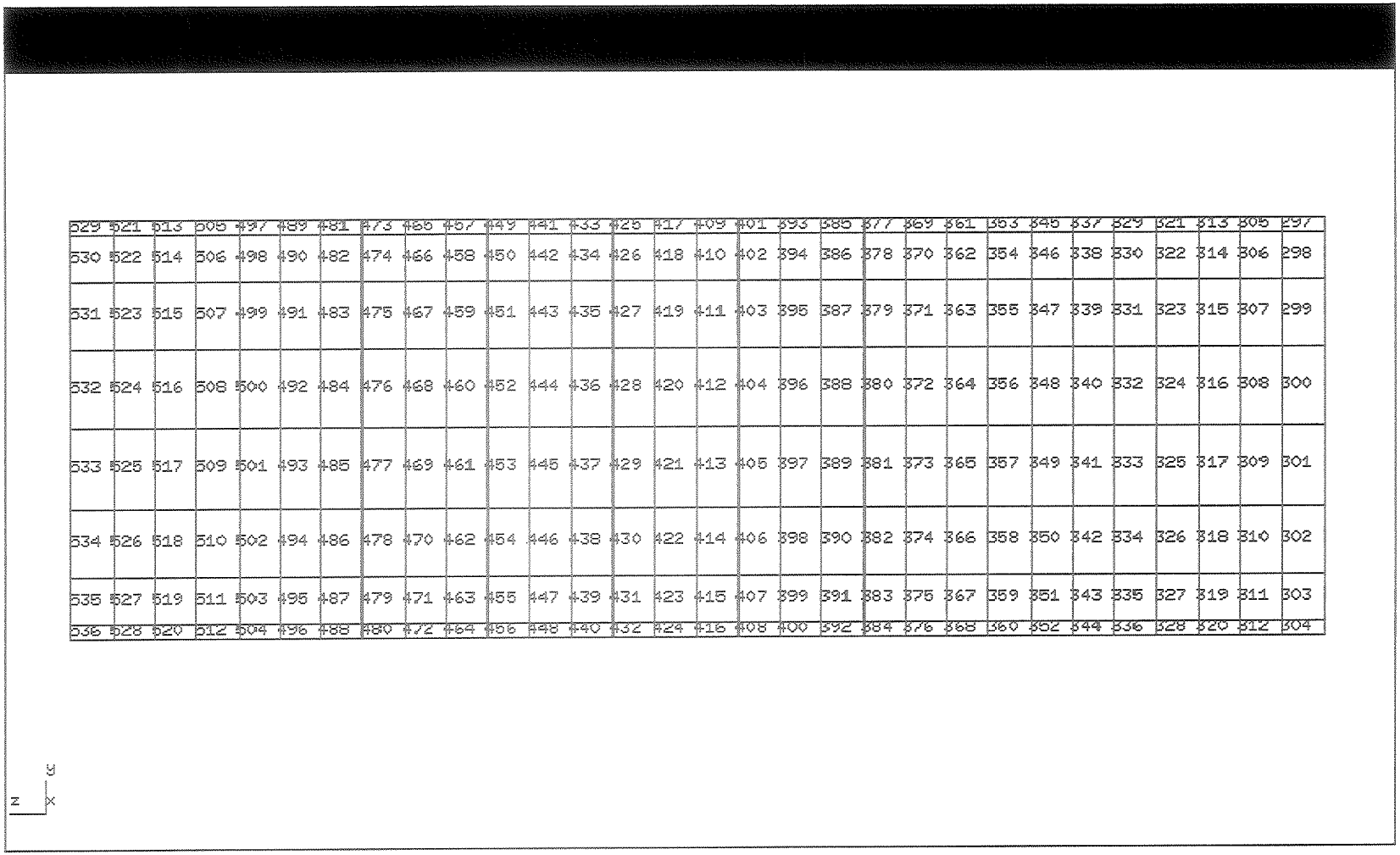

Figure 2.4 Inner Shell Element Numbers

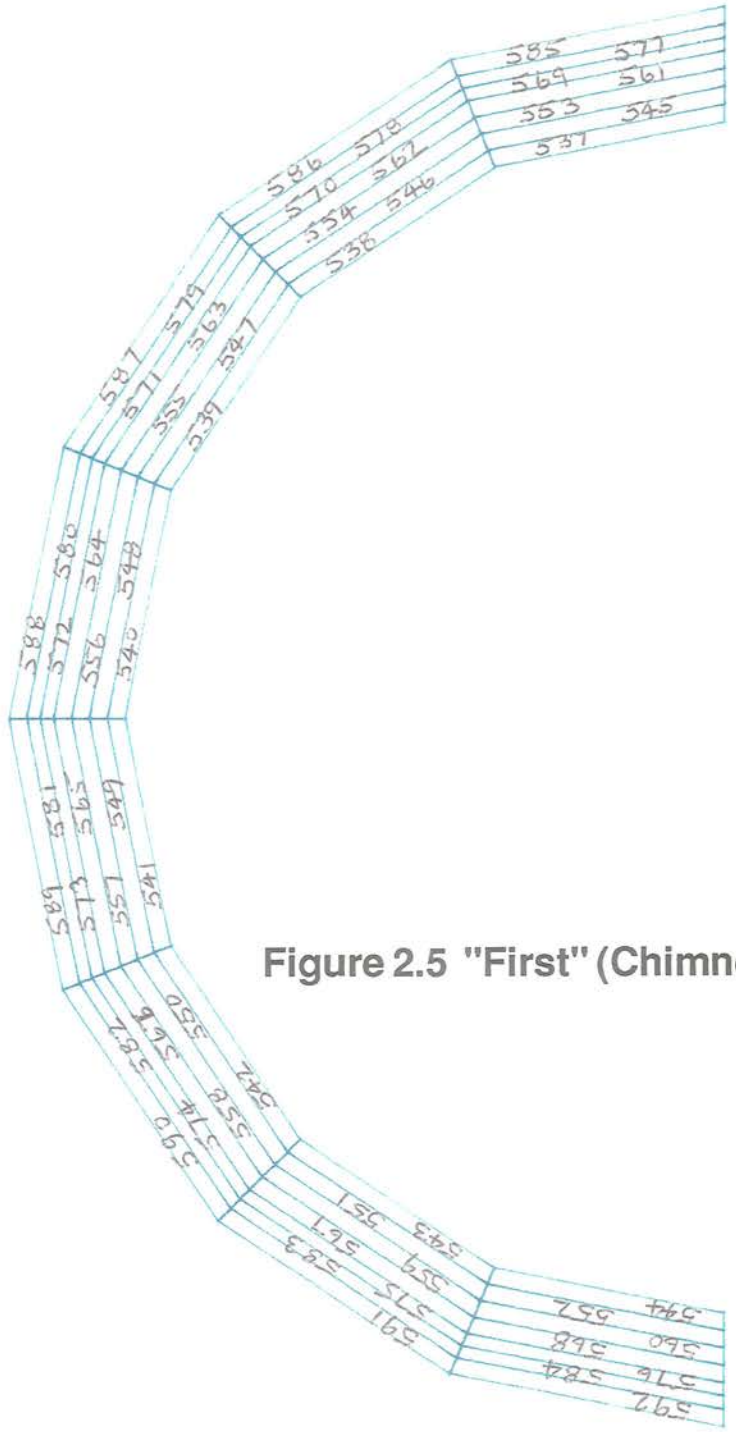

Figure 2.5 "First" (Chimney-end) Bulk Head Element Numbers

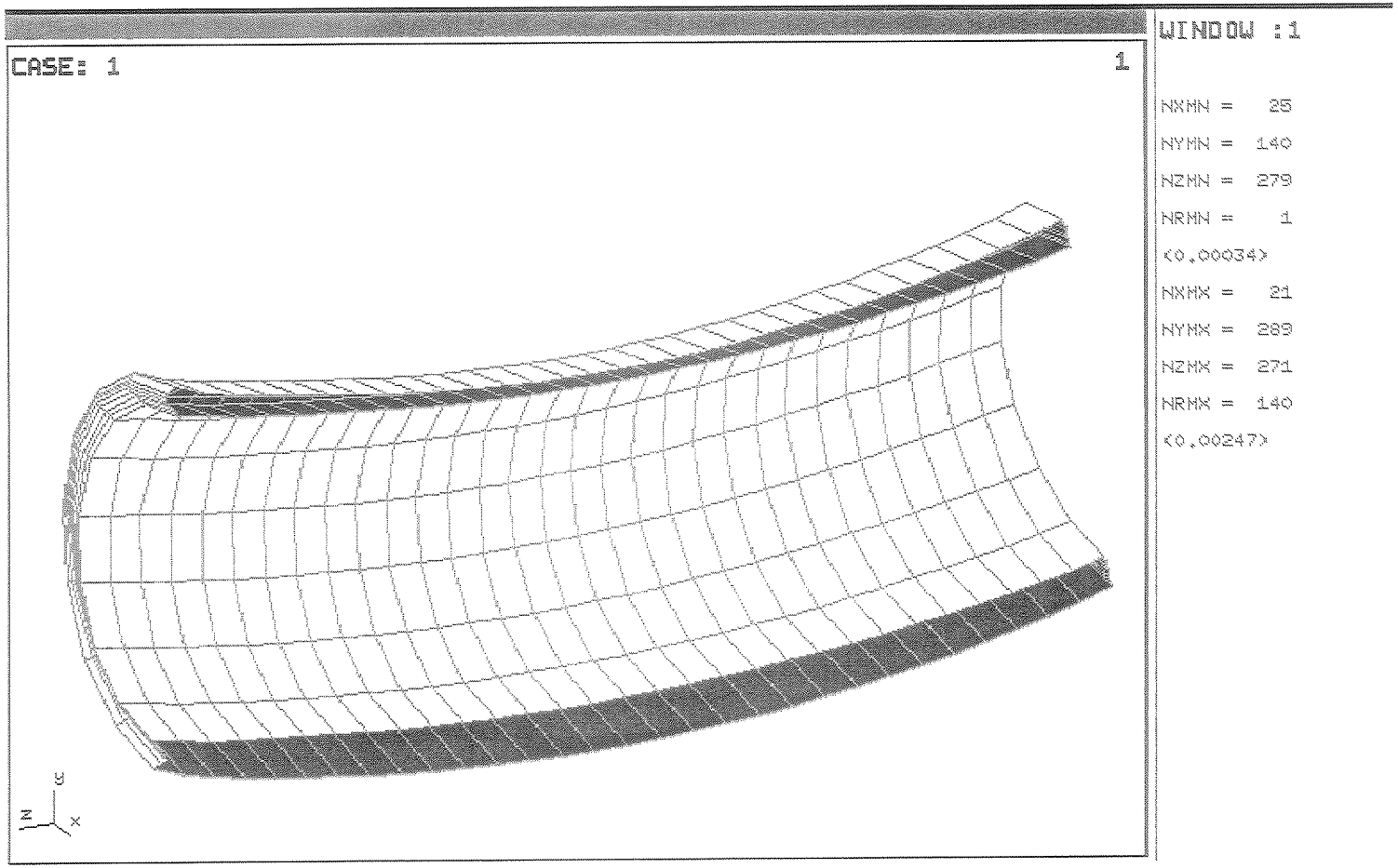

Figure 4.1 Deformed Structure (Weight Load Only)

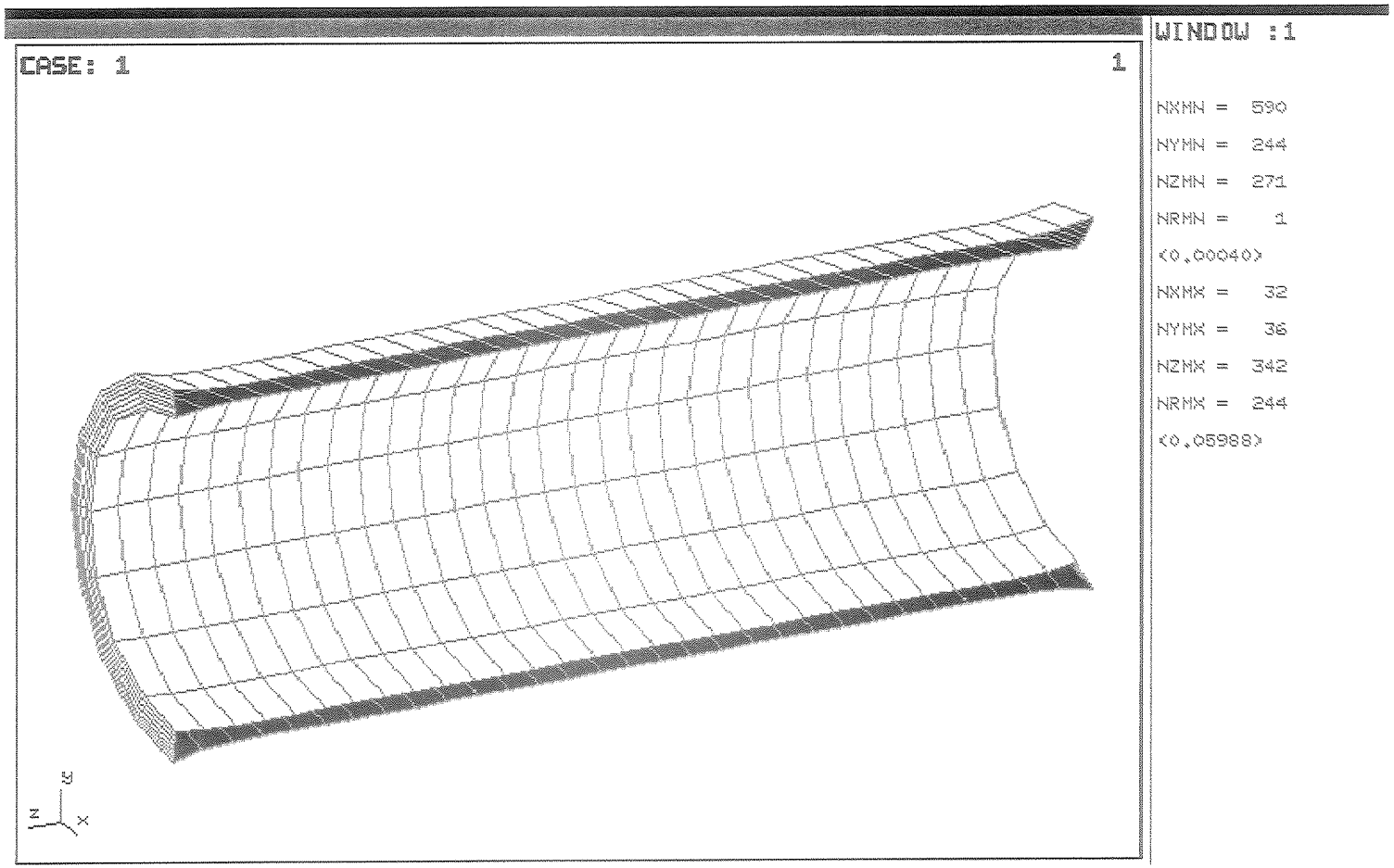

Figure 4.2 Deformed Structure (All Loads)

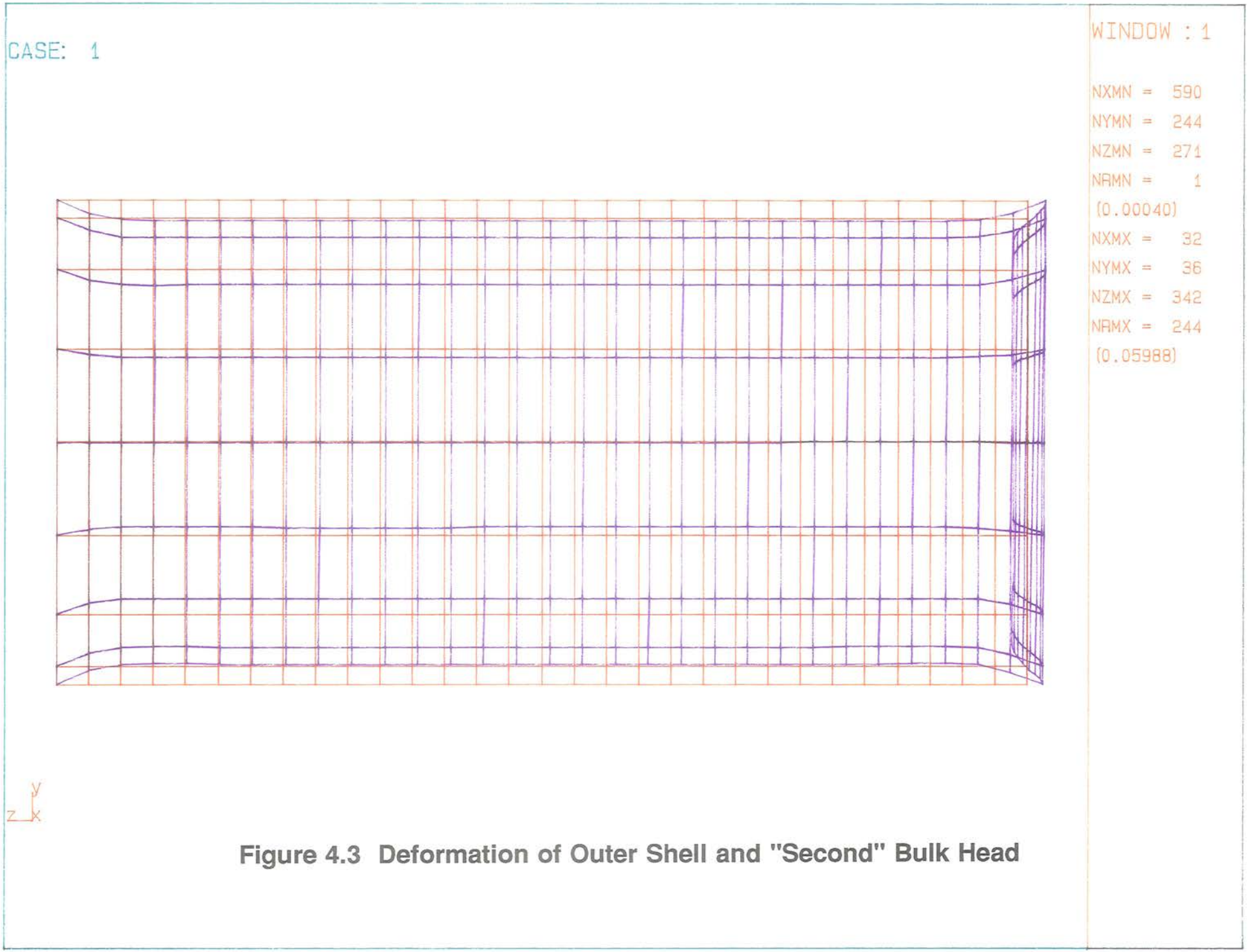

Figure 4.3 Deformation of Outer Shell and "Second" Bulk Head

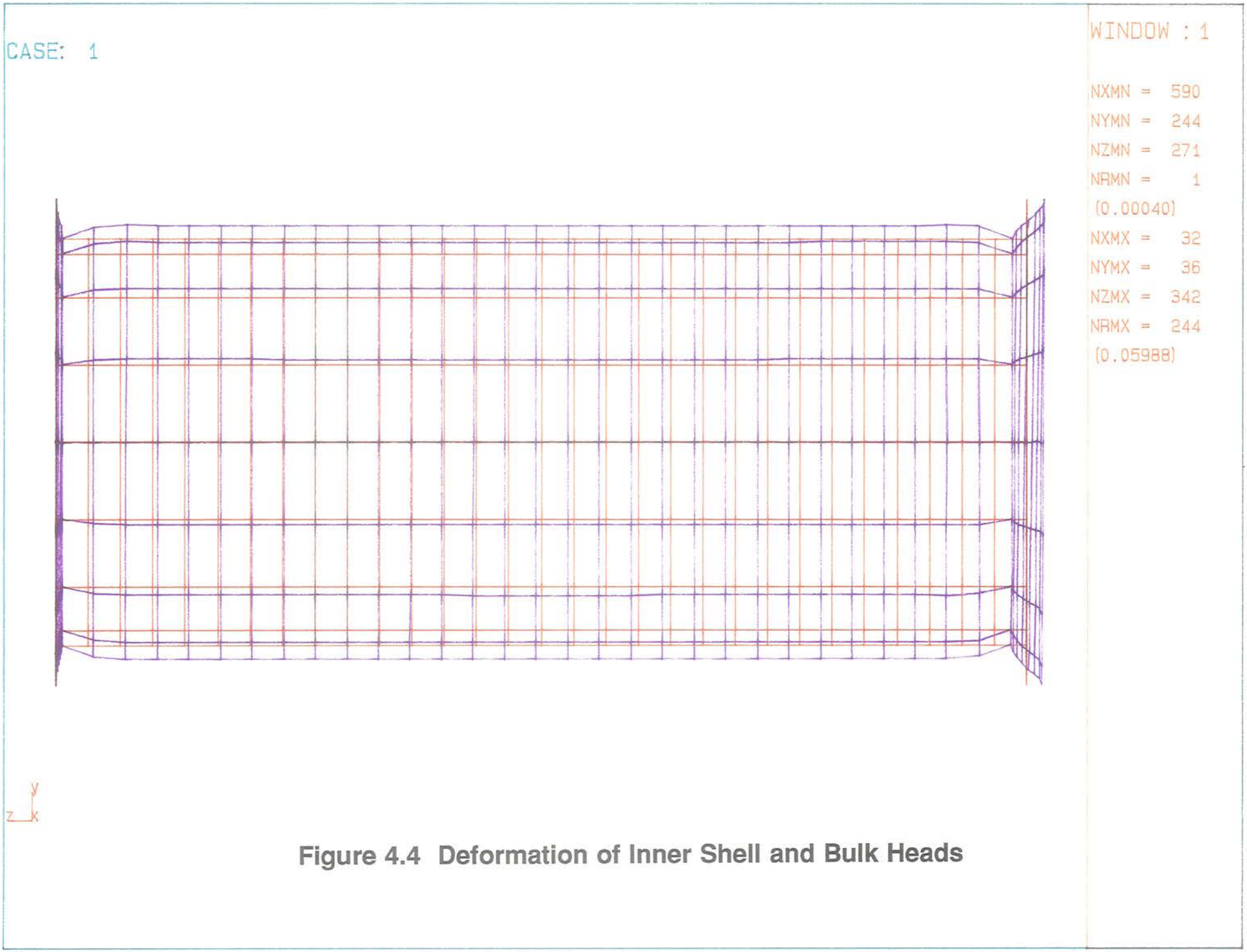

Figure 4.4 Deformation of Inner Shell and Bulk Heads

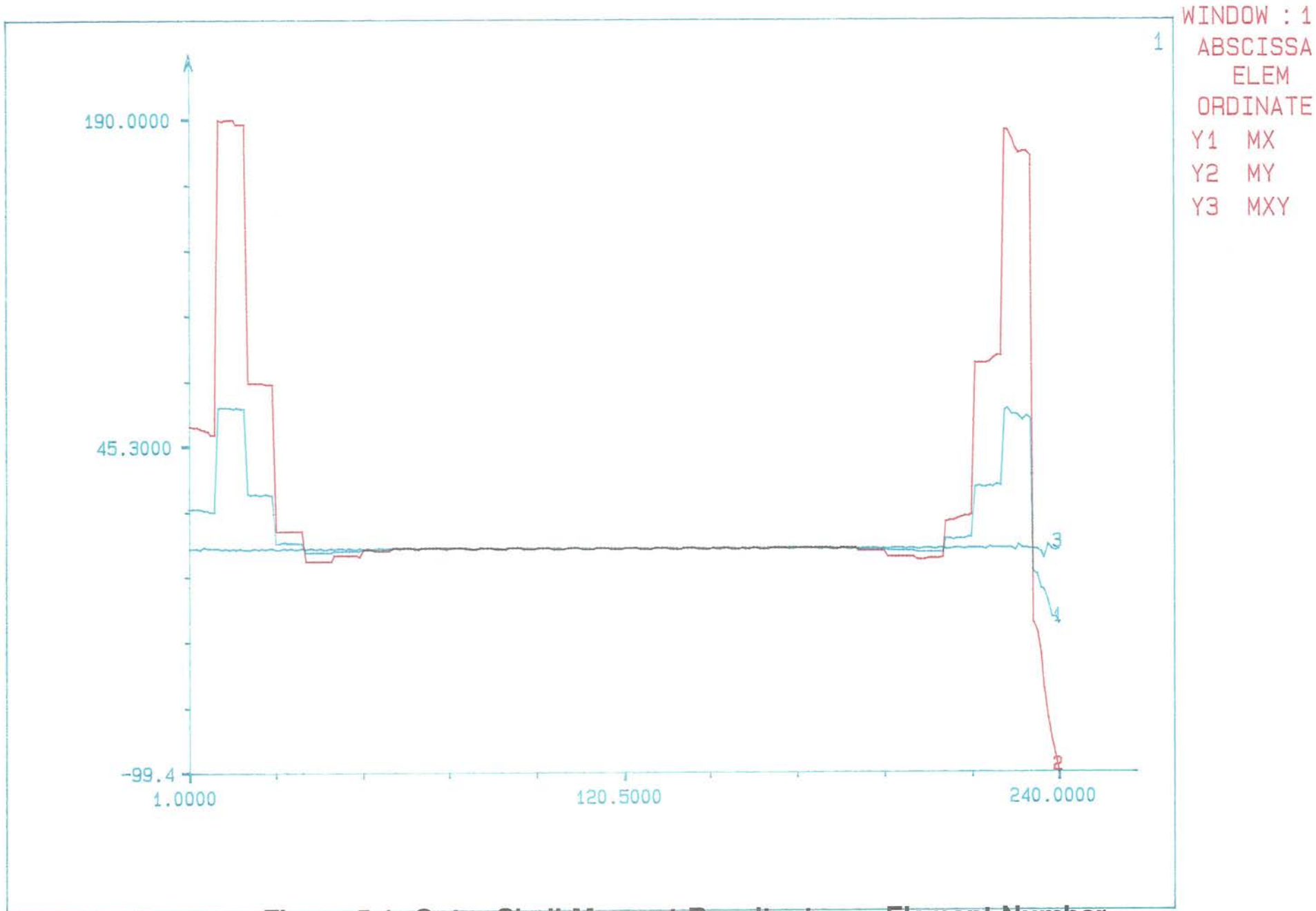

Figure 5.1 Outer Shell Moment Resultants vs. Element Number

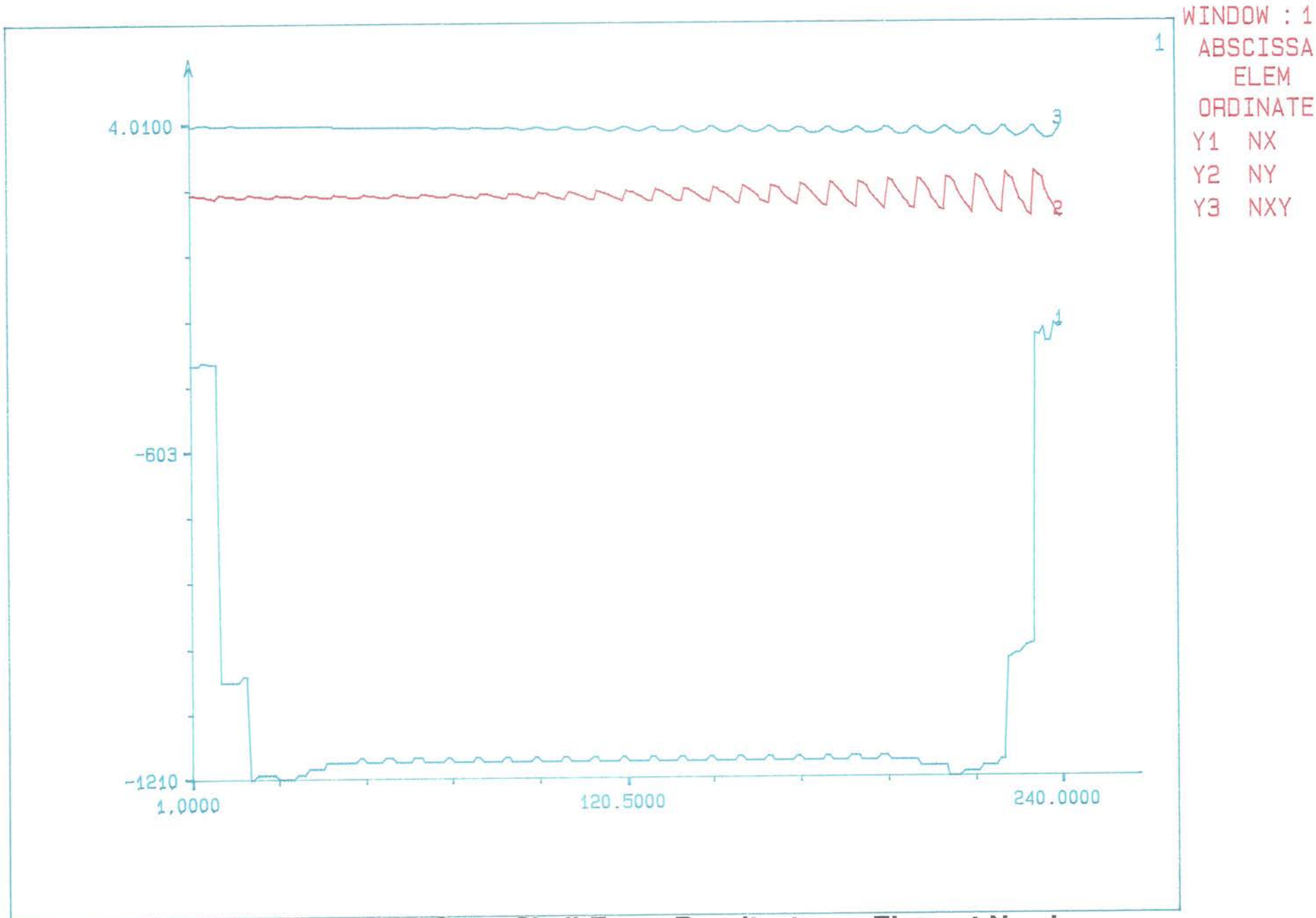

Figure 5.2 Outer Shell Force Resultants vs. Element Number

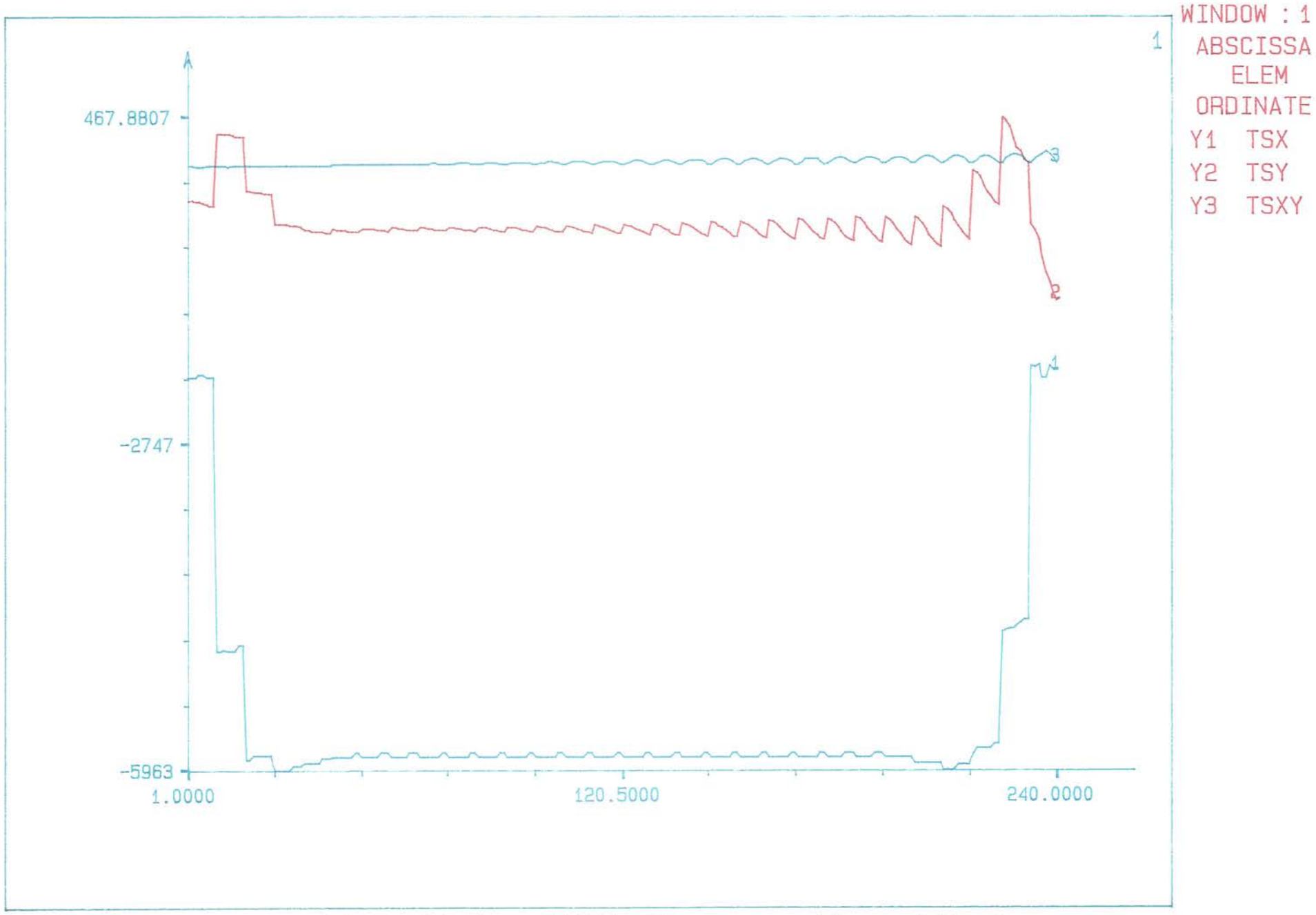

Figure 5.3 Isogrid Skin Stresses vs. Element Number

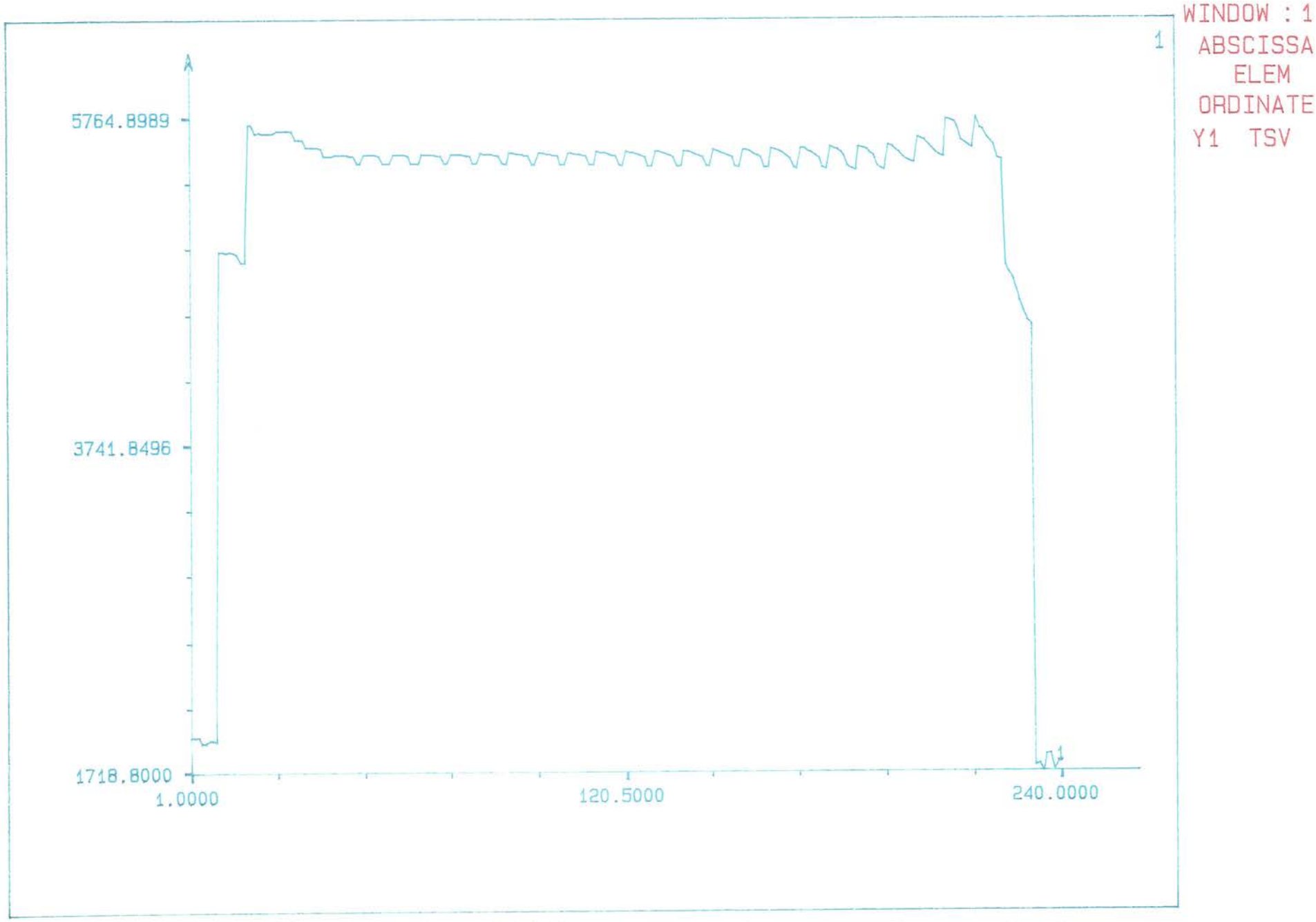

Figure 5.4 Isogrid Skin von Mises Stress vs. Element Number

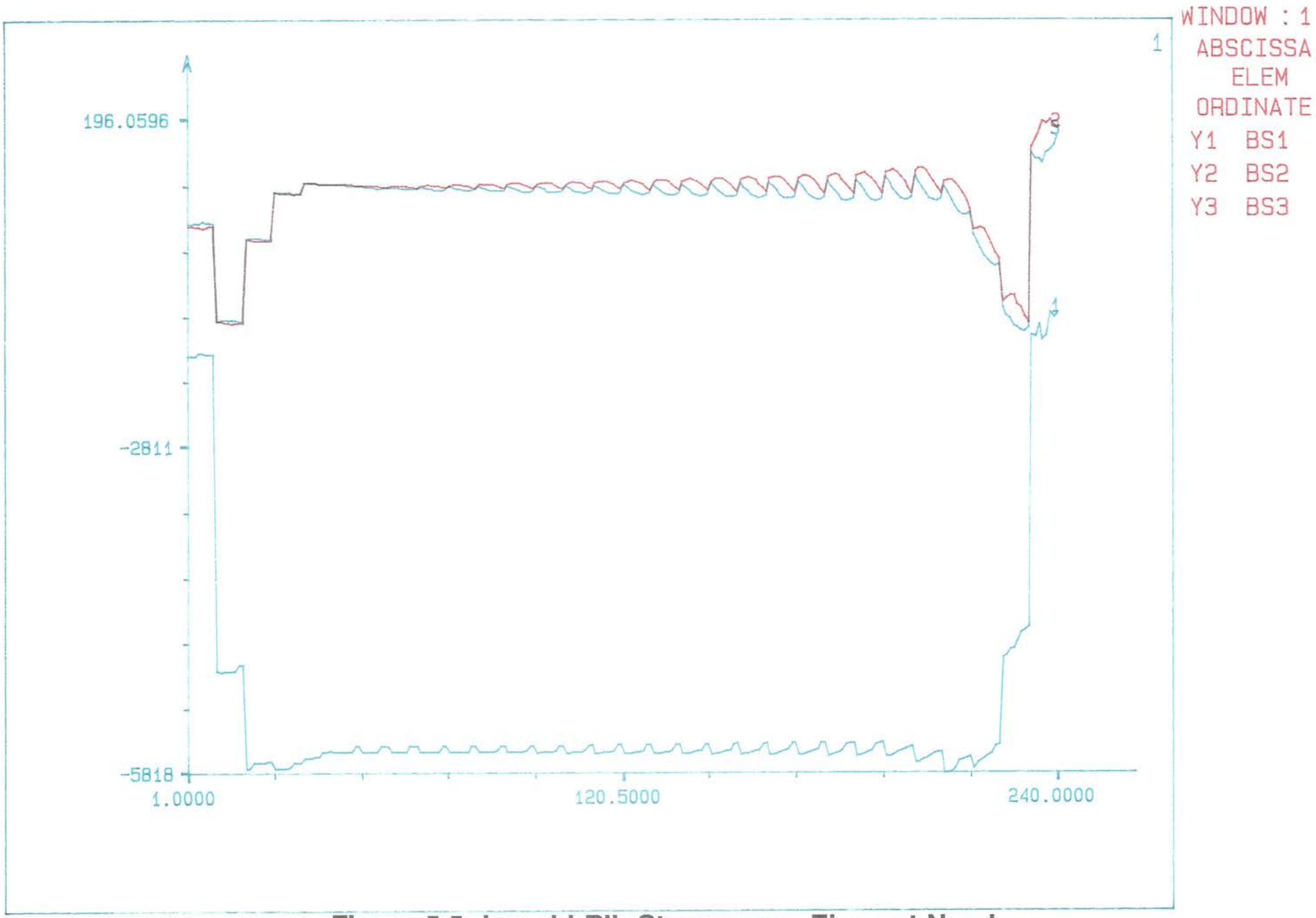

Figure 5.5 Isogrid Rib Stresses vs. Element Number

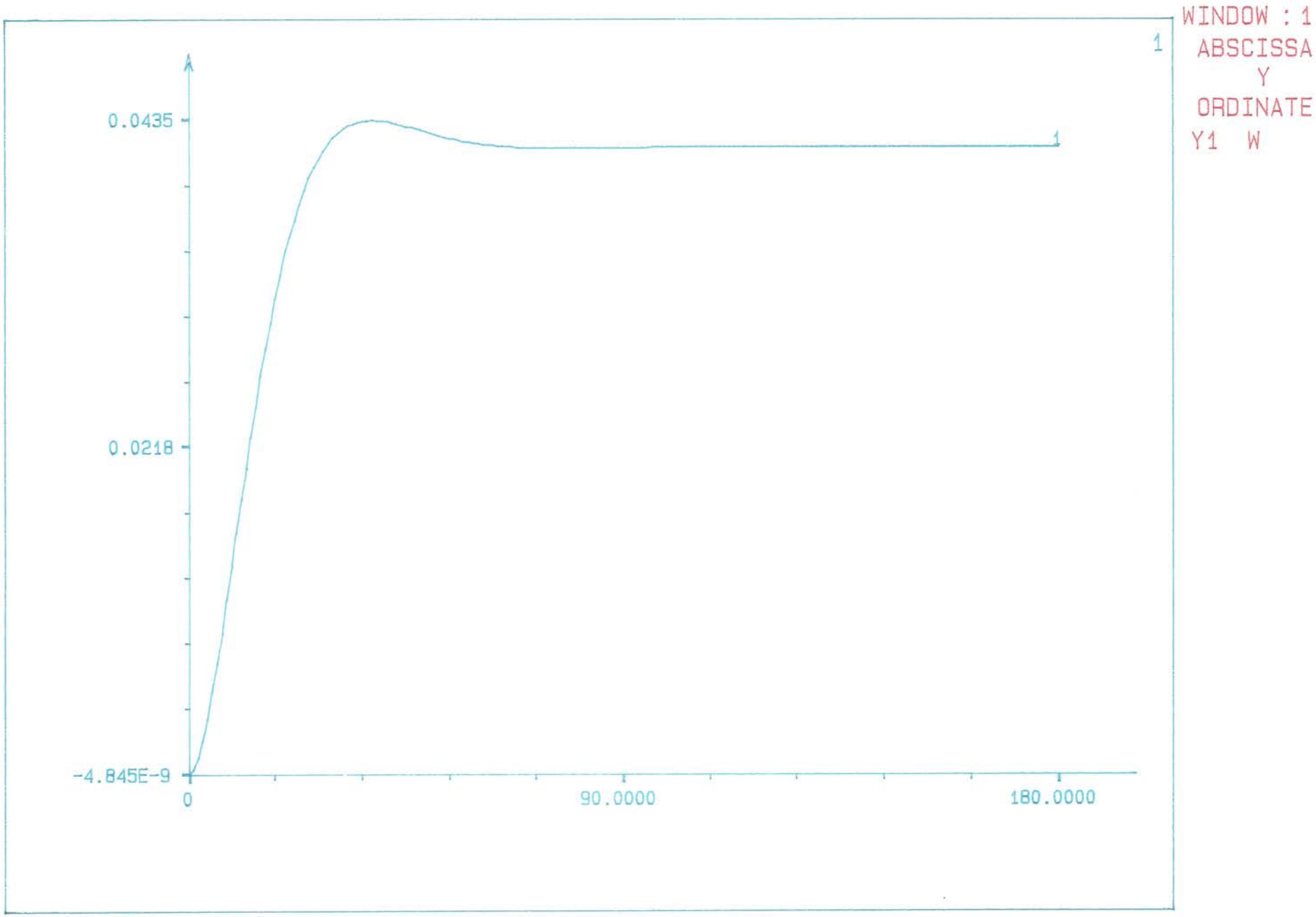

Figure 5.6 Simple Model Radial Displacement vs. Axial Position

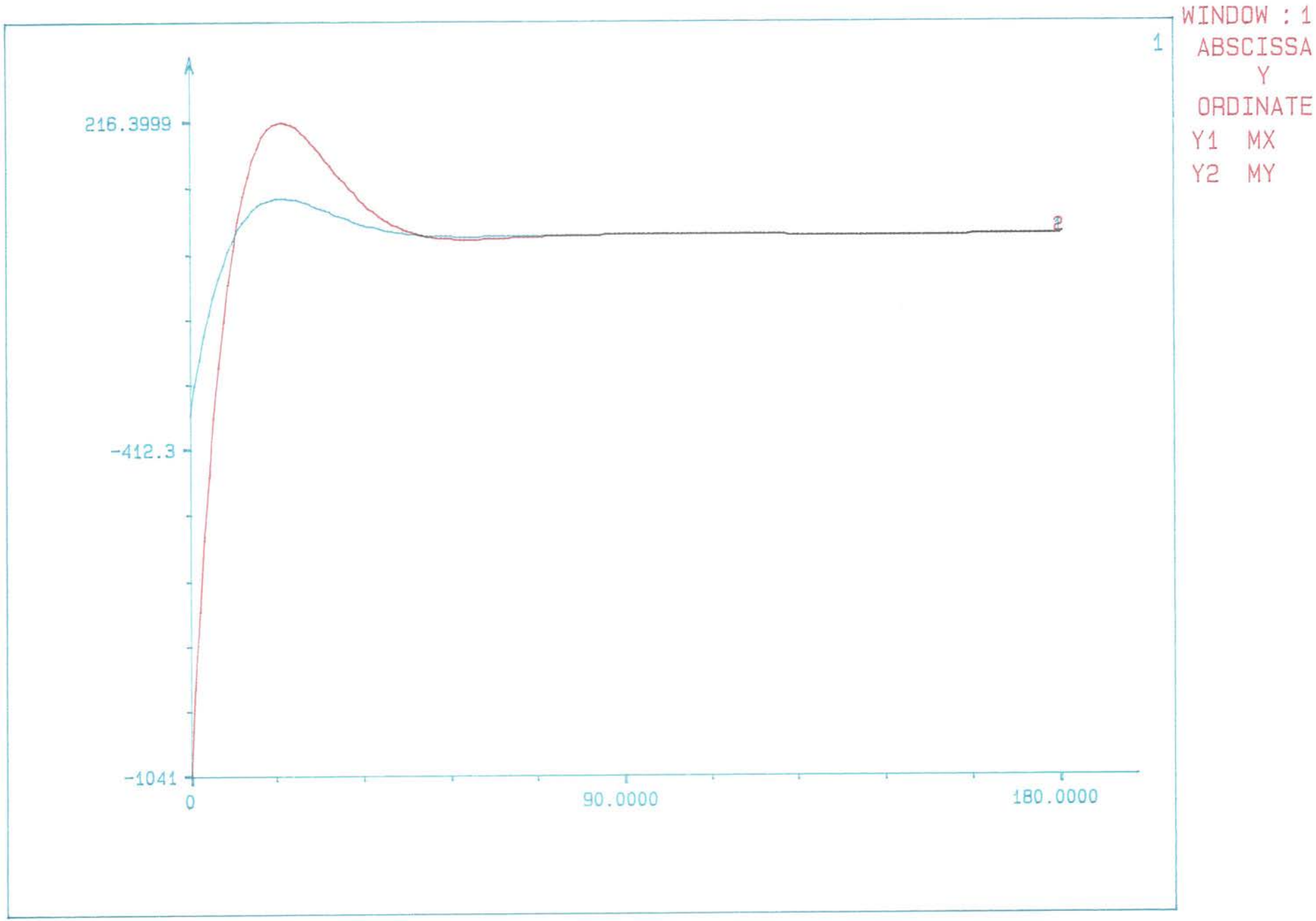

Figure 5.7 Simple Model Moment Resultants vs. Axial Position

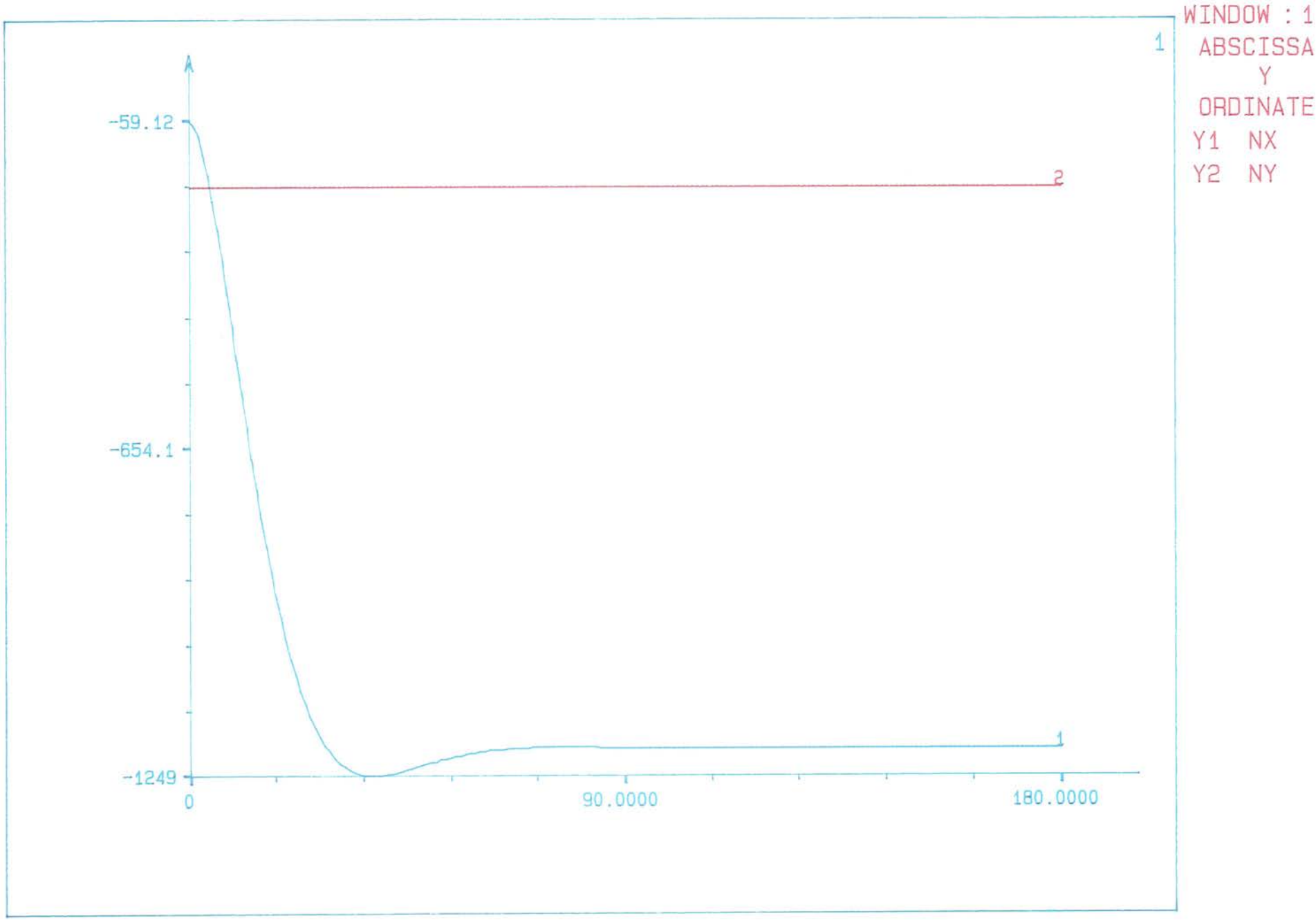

Figure 5.8 Simple Model Force Resultants vs. Axial Position

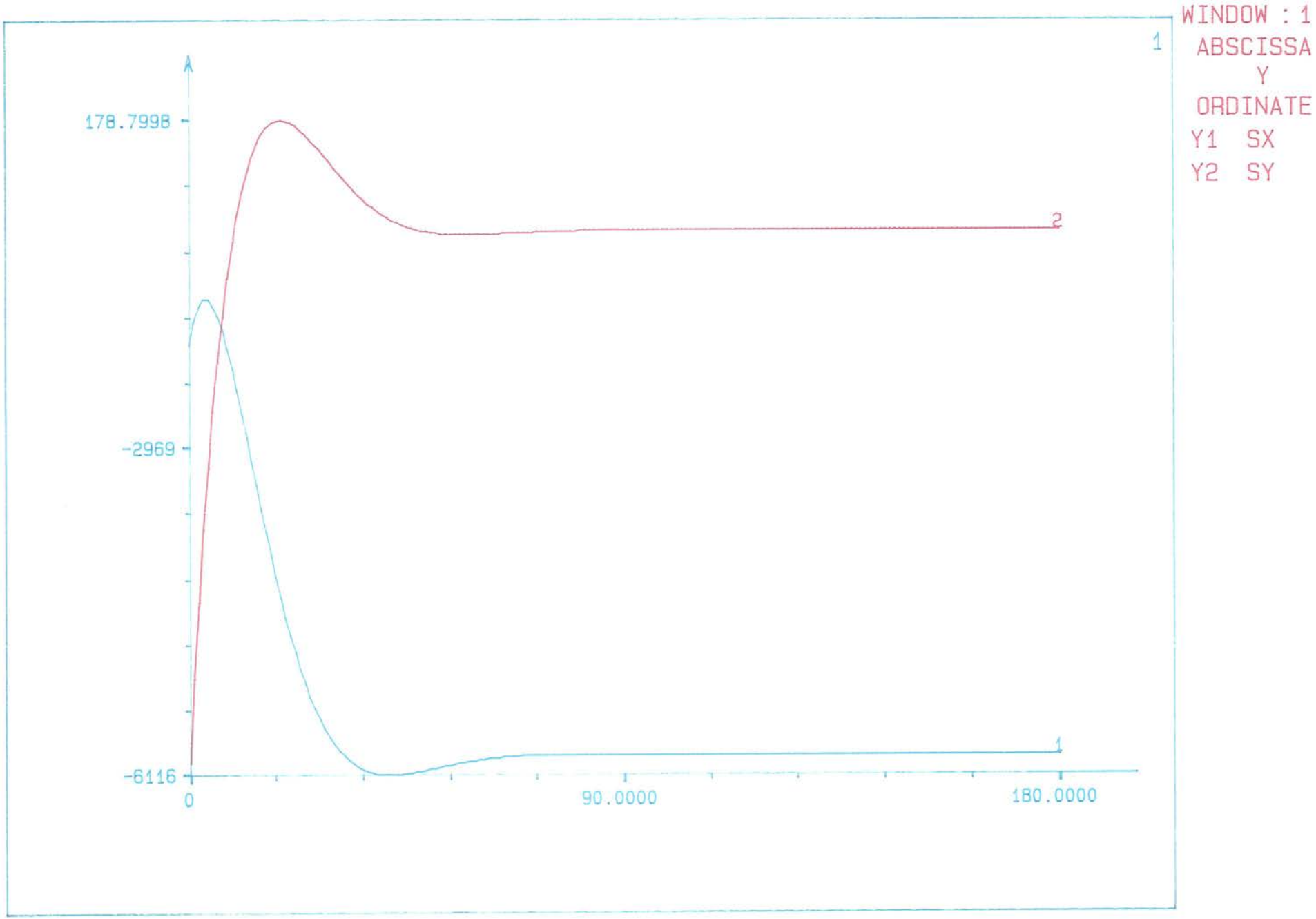

Figure 5.9 Simple Model Isogrid Skin Stresses vs. Axial Position

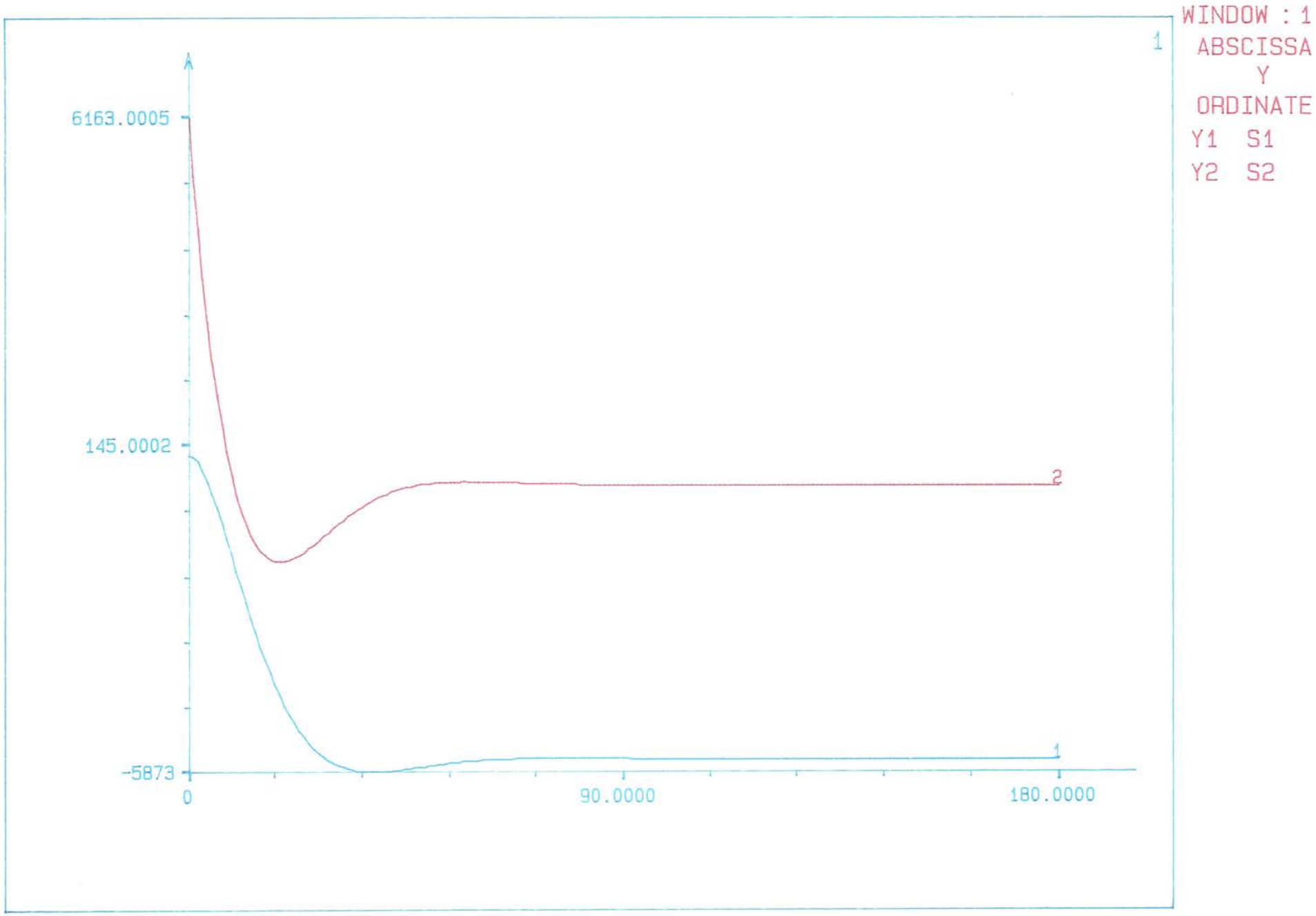

Figure 5.10 Simple Model Isogrid Rib Stresses vs. Axial Position

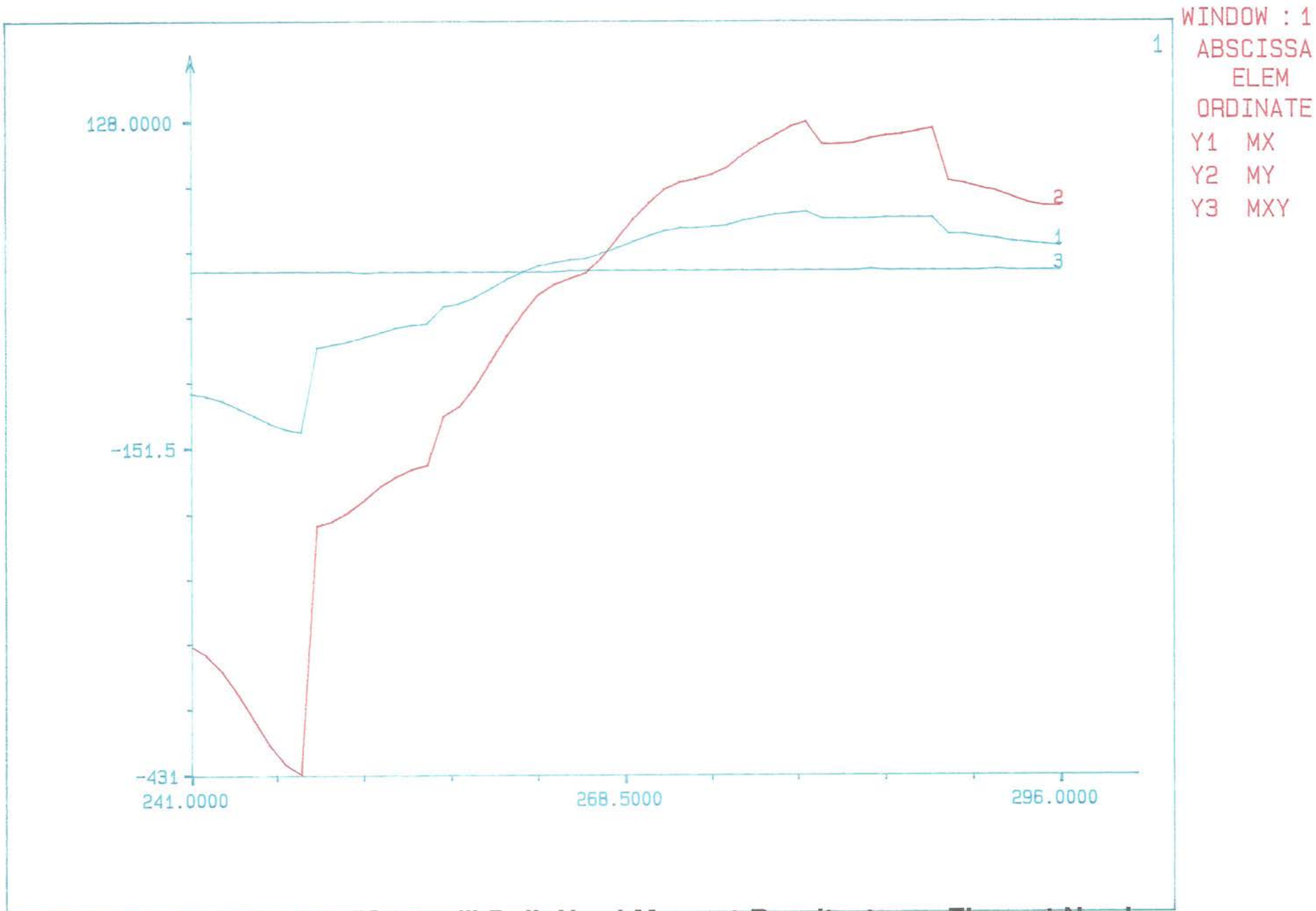

Figure 6.1 "Second" Bulk Head Moment Resultants vs. Element Number

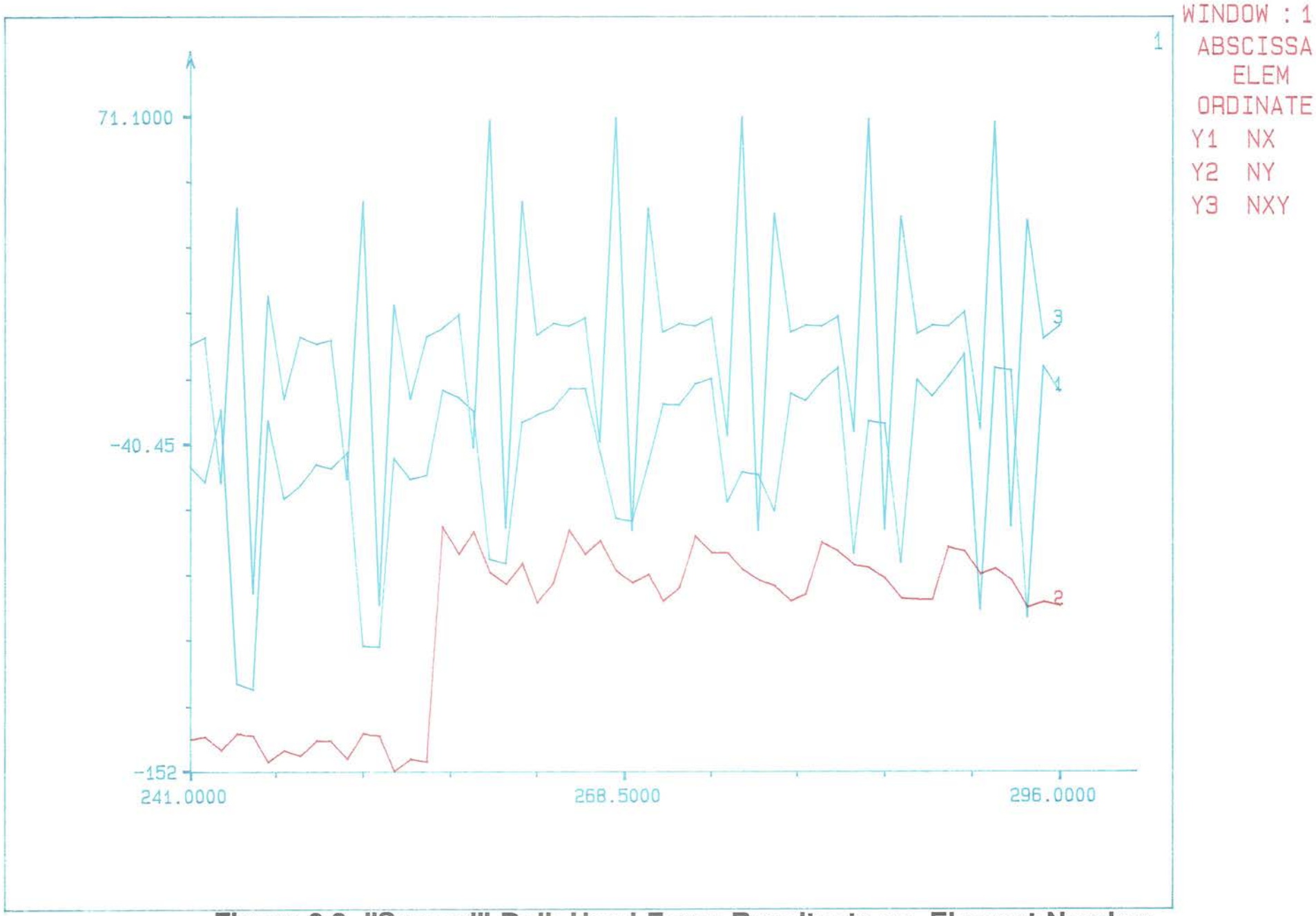

Figure 6.2 "Second" Bulk Head Force Resultants vs. Element Number

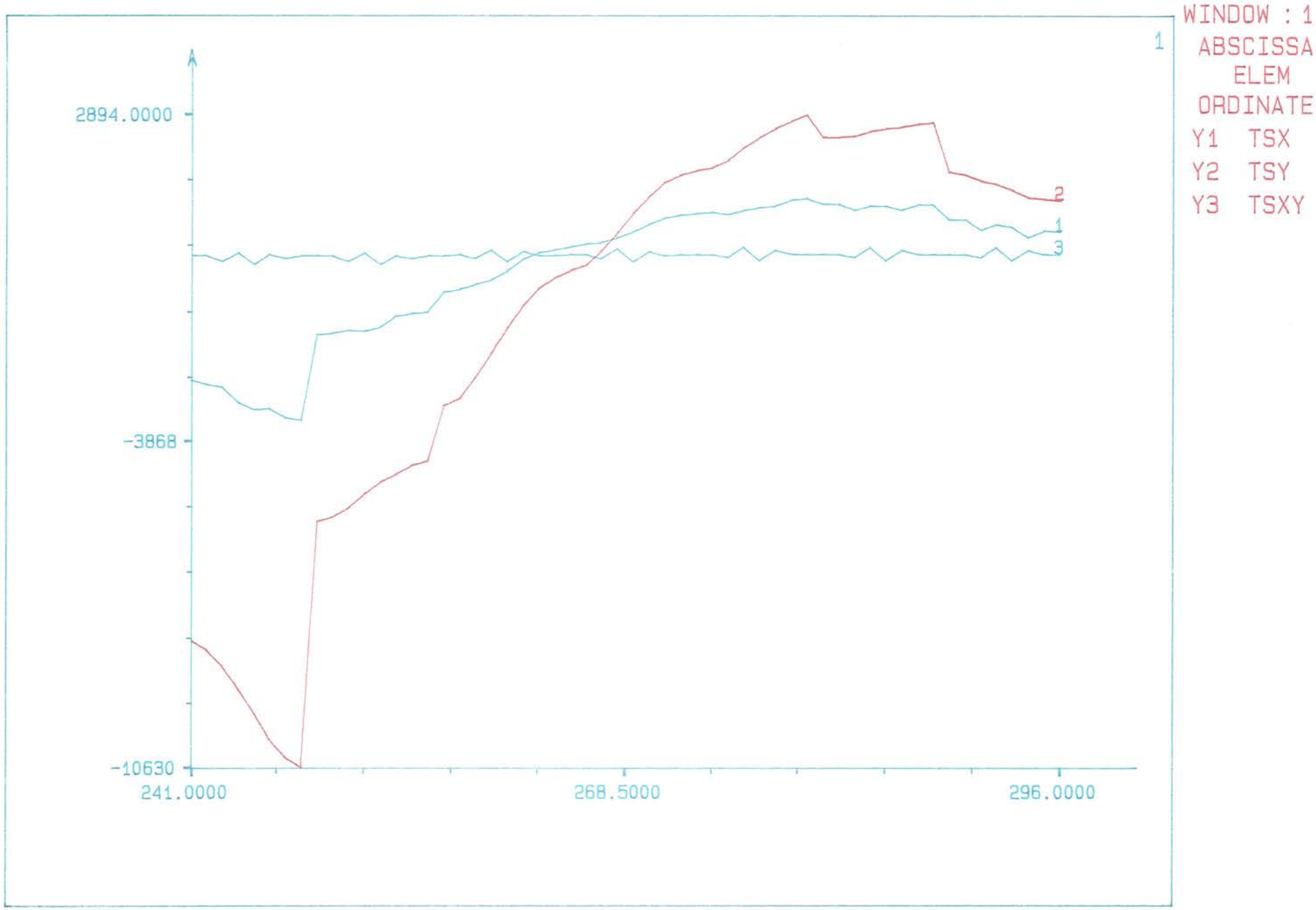

Figure 6.3 "Second" Bulk Head Inner Surface Stresses vs. Element Number

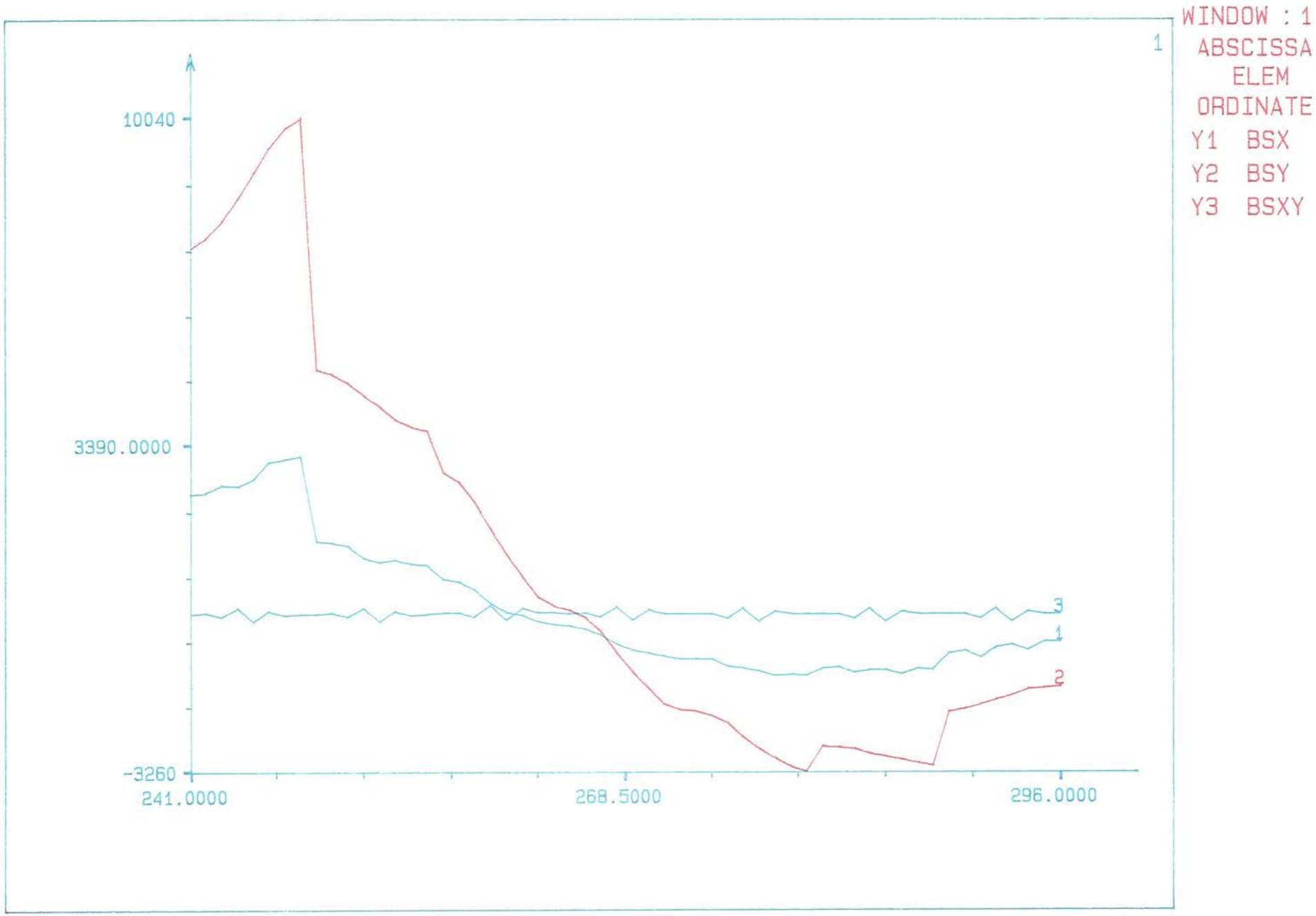

Figure 6.4 "Second" Bulk Head Outer Surface Stress vs. Element Number

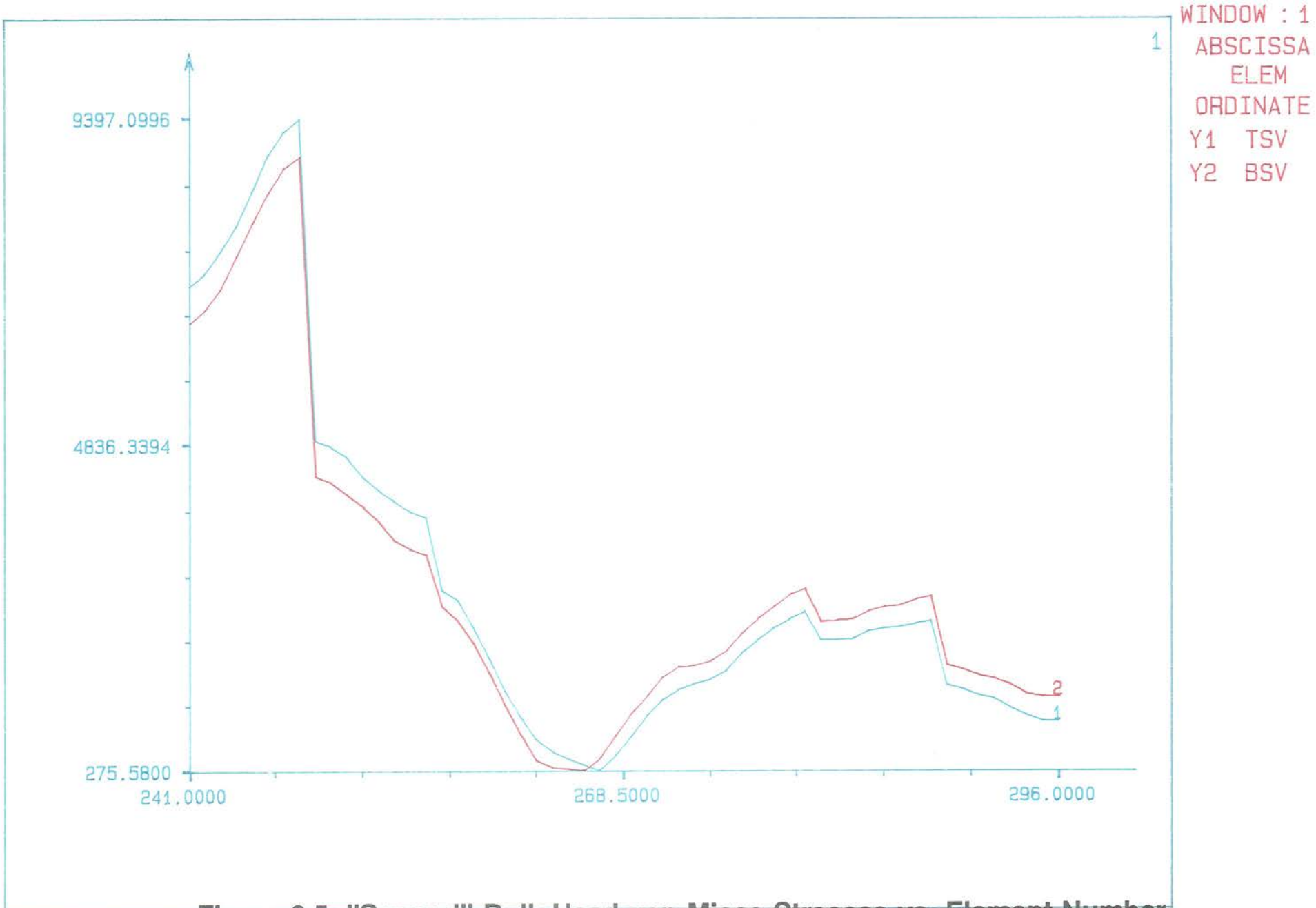

Figure 6.5 "Second" Bulk Head von Mises Stresses vs. Element Number

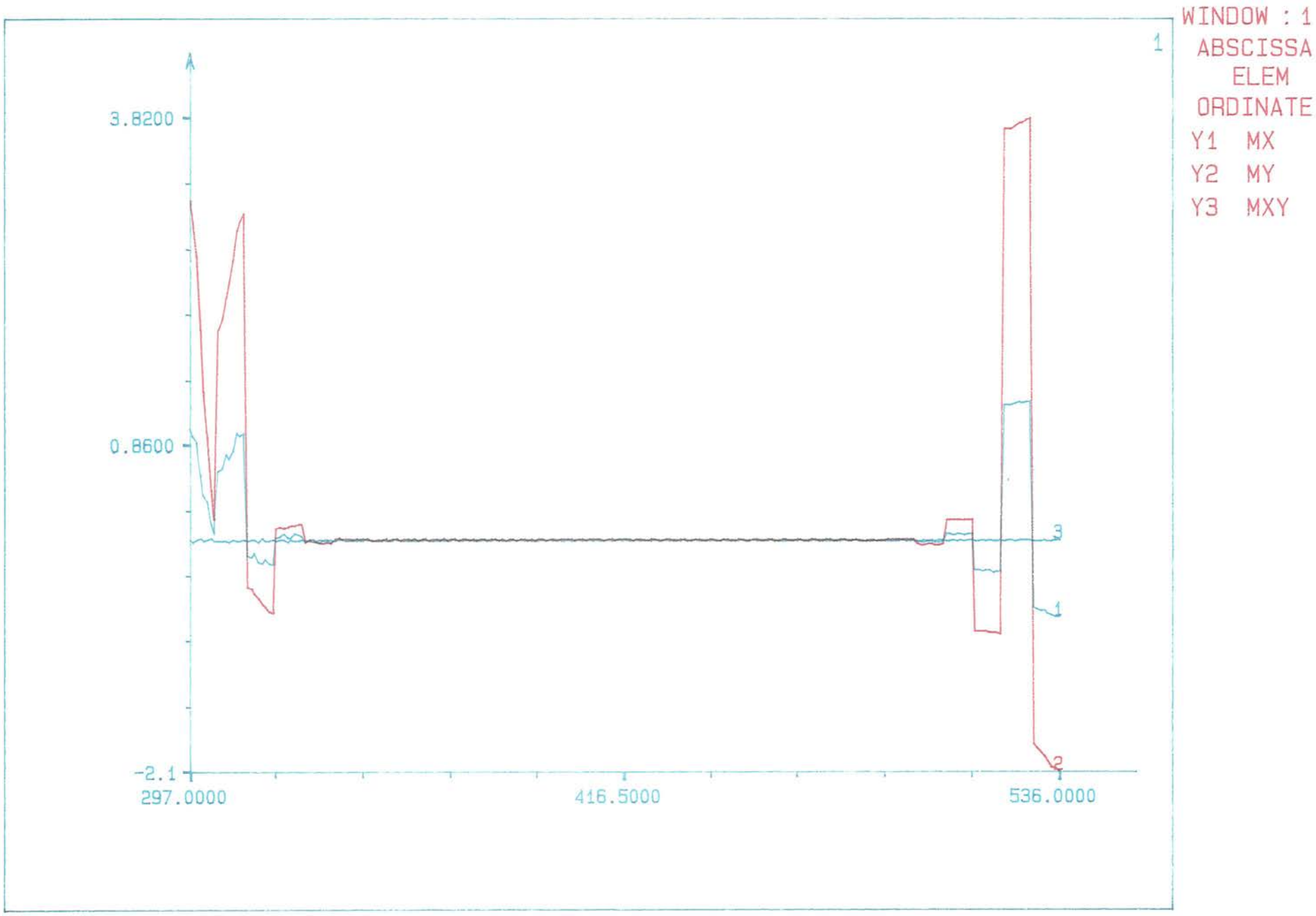

Figure 7.1 Inner Shell Moment Resultants vs. Element Number

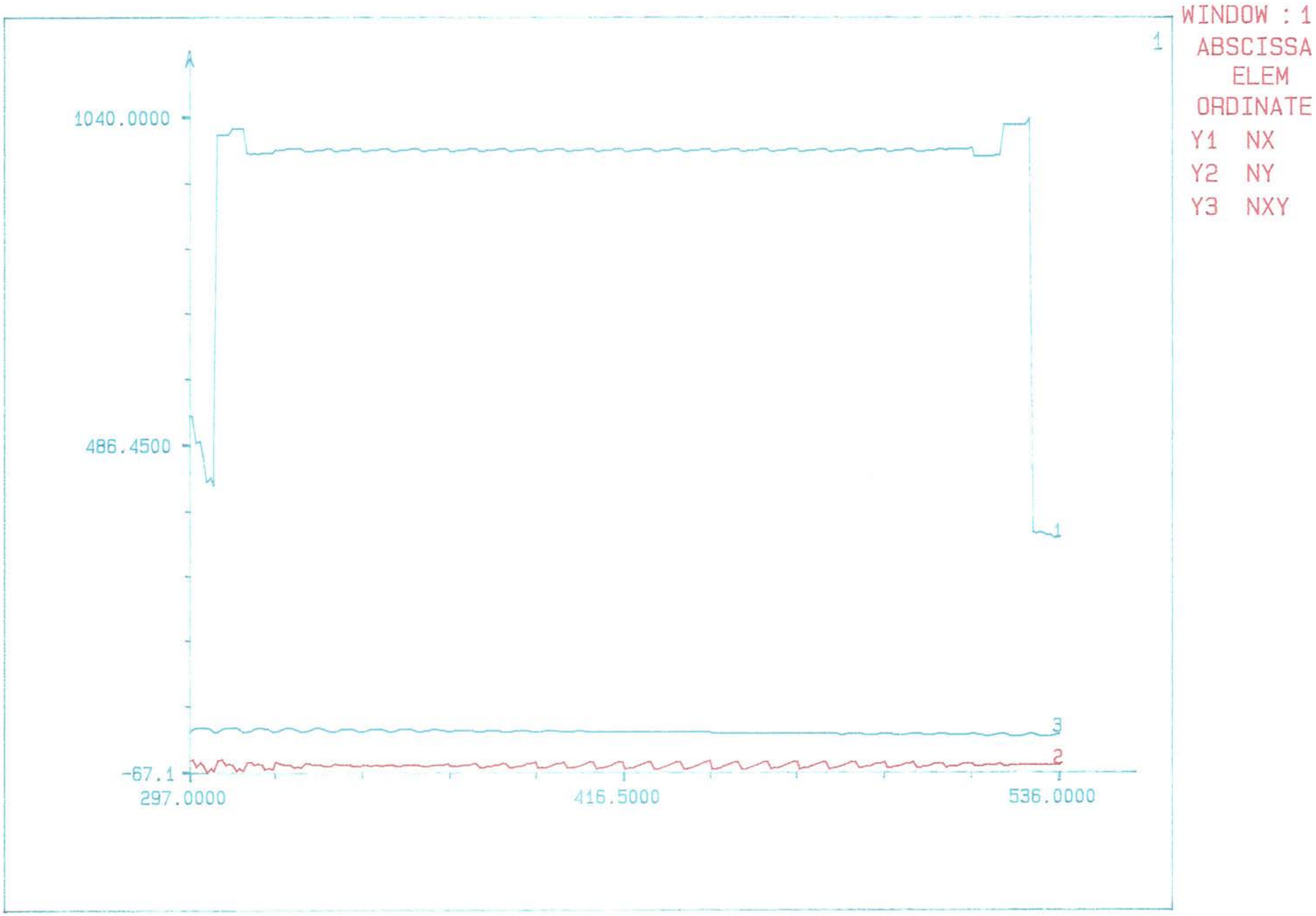

Figure 7.2 Inner Shell Force Resultants vs. Element Number

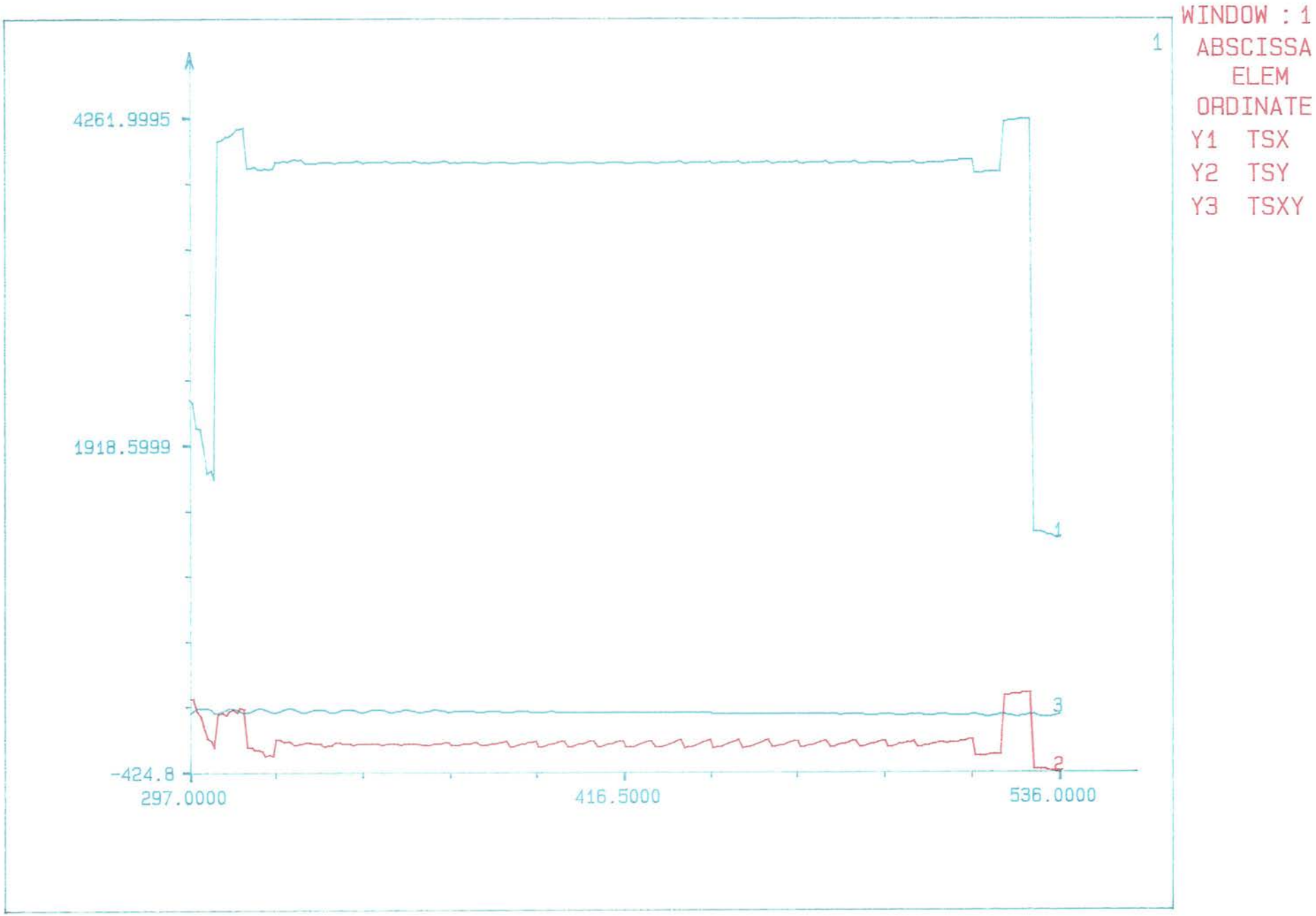

Figure 7.3 Inner Shell Stresses (Vacuum Side) vs. Element Number

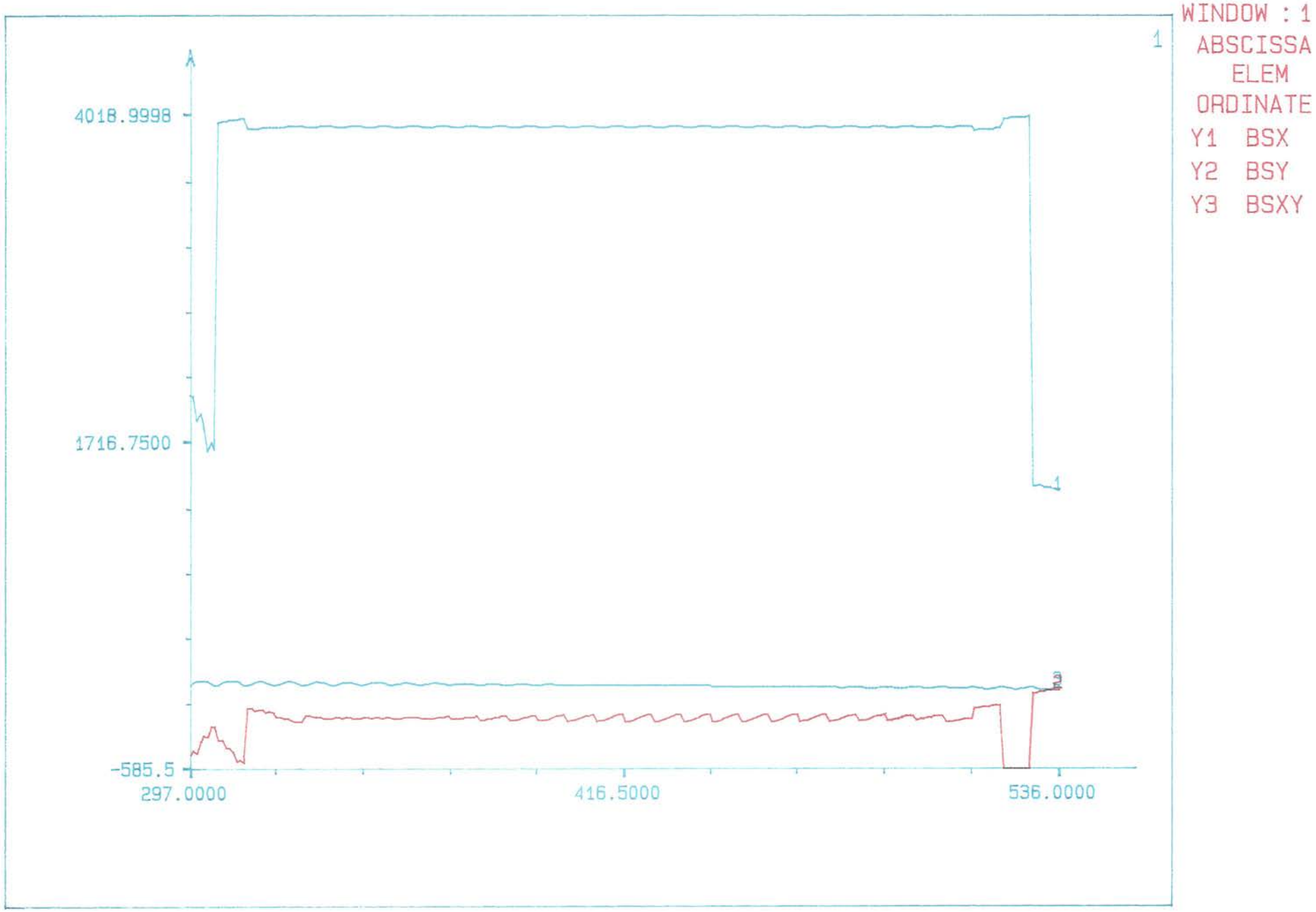

Figure 7.4 Inner Shell Stresses (Pressure Side) vs. Element Number

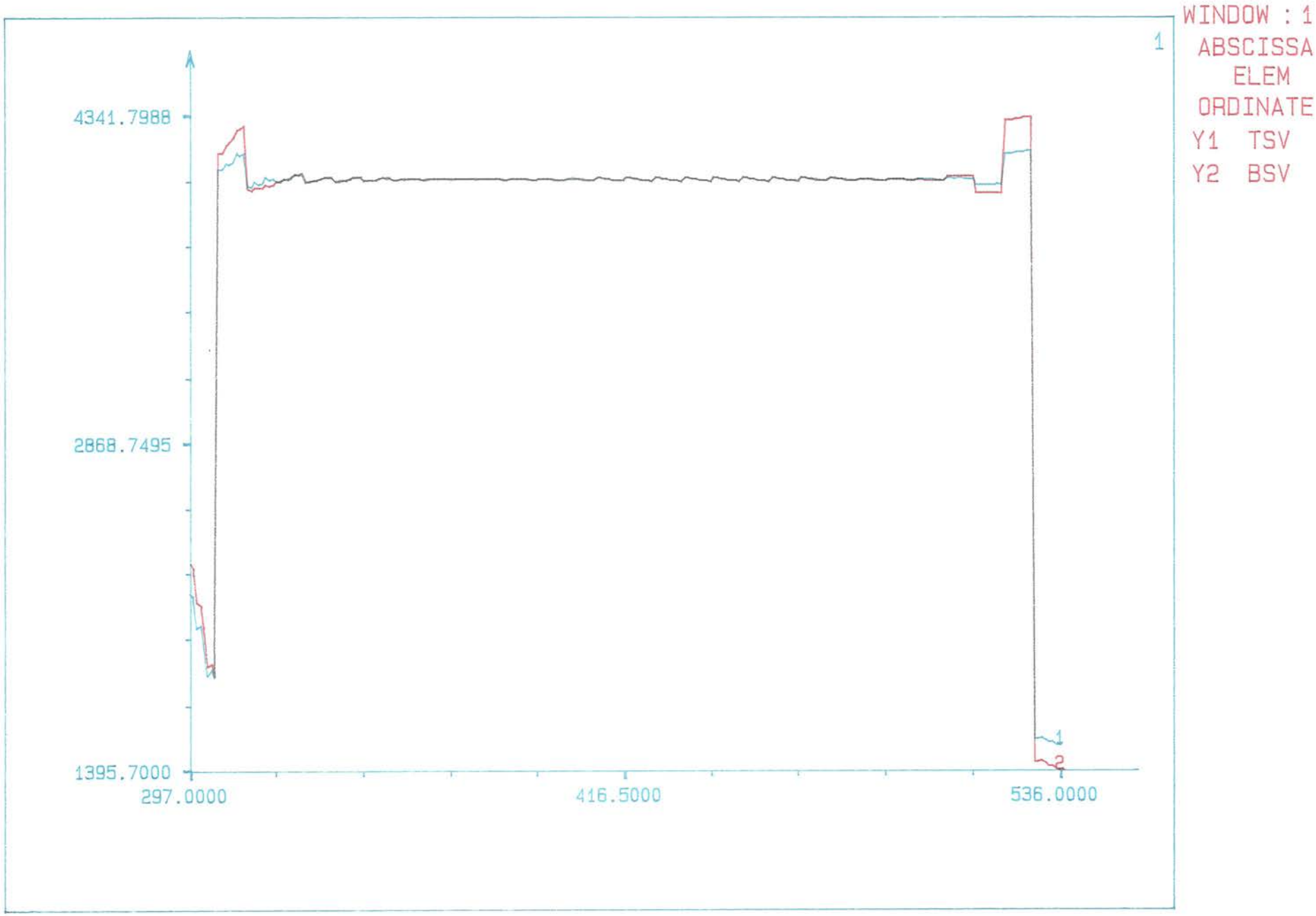

Figure 7.5 Inner Shell von Mises Stresses vs. Element Number

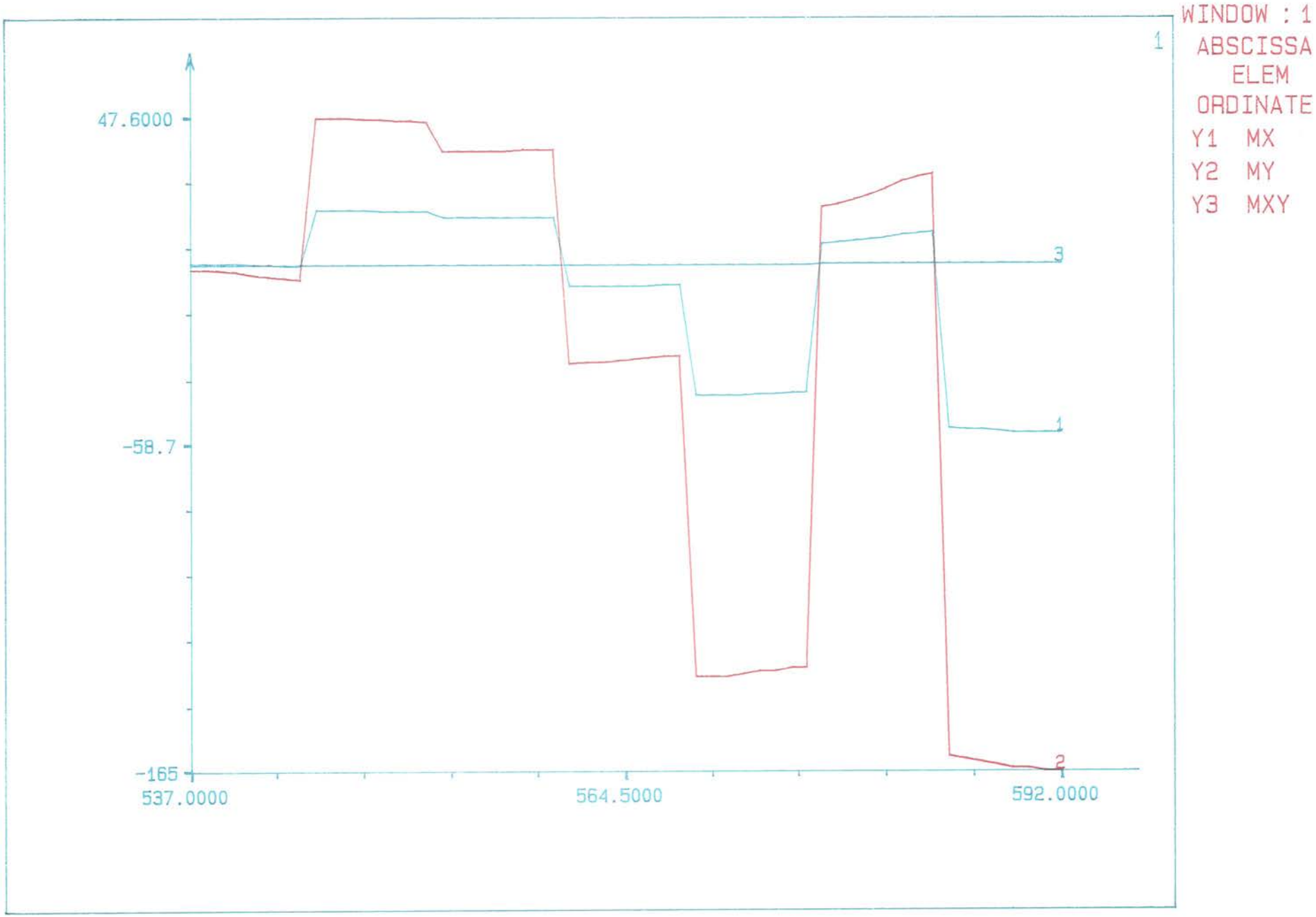

Figure 8.1 "First" Bulk Head Moment Resultants vs. Element Number

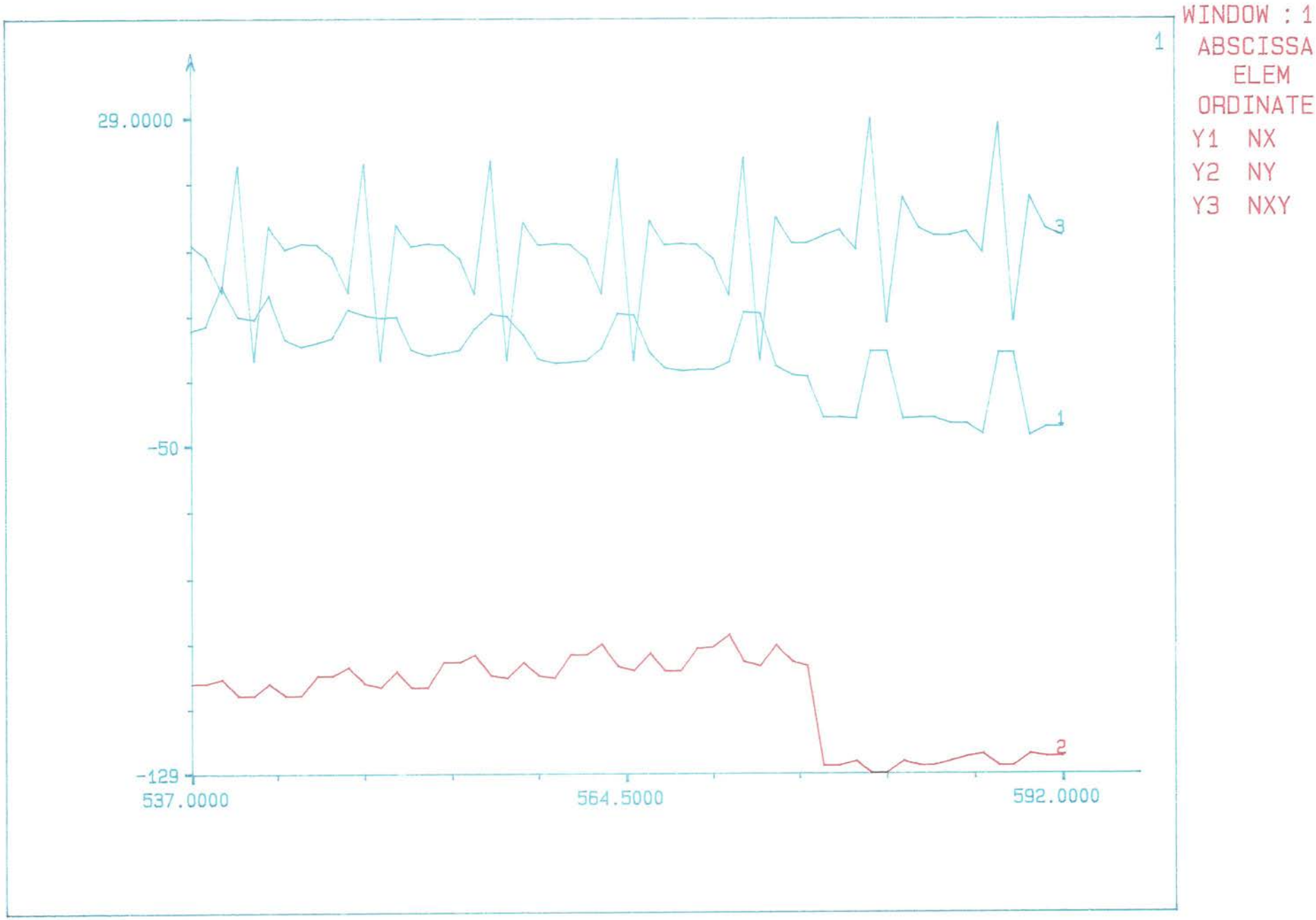

Figure 8.2 "First" Bulk Head Force Resultants vs. Element Number

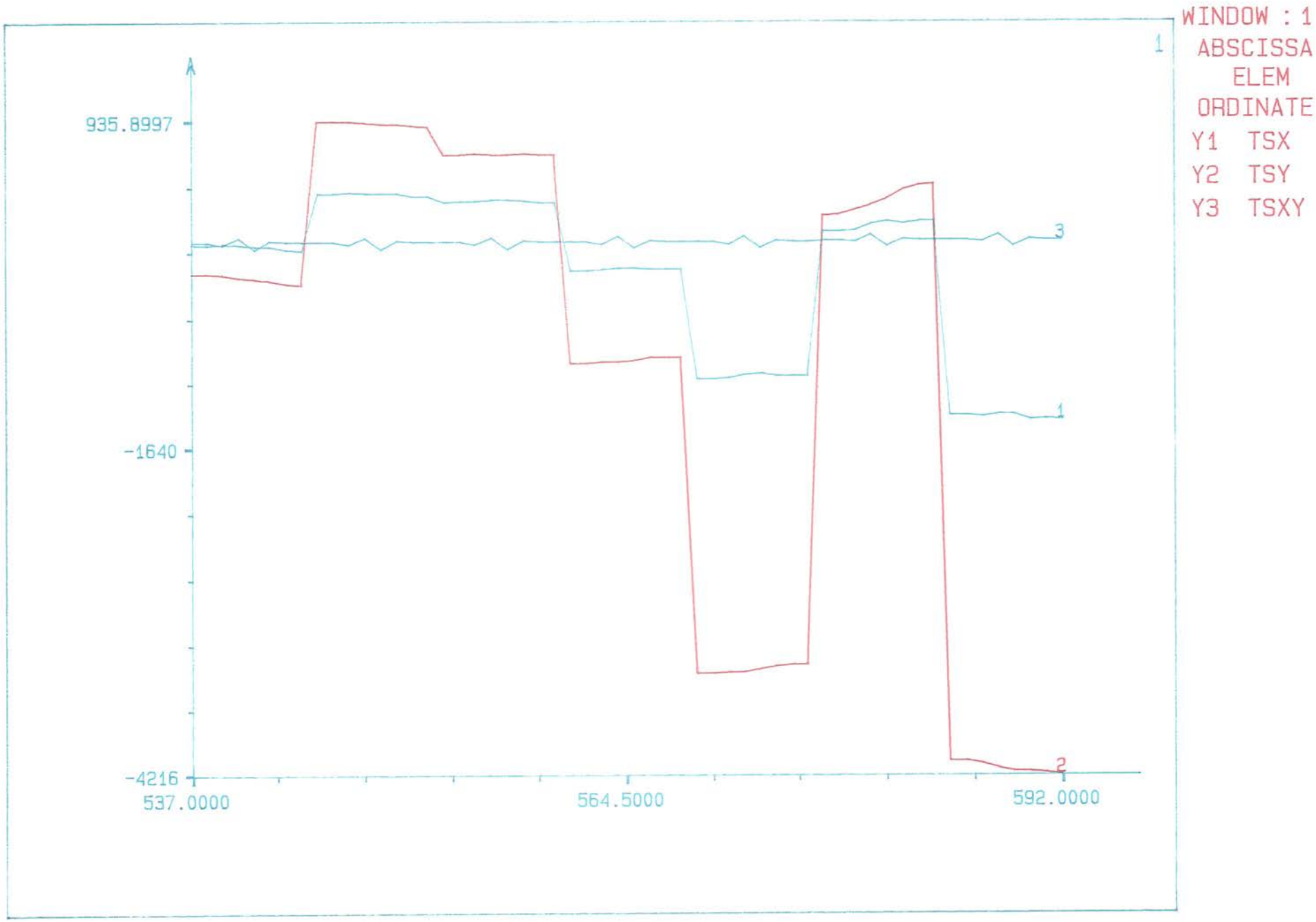

Figure 8.3 "First" Bulk Head Stresses (Vacuum Side) vs. Element Number

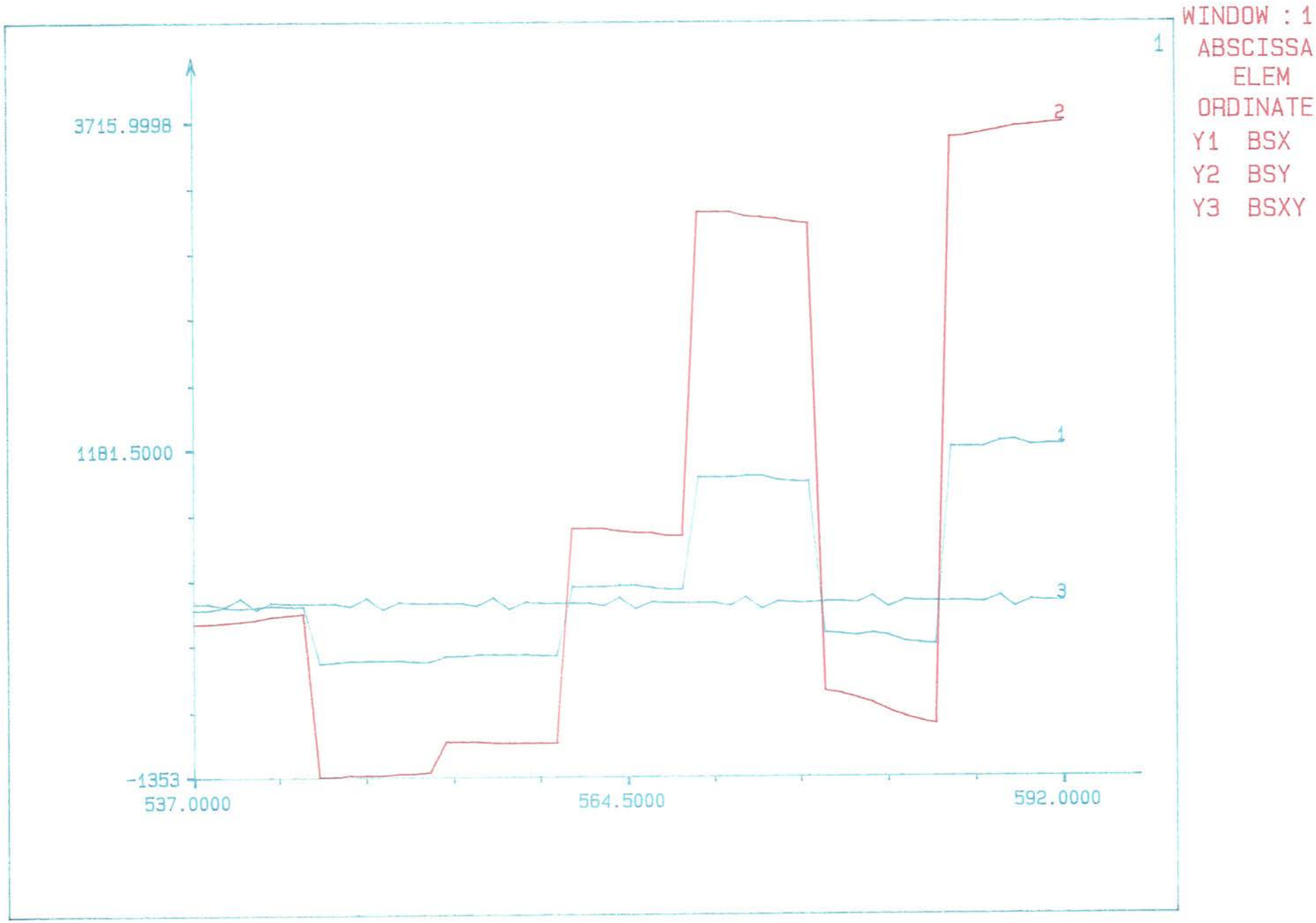

Figure 8.4 "First" Bulk Head Stresses (Pressure Side) vs. Element Number

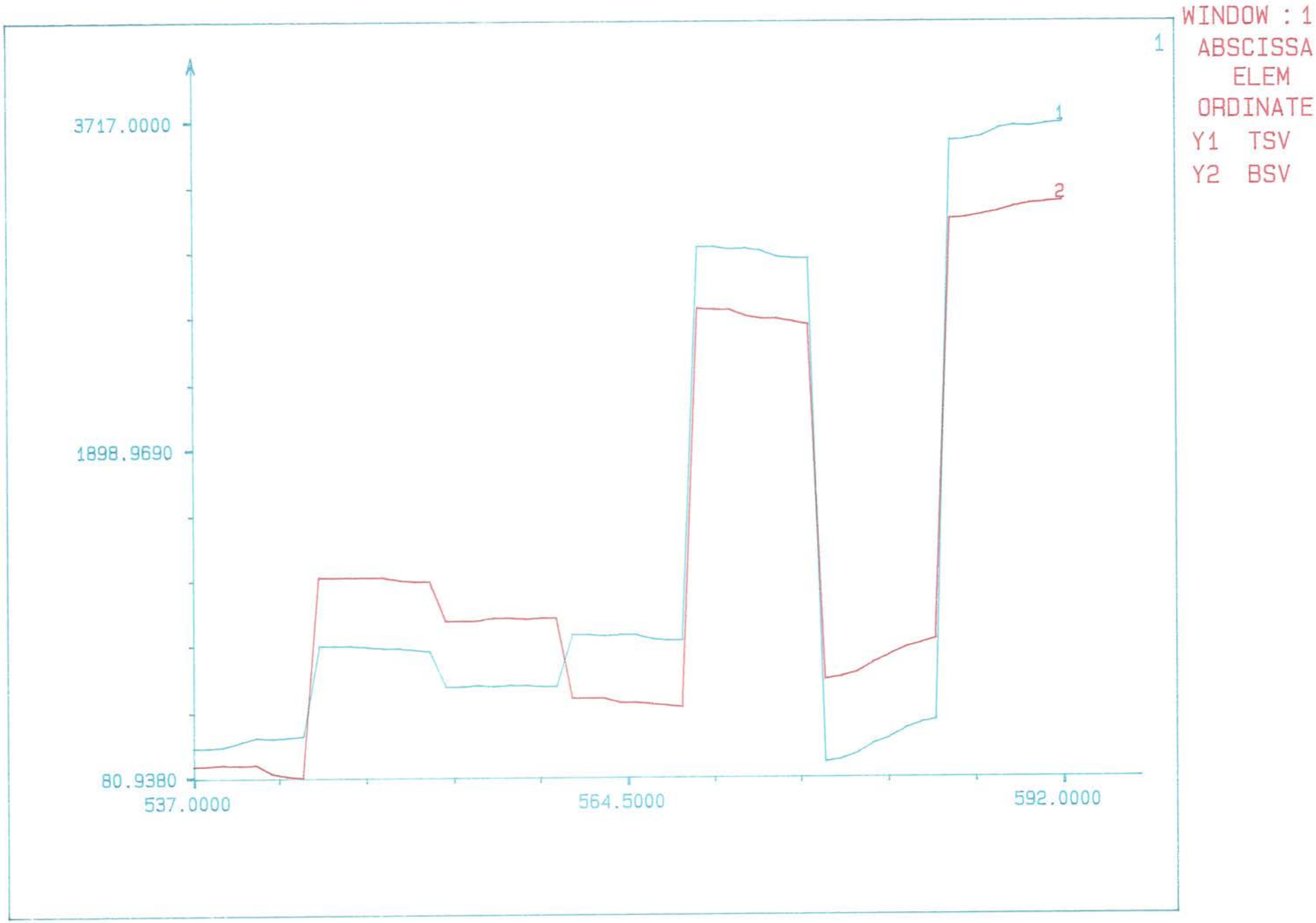

Figure 8.5 "First" Bulk Head von Mises Stresses vs. Element Number

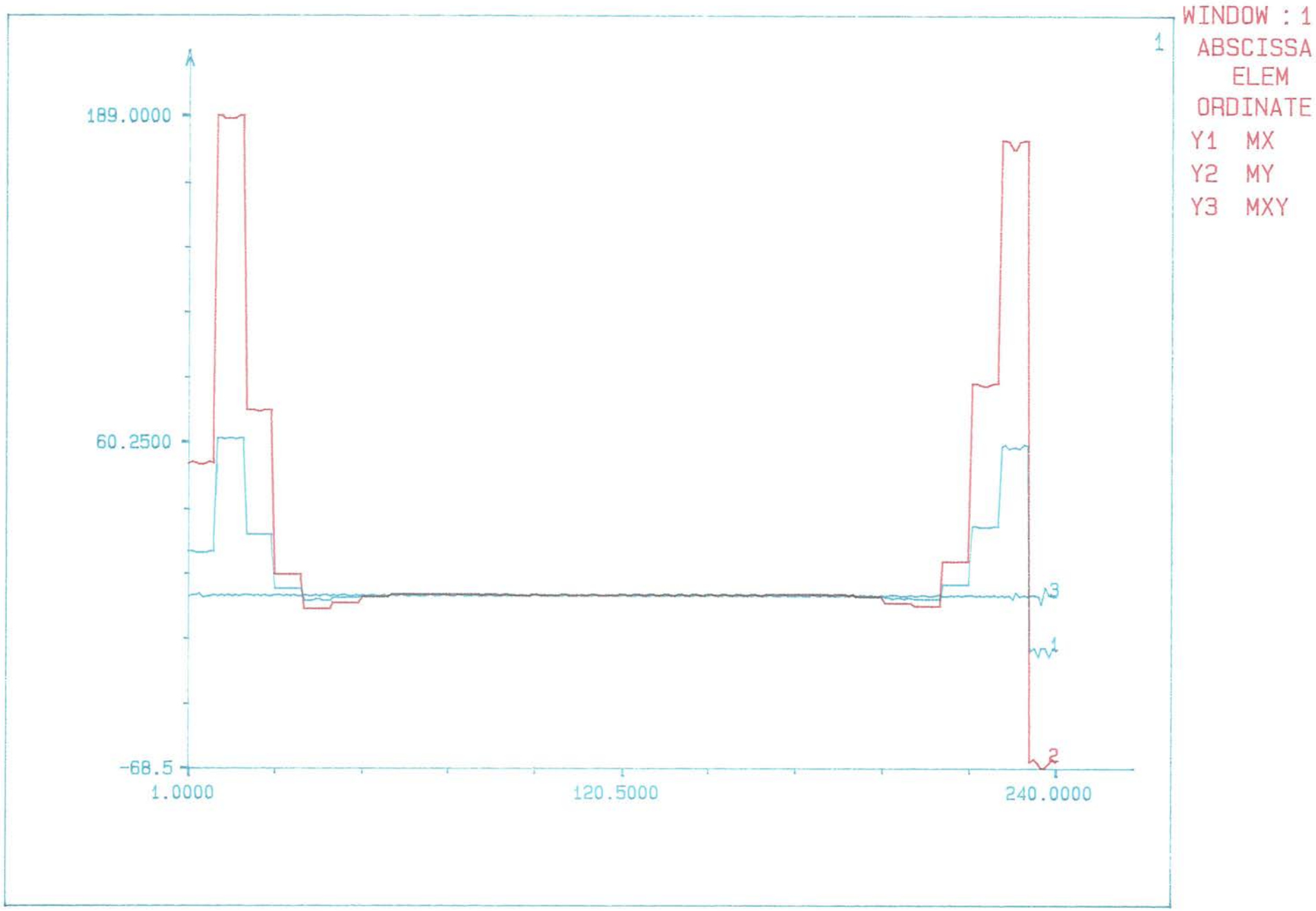

Figure 9.1 Outer Shell Moment Resultants (Pressure Load) vs. Element Number

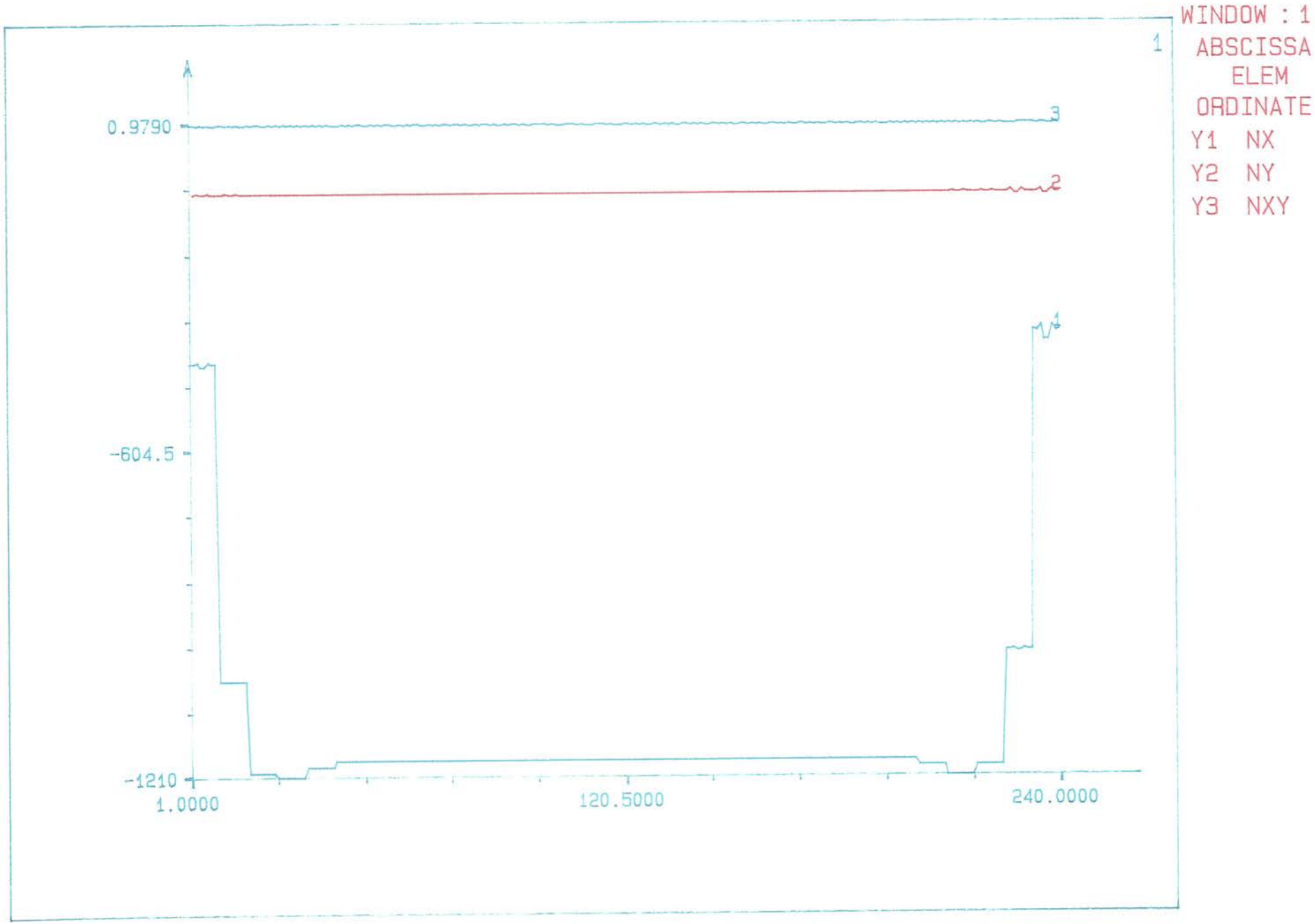

Figure 9.2 Outer Shell Force Resultants (Pressure Load) vs. Element Number

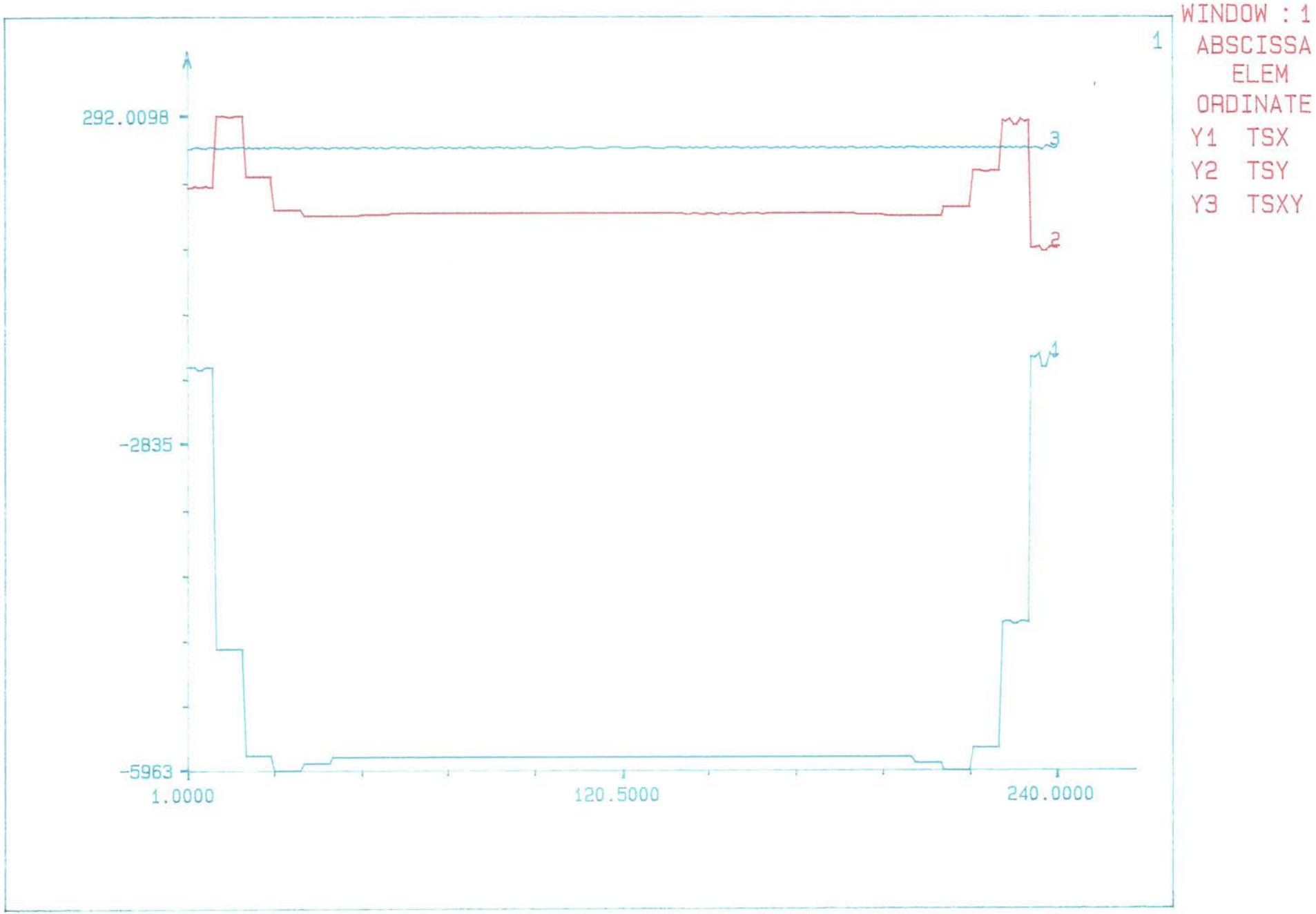

Figure 9.3 Isogrid Skin Stresses (Pressure Load) vs. Element Number

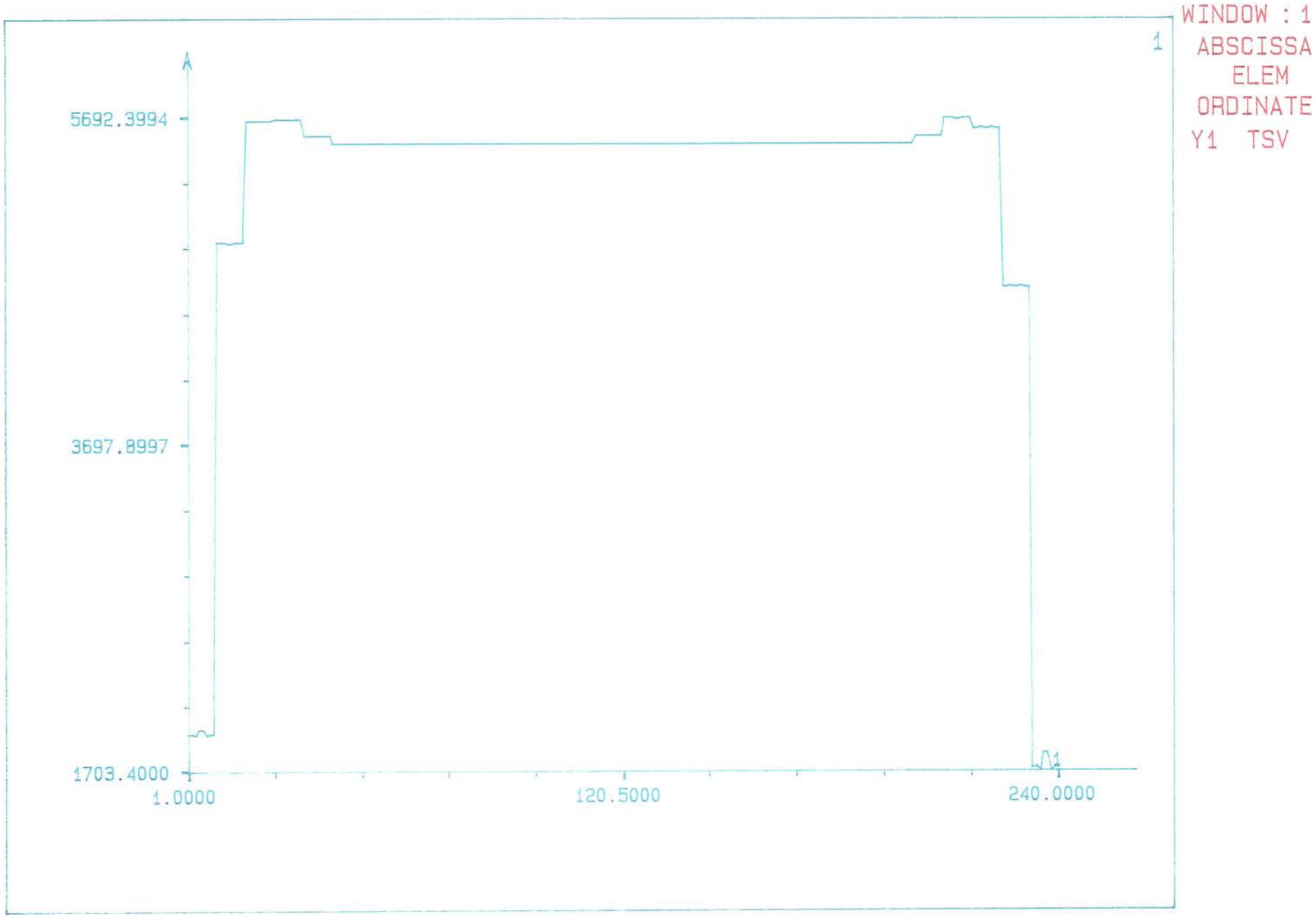

Figure 9.4 Isogrid von Mises Stresses (Pressure Load) vs. Element Number

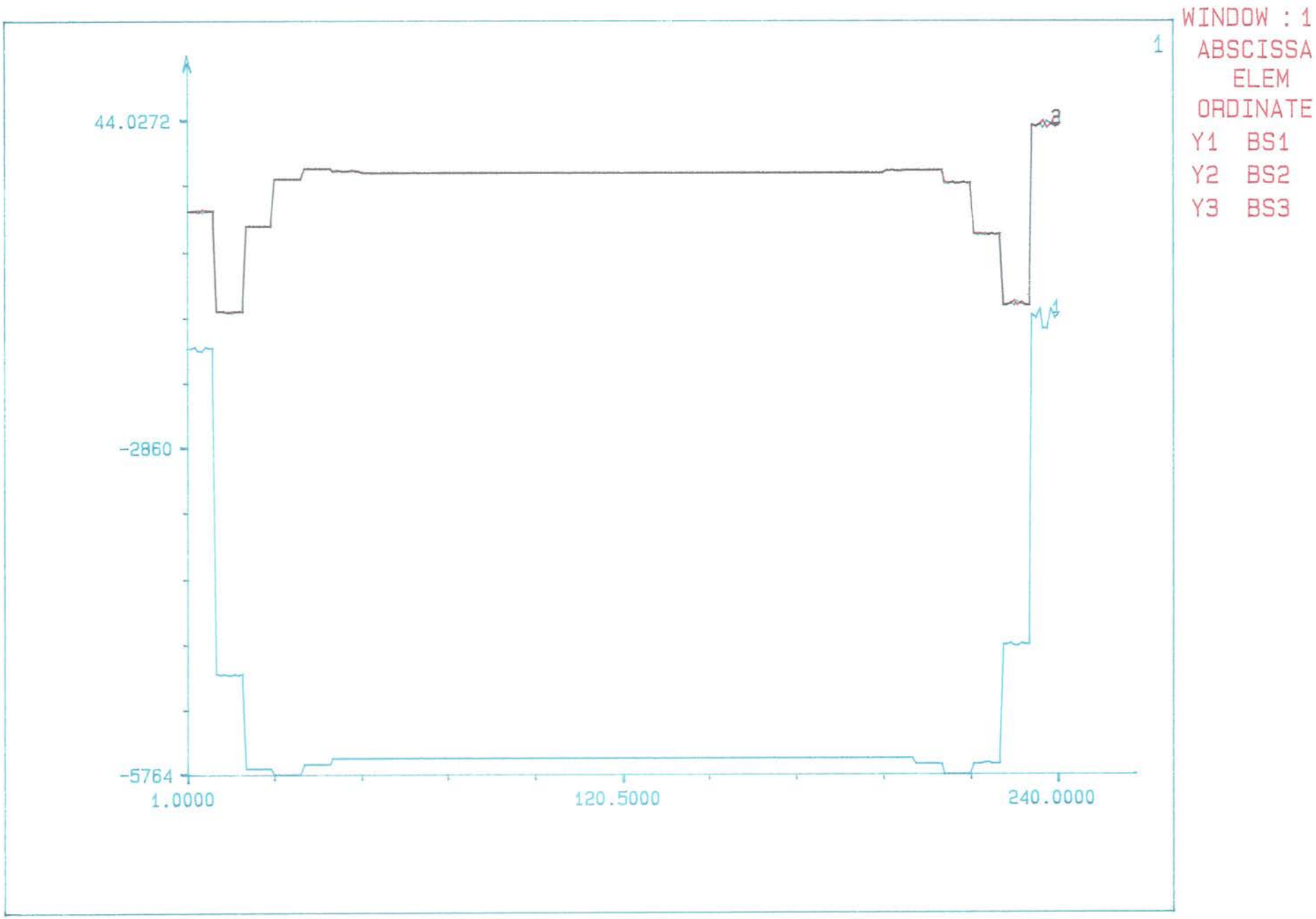

Figure 9.5 Isogrid Rib Stresses (Pressure Load) vs. Element Number

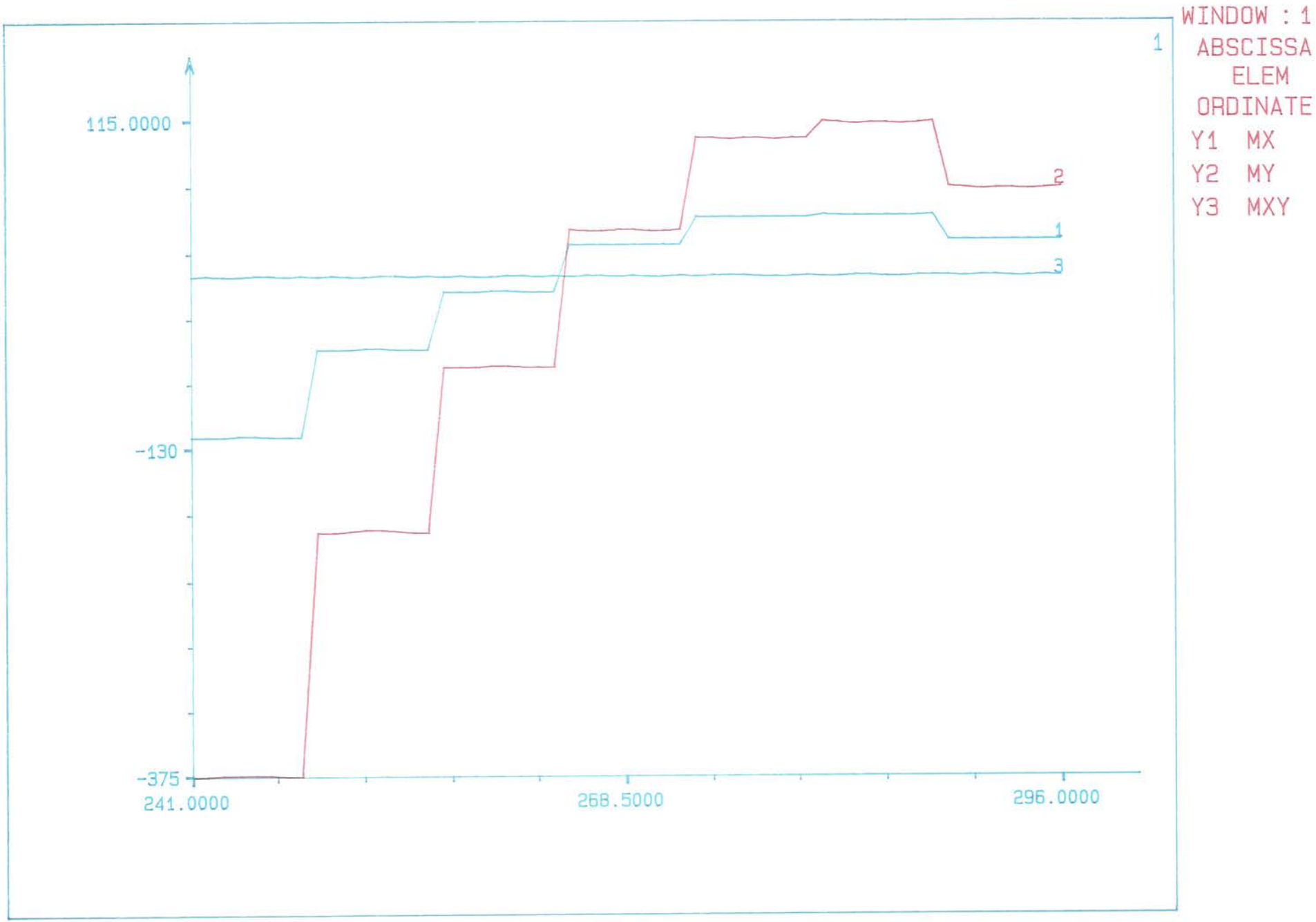

Figure 9.6 "Second" Bulk Head Moment Resultants (Pressure Load) vs. Element Number

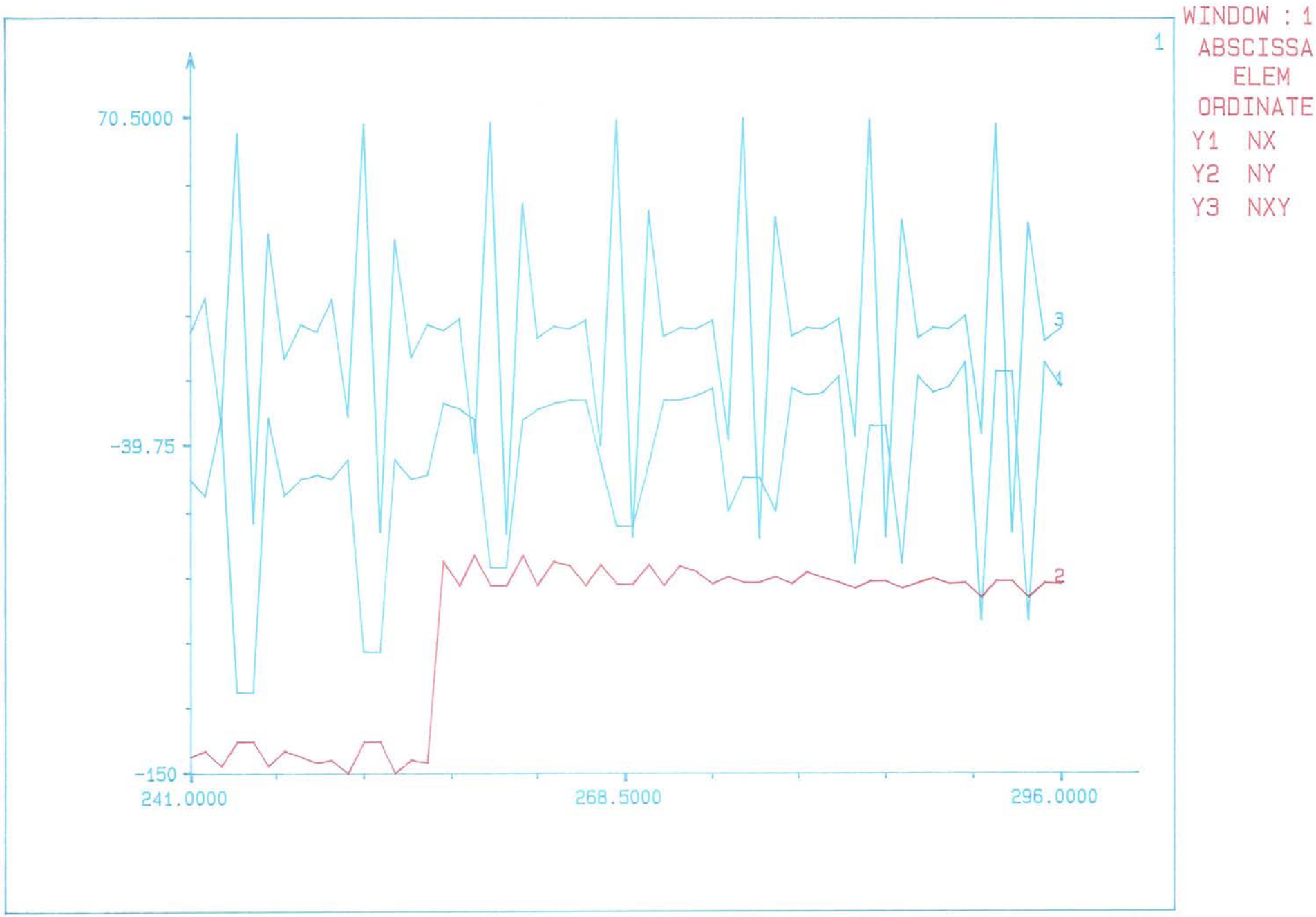

Figure 9.7 "Second" Bulk Head Force Resultants (Pressure Load) vs. Element Number

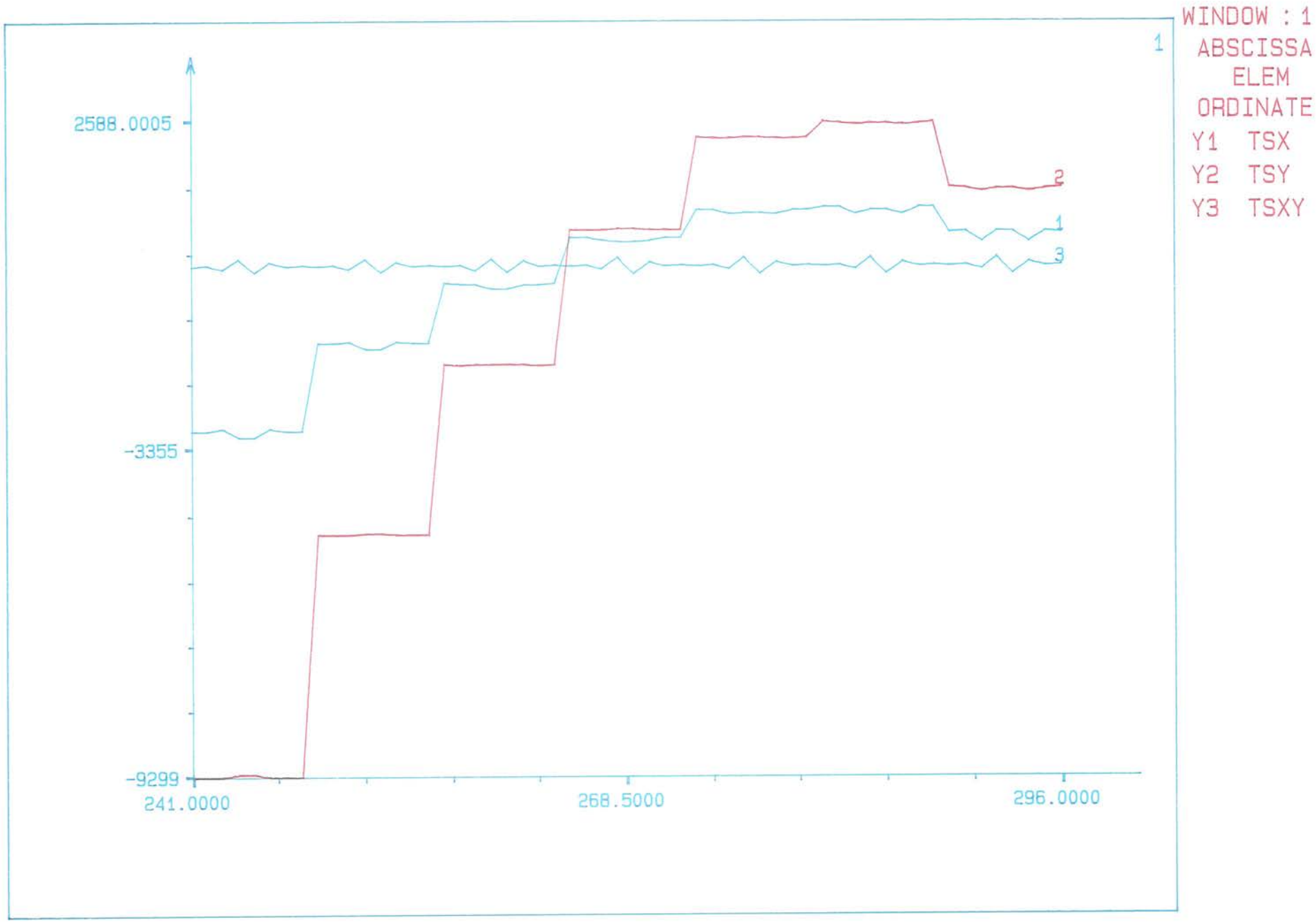

Figure 9.8 "Second" Bulk Head Inner Surface Stresses (Pressure Load) vs. Element Number

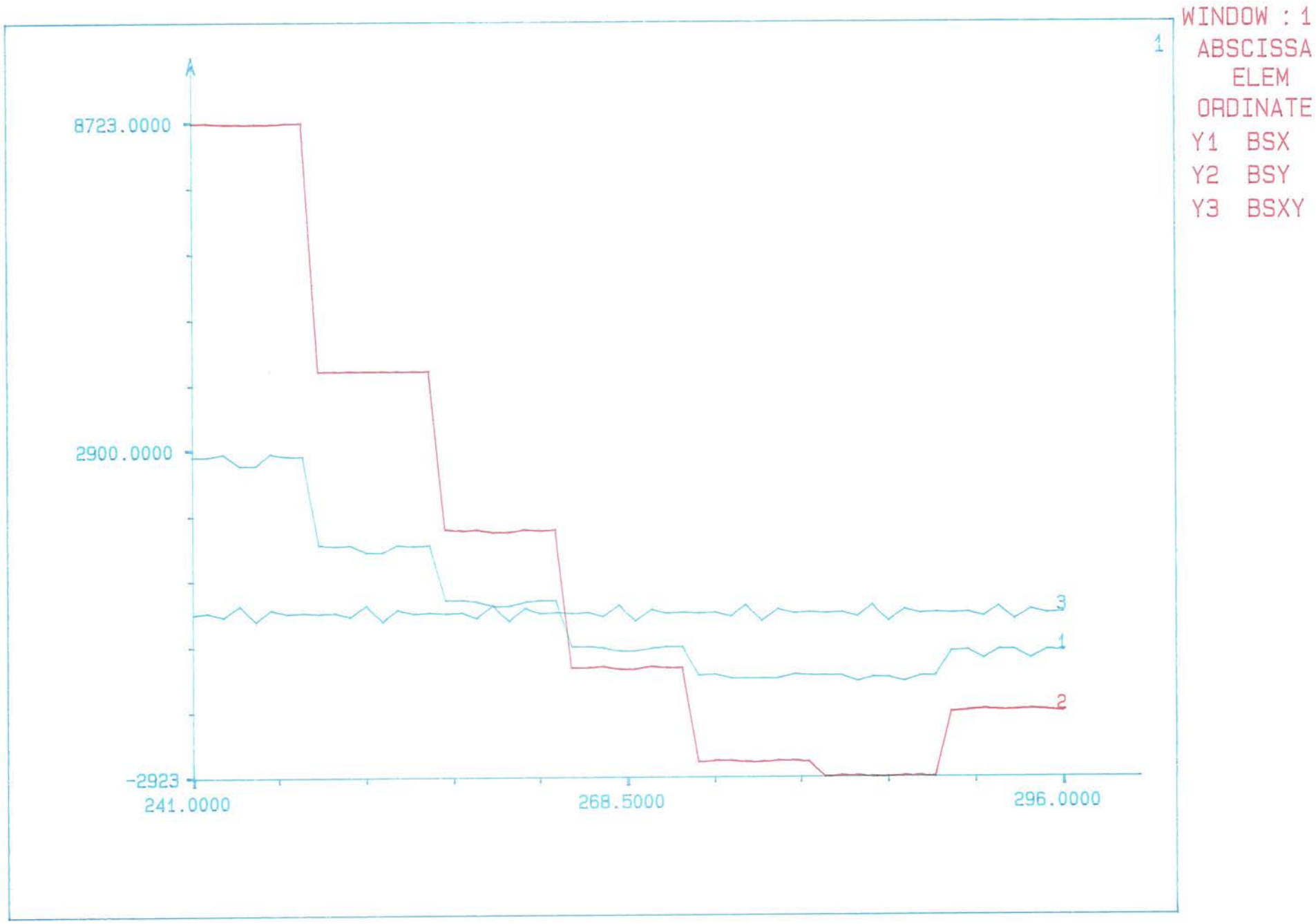

Figure 9.9 "Second" Bulk Head Outer Surface Stresses (Pressure Load) vs. Element Number

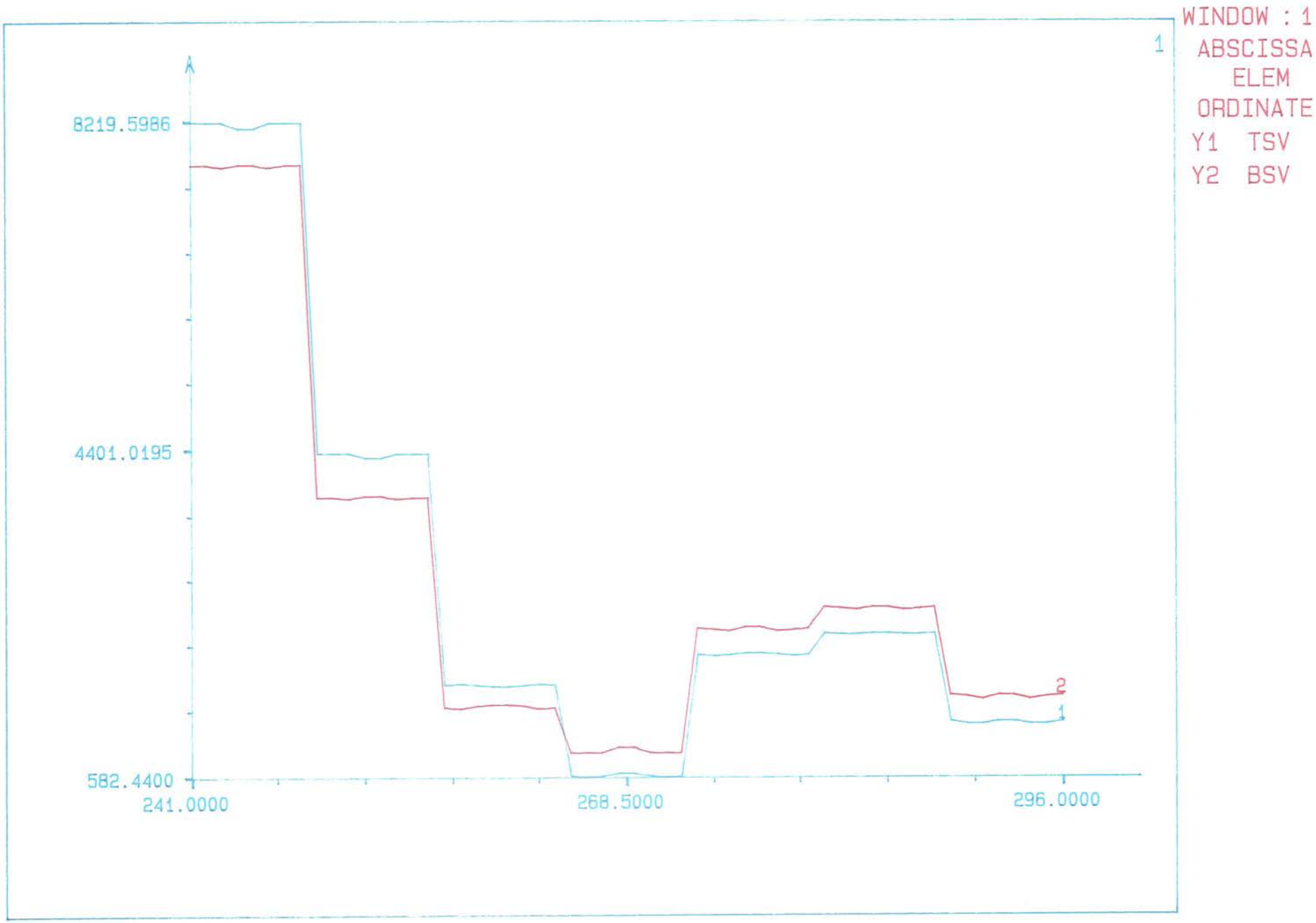

Figure 9.10 "Second" Bulk Head von Mises Stresses (Pressure Load) vs. Element Number

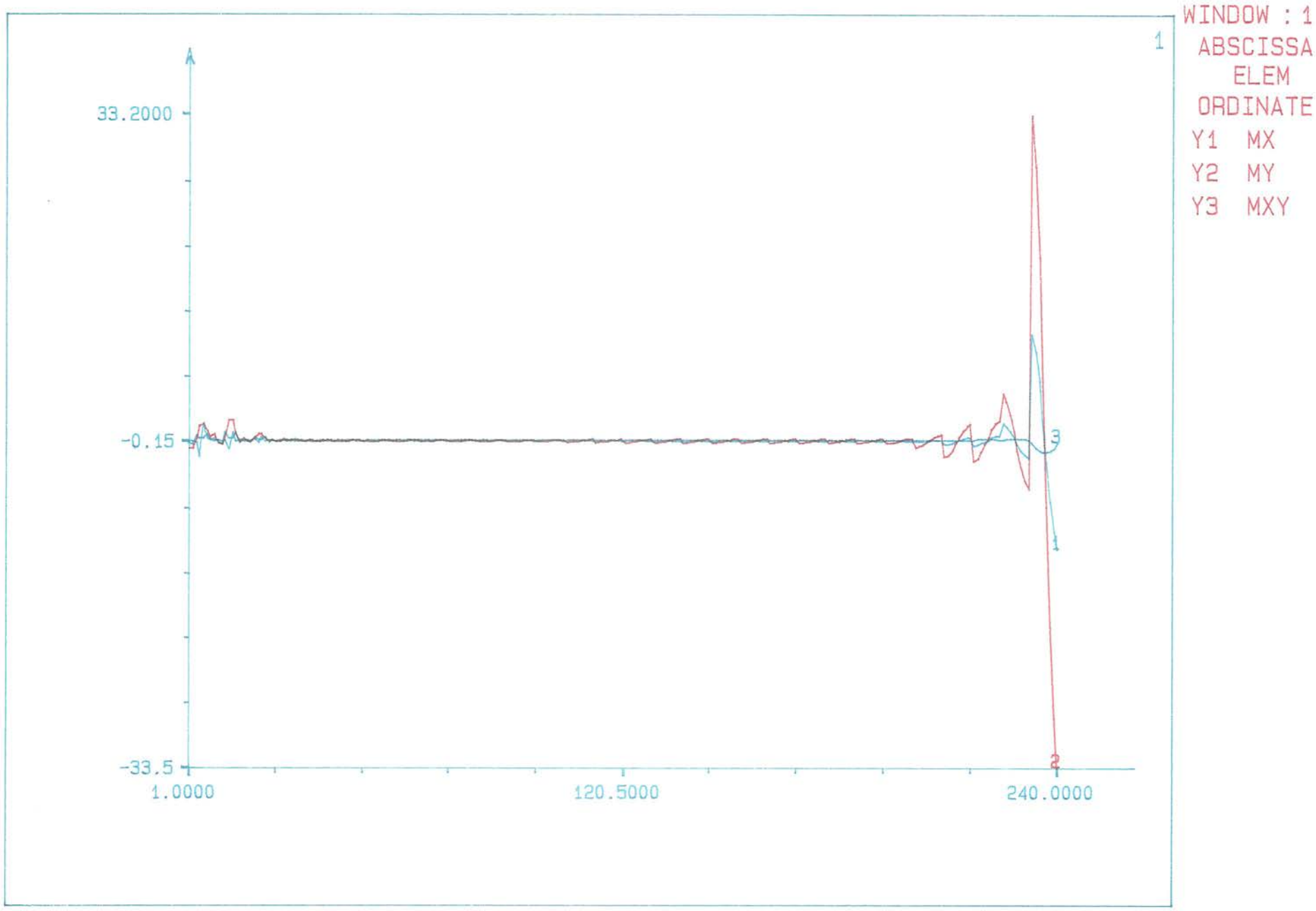

Figure 9.11 Outer Shell Moment Resultants (Bulk Head Loads) vs. Element Number

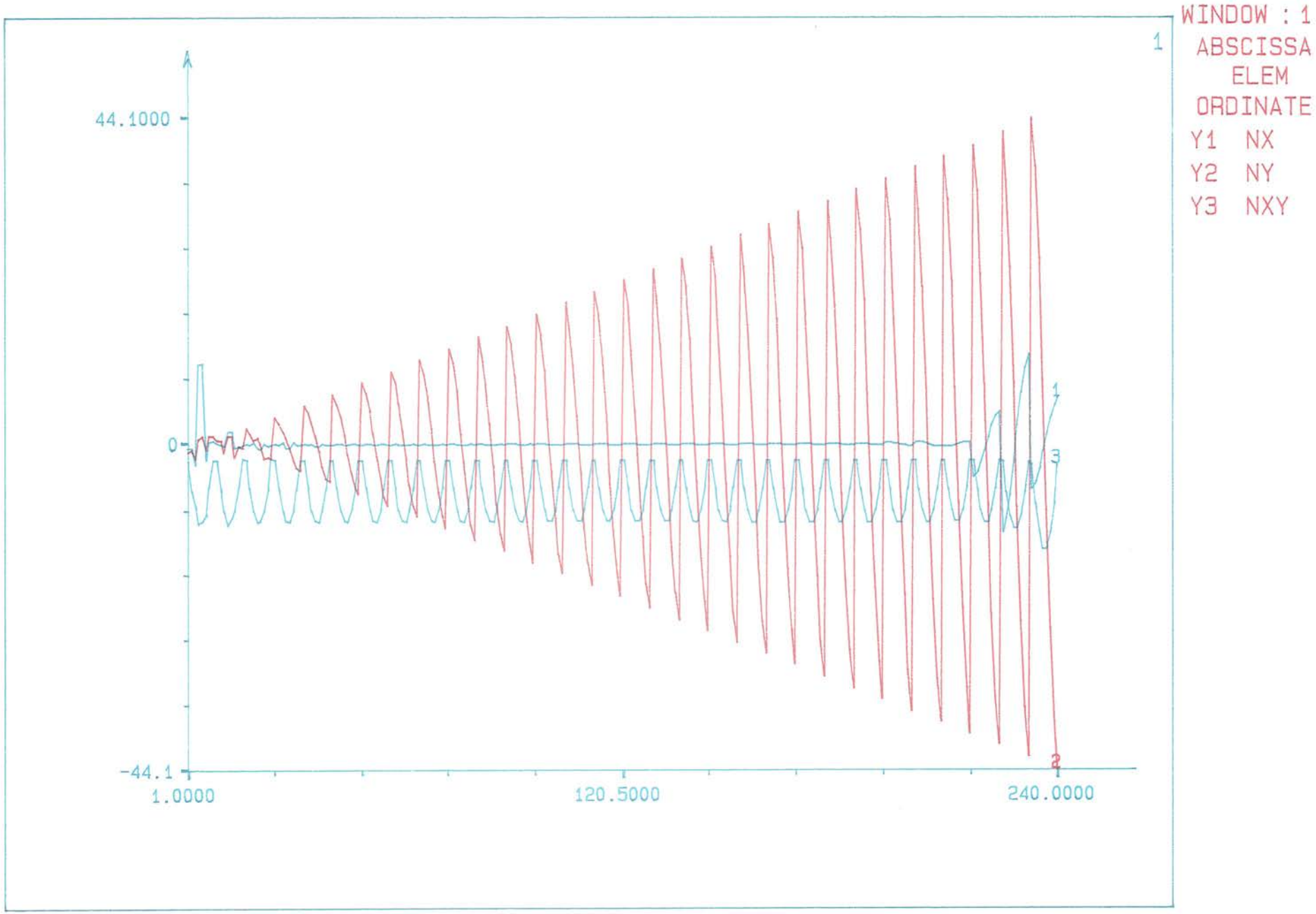

Figure 9.12 Outer Shell Force Resultants (Bulk Head Loads) vs. Element Number

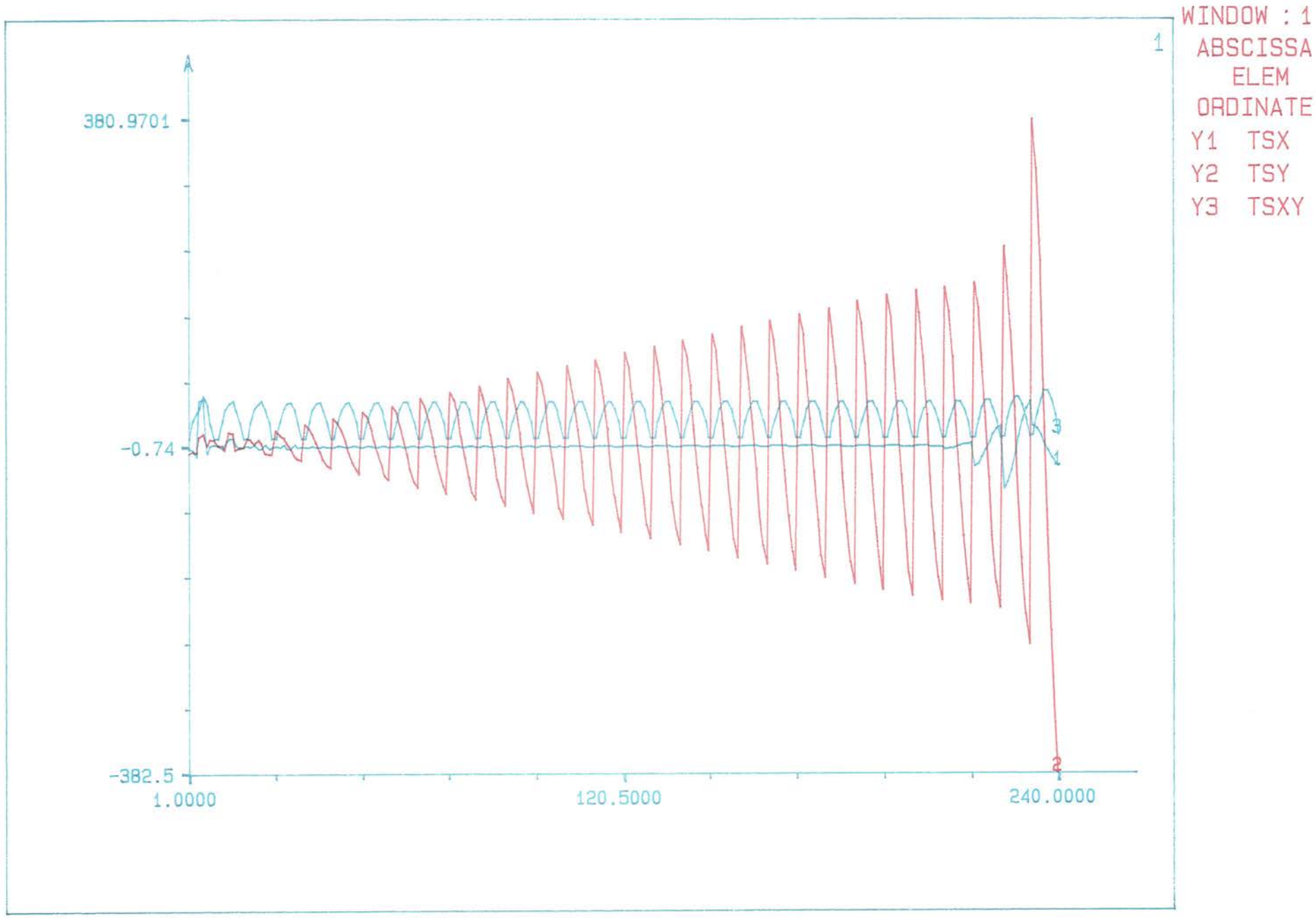

Figure 9.13 Isogrid Skin Stresses (Bulk Head Loads) vs. Element Number

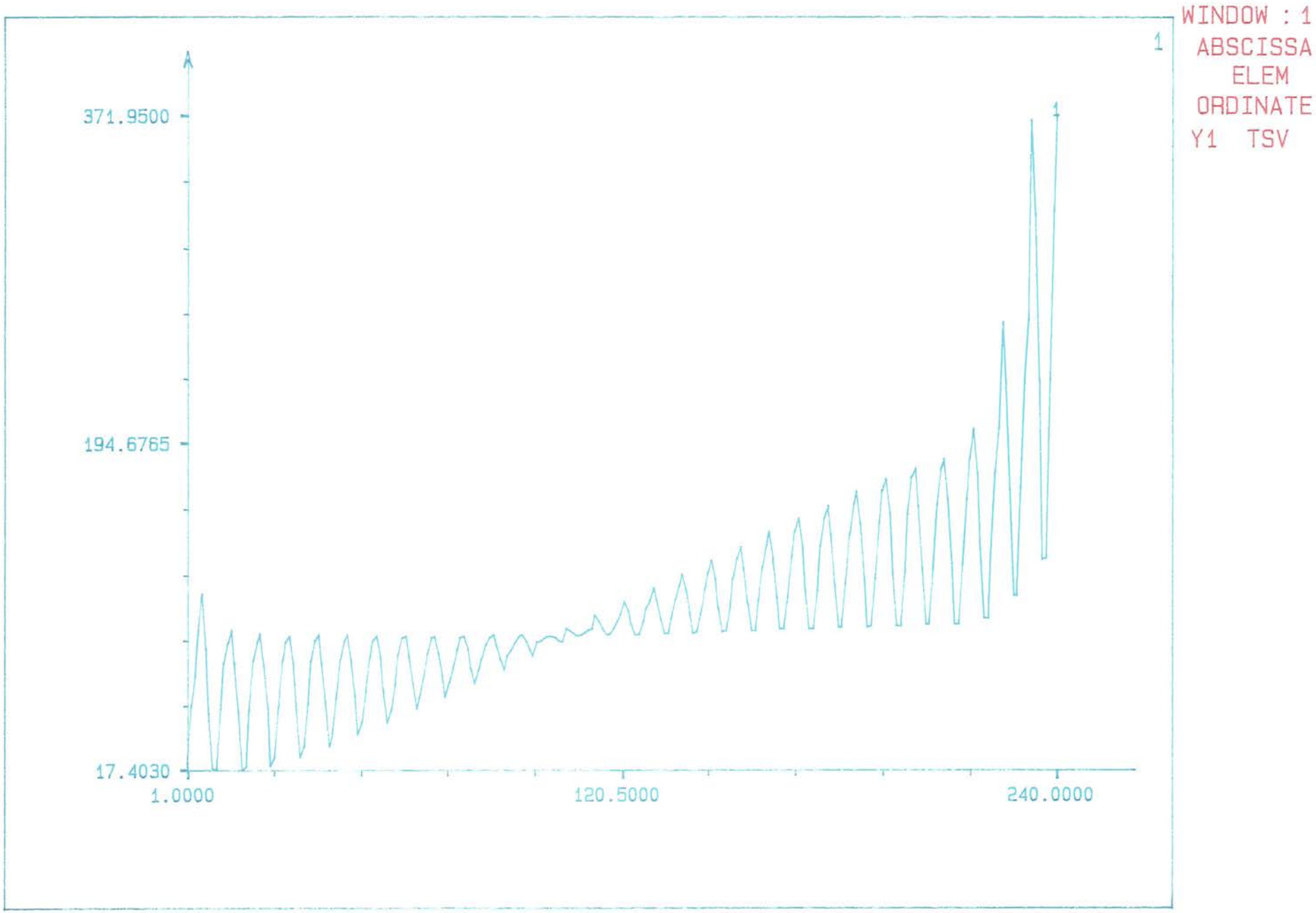

Figure 9.14 Isogrid von Mises Stresses (Bulk Head Loads) vs. Element Number

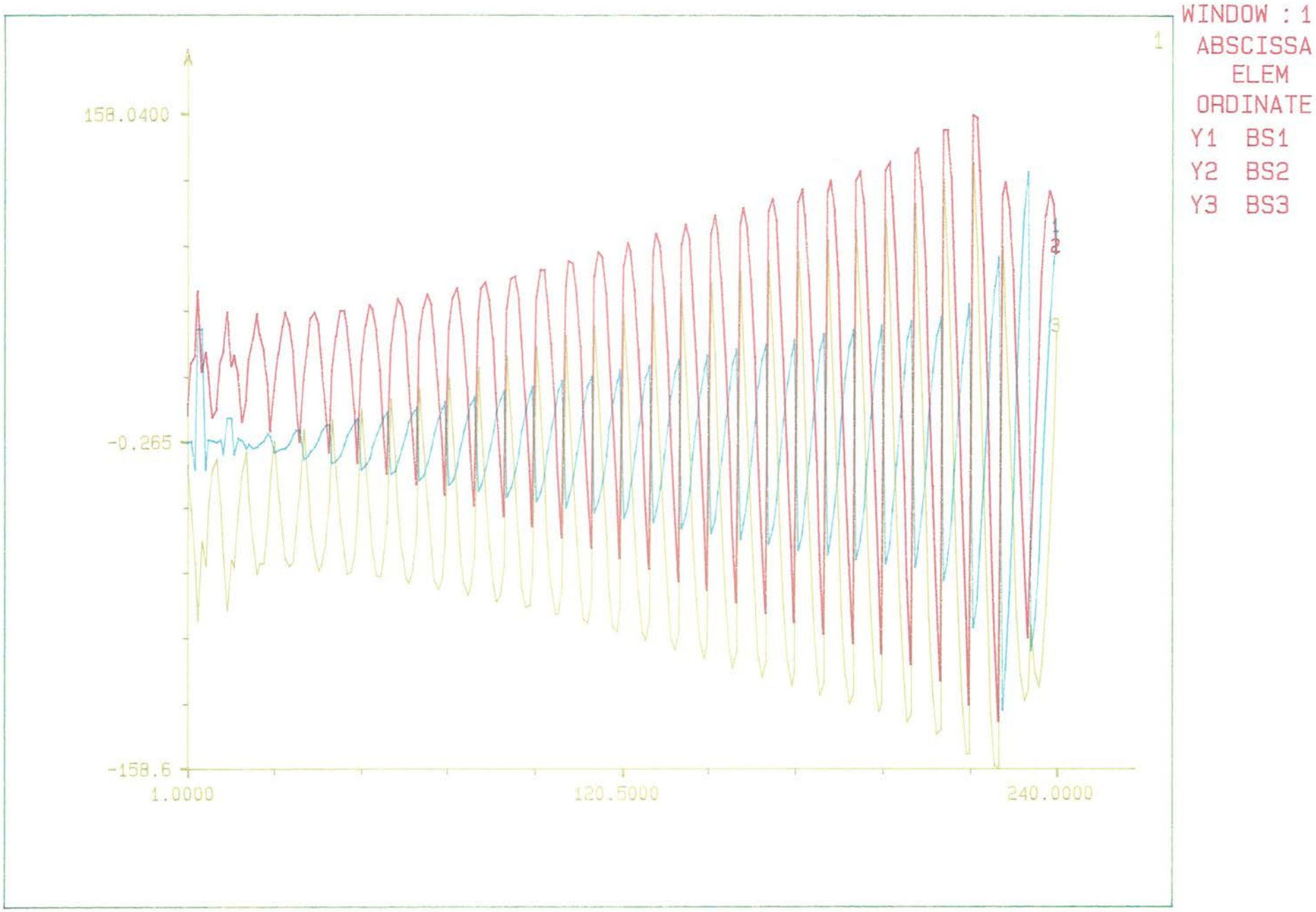

Figure 9.15 Isogrid Rib Stresses (Bulk Head Loads) vs. Element Number

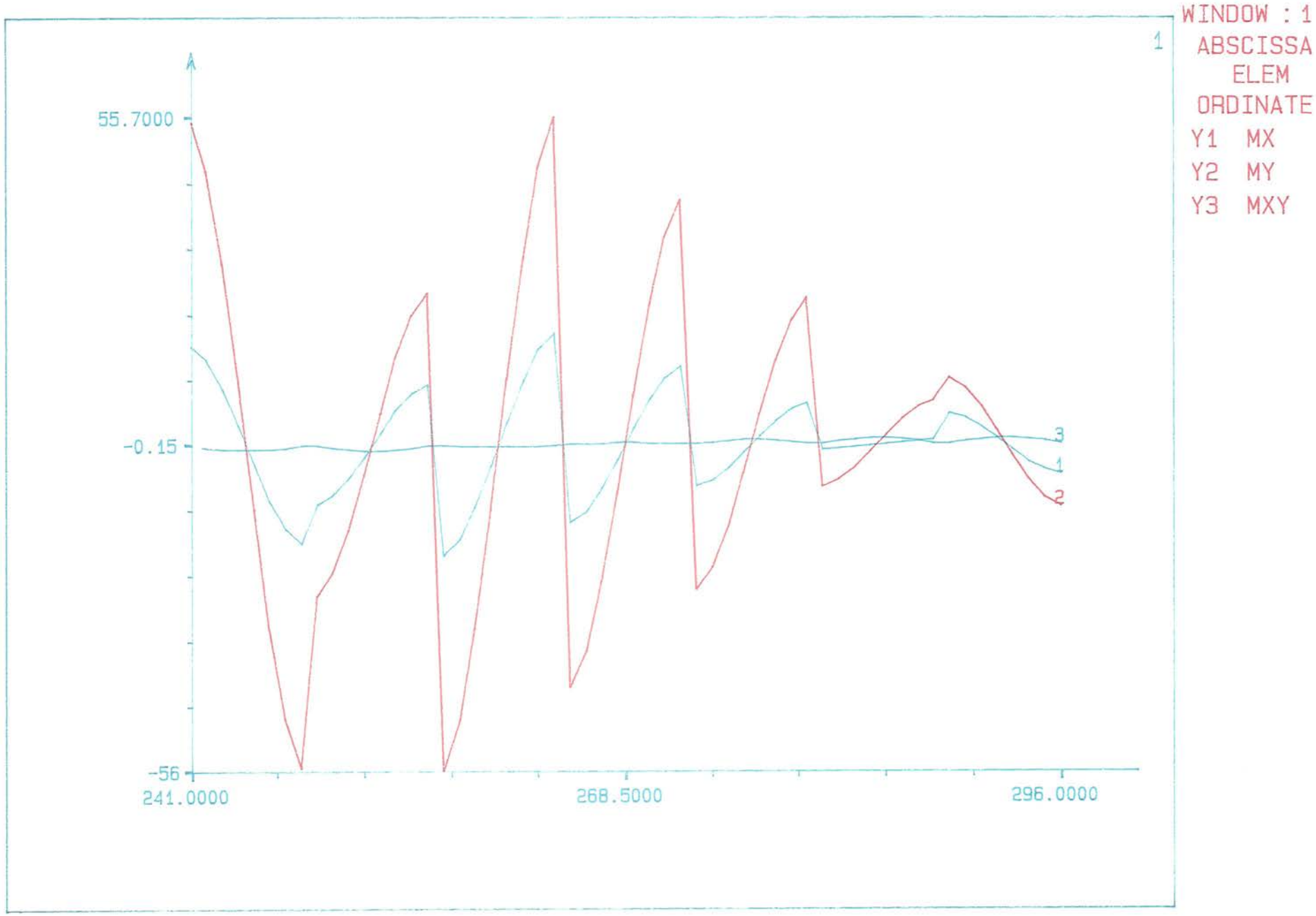

Figure 9.16 "Second" Bulk Head Moment Resultants (Bulk Head Loads) vs. Element Number

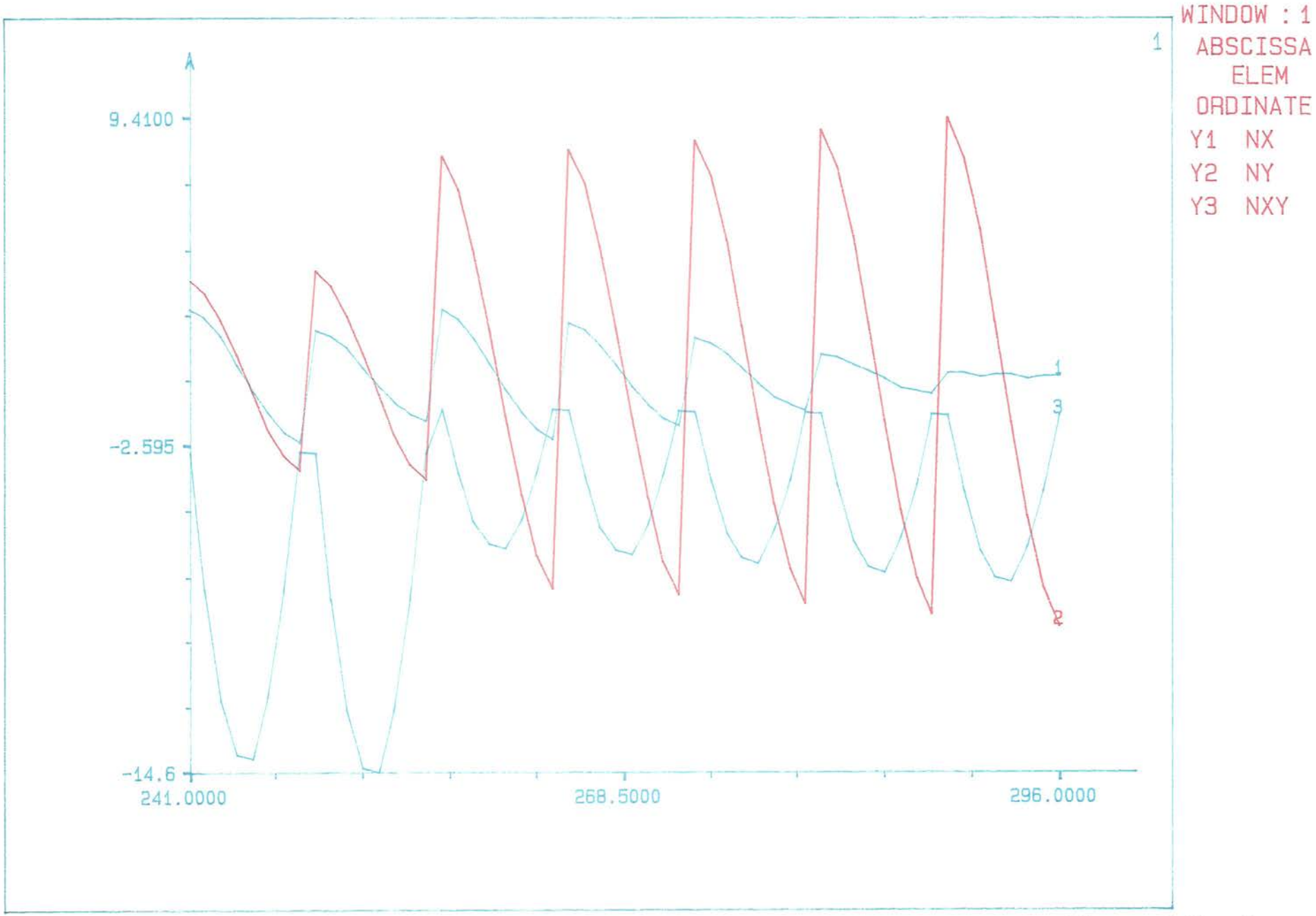

Figure 9.17 "Second" Bulk Head Force Resultants (Bulk Head Loads) vs. Element Number

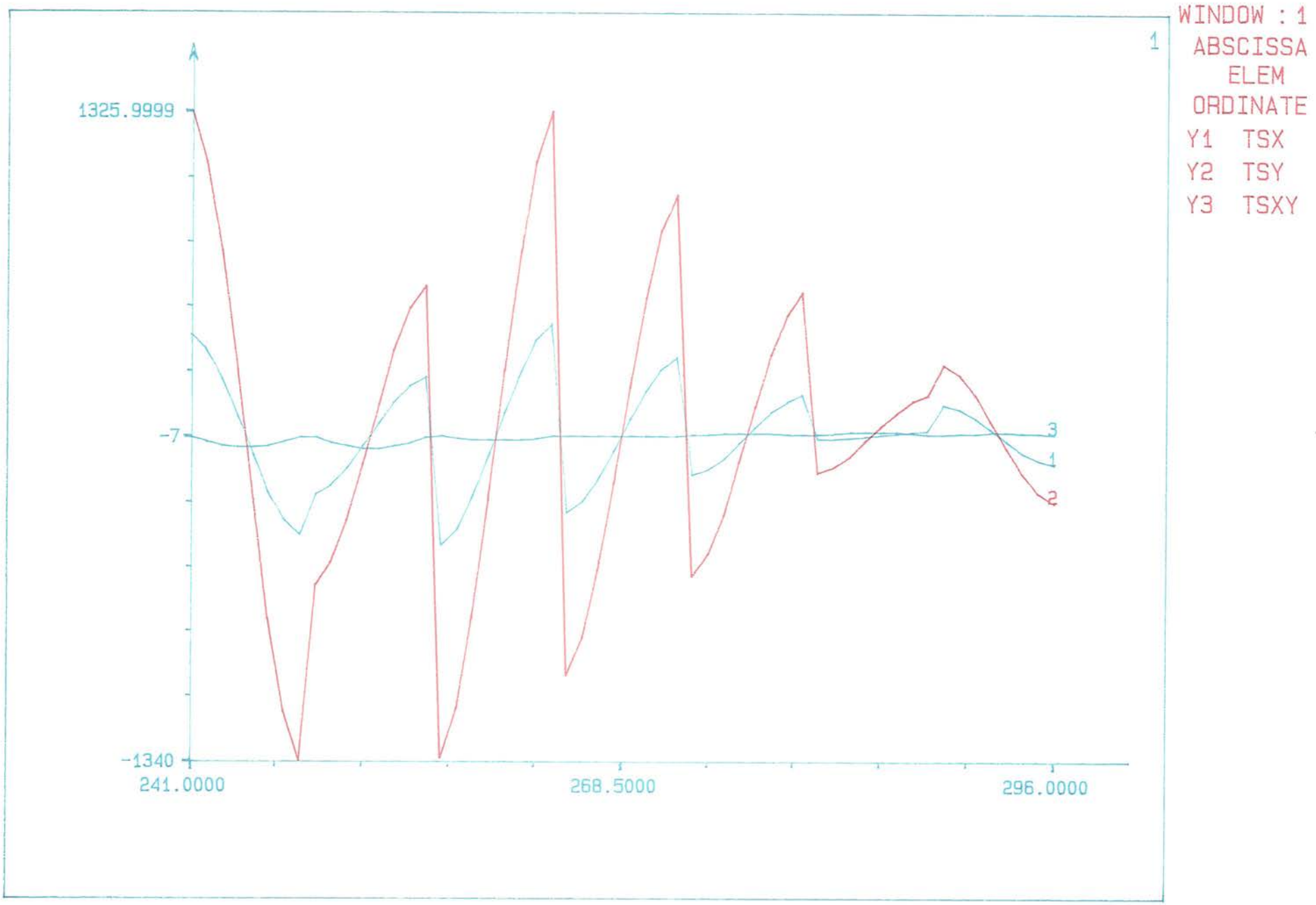

Figure 9.18 "Second" Bulk Head Inner Surface Stresses (Bulk Head Loads) vs. Element Number

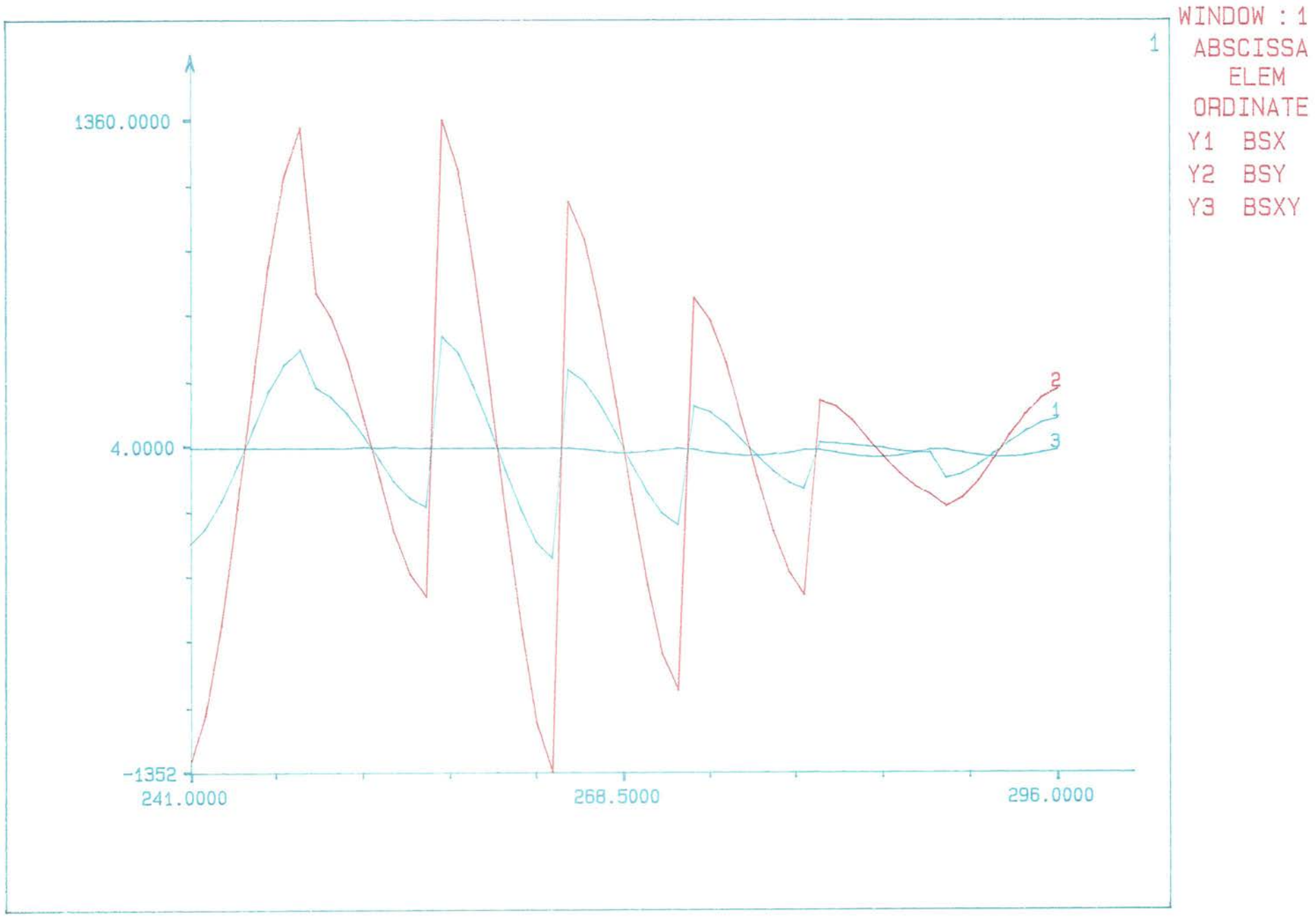

Figure 9.19 "Second" Bulk Head Outer Surface Stresses (Bulk Head Loads) vs. Element Number

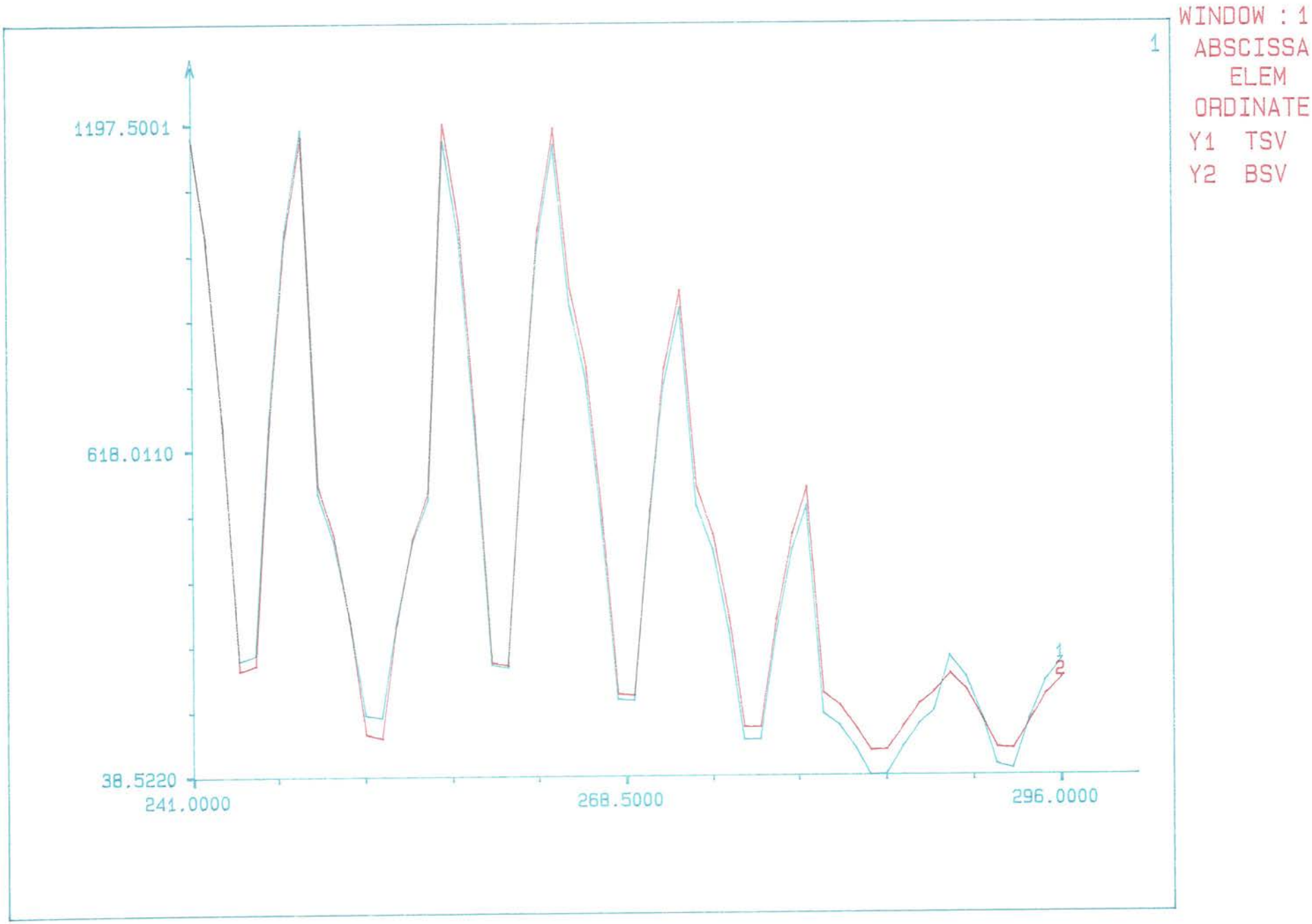

Figure 9.20 "Second" Bulk Head von Mises Stresses (Bulk Head Loads) vs. Element Number